I THE TRANSFER OF ENERGY FROM A HEATED CYLINDER TO A TURBULENTLY FLOWING AIR STREAM

II THE DIFFUSION OF ENERGY IN THE WAKE OF A HEATED CYLINDER EXPOSED TO A TURBULENTLY FLOWING AIR STREAM

Thesis by

Glenn Wagner Billman

In Partial Fulfillment of the Requirements

For the Degree of

Doctor of Philosophy

California Institute of Technology

Pasadena, California

1948

Acknowledgment

The design, construction, and operation of the apparatus described in this thesis would have been impossible without the constant, untiring efforts of my co-worker William H. Corcoran. David M. Mason (in particular), Robert C. Beacham, George A. Griffith, Willard M. DeWitt and H. Hollis Reamer also assisted, often during emergencies when such assistance was sorely needed.

The experimental project was initiated, and financial support for it was secured through the efforts of Dr. B. H. Sage. Dr. Sage, in addition, served as technical advisor for the project and contributed much in the way of guidance and encouragement. Dr. W. N. Lacey gave helpful advice during progress of the work.

The preparation of this thesis was aided by Mary Torrance who typed the manuscript.

Abstract

An experimental apparatus is described which was designed to accomplish:

(1) The production of a stable, two-dimensional, turbulently flowing air stream, and

(2) The measurement of temperature and velocity distributions associated with the thermal transfer of energy from heated bodies to the turbulent air stream.

Particular emphasis is placed upon design details of the apparatus which are unique.

Experimental data are presented for measurements of:

(1) The transfer of energy from a heated cylinder to the turbulent air stream

(2) The diffusion of energy in the wake of a heated cylinder.

These data are analyzed and the results presented in numerical and graphical form. The data are compared, where possible, with published data of a similar nature.

I Introduction

The apparent analogy between transfer of momentum and transfer of energy in flowing fluids has attracted considerable theoretical but little experimental attention since it was proposed by Reynolds (Reference 5). The theorists, notably Prandtl, von Karman, and Taylor, have proposed various mechanisms (References 6, 7, 8) by which such momentum and energy exchanges may take place. Each mechanism yields results which are in semiquantitative agreement with the meager amount of experimental data available in the literature. In the interests both of further theoretical progress and of practical engineering application of the analogy, it is essential that additional data be made available to permit confirmation or refutation of the mechanisms proposed.

The Department of Chemical Engineering at the California Institute of Technology has initiated an experimental program which, it is hoped, will provide sufficient data relating to the temperature and velocity distributions associated with thermal transfer of energy in flowing media to permit such confirmation or refutation.

The experimental investigation described in this thesis was a first step in this program. The physical situation investigated was that of a heated cylinder exposed to turbulent air flowing normal to the cylinder axis. Two aspects of this situation were considered:

(1) The transfer of energy from the heated cylinder to the turbulent air stream

(2) The diffusion of energy in the wake of the heated cylinder.

II Apparatus

A. General Characteristics

The apparatus employed in this investigation is a small, closed-circuit wind tunnel of rectangular working section designed to produce stable two-dimensional air flow over a wide range of velocity. As a necessary adjunct to the tunnel, instrumentation is provided which permits:

1. Control of bulk temperature and velocity of air entering the wind tunnel working section.
2. Control of thermal environment of air while in working section.
3. Measurement of point temperature and velocity as functions of position throughout the volume associated with the working section.
4. Measurement of surface temperature and of energy added to heated bodies exposed to air flow in the working section.

A general view of the wind tunnel is provided in Figures 1 and 2. The dimensions of the apparatus may be estimated from the 10 foot height and 15 foot length of the 4 x 4 wide flange framework which, exclusive of its own weight, supports a distributed load in excess of 5000 pounds. The instrument bench and control panels which serve the wind tunnel are shown in Figures 3-5. The instrument bench is located at the room wall opposite the wind tunnel while the control panels are in the positions indicated by Figures 1 and 2.

B. Details of Apparatus

1. Air System

The air system, which may be traced in part in Figures 1 and 2, is presented in schematic detail in Figure 6. The blower is driven by a 3-horsepower motor operating through a Speed-trol unit which employs variable diameter sheaves to provide rotative speeds over a wide, continuous range. Extension of the range of operation beyond that provided by the Speed-trol unit may be accomplished by variation of sheave ratio between blower and Speed-trol or by insertion of orifice plates in blower outlet.

The motor-blower unit is shock-mounted and joined to the remainder of the air system by canvas connectors as indicated in Figure 7. Under these conditions, virtually no vibration is transmitted to the remainder of the system, and readings with delicate instruments are not disturbed.

Air leaving the blower passes through an expansion section to the heater-cooler unit shown in Figure 8. The heater is manually controlled and consists of three 500 watt nichrome strip heaters mounted on transite frames. One of the heater sections is Variac controlled and permits continuous variation in power output through the range 0-1500 watts when used in conjunction with the two remaining steady heaters. The cooler section is a 5000 B.t.u. per hour unit designed to operate

on the standard laboratory freon system. Manual control of cooling rate is provided by a standard diaphragm-type pressure reducing valve.

Gross flow of air (approximately conditioned to the desired operating temperature) is measured by means of a low-loss Venturi meter of the type shown in Figures 9 and 10. Maximum working section velocities are desired in the range between 4 and 160 feet per second. These limits correspond to volumetric flow rates of 0.25 and 10 cubic feet per second, respectively. In order to cover such a volumetric flow range with readable pressure differentials, a set of four Venturi meters is employed with characteristics given in Table I and Figure 11. Upstream calming lengths, contraction, and diffuser angles recommended by Reference 1 are employed in the meters, their only distinctive feature being use of a slot-type piezometer section rather than a series of small diameter holes susceptible to clogging.

Final thermal conditioning of the air is accomplished by a 250-watt automatic control heater mounted between the exit of the expansion sections following the Venturi meter and the entrance to the upstream plenum chamber. This heater, shown in Figure 12, is actuated by a platinum resistance element mounted in the convergent section which precedes the tunnel working section (Figures 12 and 13). The control and heater power circuits involved will be described under instrumentation.

Air leaving the automatic heater enters the upstream plenum chamber (Figure 13) and is turned through 180 degrees by two sets of turning vanes designed in accordance with the recommendations of Reference 2. These vanes are of such form and spacing as to minimize eddy formation associated with the change in direction. They serve, additionally, to distribute the flow over the cross section and thereby to minimize centrifugal effects. As a means of damping out eddies or other irregularities produced by the change in direction, a filter and a honeycomb calming section are employed at the exit of the plenum chamber. The filter also removes dust which might otherwise interfere with operation and calibration of the hot wire anemometer and pitot tube employed to measure air velocity. The air next enters the convergent section which, by reason of a 10 fold contraction ratio, produces a substantially uniform velocity distribution at the entrance to the working section.

The working section, to be described under that title, conducts the air past the heated cylinder and measuring instruments and delivers it to a downstream end box (Figure 14). From this end box the air is returned to the blower.

2. Working Section

The working section of the tunnel is a horizontal, rectangular duct 3/4 inch high, 12-3/8 inches wide and 13 feet 6 inches long. The upper and lower walls of the duct are

polished copper plates, 3/8 inch thick, whose external surfaces are in contact with separate systems of rapidly circulating, thermally conditioned oil. A cross-section of the working section duct is presented in Figure 15.

The 3/4 inch sidewalls of the working section are laminated cotton micarta blocks designed to slide between the upper and lower duct surfaces and thus permit longitudinal motion of temperature and velocity measuring instruments which enter through specialized blocks associated with the traversing unit (Figure 22). Metal backing strips attached to the micarta blocks (Figure 15) bear against machined surfaces and thus provide positive alignment of the block surface exposed to the air stream. The micarta blocks were ground with tolerances on vertical and lateral dimensions of $\pm$ 0.002 inch. They therefore present a smooth, uninterrupted surface from block to block on the air stream side. A standard block is shown in place between the duct surfaces in Figure 16, while Figures 17 and 18 present two views of the specialized block associated with the traversing unit. Felt sealing strips mounted in grooves (Figures 16 and 17) on the top, bottom, and ends of the blocks provide compression against the duct surfaces and adjacent blocks sufficient to prevent significant loss of air from the section.

The sidewall blocks are constrained to move as a unit with the traversing gear while they are in the working section. If the longitudinal motion of the traversing gear is sufficient to

require addition or removal of sidewall blocks (to permit further motion or to maintain working section closure), this may be accomplished at either end of the apparatus on rails of the type shown in Figure 12.

3. Oil System

The upper and lower walls of the working section, as previously noted, are in contact with separate systems of rapidly circulating, thermally conditioned oil. The physical relation of the oil and air systems may be observed in Figures 6 and 15, the former presenting both systems in their entirety.

The portions of the oil systems external to the oil baths are shown in Figures 19 and 20. Oil flows from left to right through the 6 inch pipe lines visible in these figures, passing successively through a cooler, a heater, and a pump section.

The cooler unit employs freon refrigerant from the laboratory compressor and is designed as a combination external and internal unit. The circumstance responsible for this design was the excessive oil-side pressure drop associated with an all internal unit. The external cooler element is shown as the spiral (four 3/8 inch copper tubes, 25 feet long, in parallel) soldered on the exterior of the 6 inch oil lines. The internal cooler element (two 3/8 inch copper tubes, 25 feet long, in parallel) enters the 6 inch pipe through special fittings (Figures 19 and 20.) Inside the pipe, this element is a double helix, $4\frac{1}{2}$ inches in outside diameter.

The refrigerating capacity available is approximately 24,000 B.t.u. per hour per system. The most satisfactory design for this capacity, based upon a compromise between refrigerant pressure drop and oil system pressure drop, was found to be one in which the internal element removes approximately 10,000 B.t.u. per hour and the external element 14,000 B.t.u. per hour. The research program described in this thesis did not require the entire design capacity of the cooler unit, for this capacity is based upon conditions described in Reference 15. The capacity required for this program was determined by the thermal input of the pumps (less losses to the atmosphere from the oil baths) and amounted approximately to 3,800 B.t.u. per hour per system.

The heater unit was also designed as a combination external and internal element. In this instance, space considerations and the desire to avoid excessive pressure losses and charring in the oil system were responsible for the design. The heating capacity available is approximately 20,000 B.t.u. per hour per system or 6,000 watts per system. The external heater unit consists of two 2,000 watt heaters (mounted in the cooler section spiral), one 1,000 watt heater and two 500 watt heaters (mounted in the muff shown in the upper right of Figure 19). The heaters are fabricated by wrapping suitable lengths of chromel wire strip about the oil line and insulating with properly disposed layers of alundum cement and 85 per cent magnesia. One 500 watt heater is Variac controlled in order to permit manual adjustment, and all heaters

are capable of independent operation which therefore permits continuous variation of power output in the range 0-6000 watts.

The internal heater unit consists of a 250 watt chromel wire heater wound upon a support element which fits inside the 6 inch return line. This heater is automatic in operation and is actuated by a copper resistance element mounted in the oil bath inlet line (Figure 21). The control and power output circuits associated with the heater and control element will be described in succeeding sections.

The relative arrangement of the cooler and heater sections was dictated by the fact that the cooler section is not susceptible to automatic control. With the arrangement employed, the cooler can be set at a capacity sufficient to cool the oil stream slightly below the desired operating temperature. The automatic control circuits compensate for this temperature error by selecting an energy input which brings the oil stream to the correct temperature.

As the oil leaves the heater-cooler section it is drawn into the low-head, high capacity axial flow pumps illustrated in Figure 20. These pumps are rated at 400 gallons per minute at 5 feet head of S.A.E. 10 oil (or equivalent) when driven at 1140 revolutions per minute by the 1½-horsepower motors shown in Figure 14. The action of the impeller mixes the oil thoroughly, eliminating temperature irregularities, and forces it past the

temperature control element and through the oil bath where it conditions the working section of the wind tunnel. Return of the oil to the cooler and heater sections completes the circuit.

4. Instrumentation

a. Temperature measuring instruments

Platinum resistance thermometers of conventional design are employed in measurement of both air and oil system temperatures. The air thermometer is located at the inlet to the convergent section (Figure 6) while the oil thermometers are located in the riser sections of the oil baths as indicated in Figures 6 and 21. The resistance values of these instruments are read with Mueller bridges capable of measuring resistance to $\pm$ 0.0001 ohm. This resistance uncertainty corresponds approximately to a temperature uncertainty of $\pm$ 0.003°F. for the thermometers employed. The lack of temperature calibration curves for the coils of the Mueller bridges reduces the precision of measurement to a significant but unknown extent. Limitations imposed by time precluded any attempt to calibrate the bridges against standard resistances.

Point temperature is measured in the working section of the tunnel in terms of resistance value of

the platinum wire element of the thermanemometer* shown in Figure 22. Four cotton covered No. 36 copper leads carried out to the tips of the steel needles (Figure 22) permit cancellation of lead resistance as in a standard four wire resistance thermometer. Resistance, as in the case of the air and oil bath thermometers, is read on a Mueller bridge with ± 0.0001 ohm accuracy. The wire element has a resistance approximately one-tenth that of the standard thermometers. Temperatures are thus measurable to one less significant figure or ± 0.03°F.

Butt-soldered copper constantan (1938 calibration, Leeds and Northrup) thermocouples are employed to measure the surface temperature of the copper plates forming the upper and lower walls of the working section. These thermocouples are mounted in the manner indicated by Figure 23 at the positions along the plate shown in Figure 6. Fourteen additional thermocouples, disposed as indicated in Figure 31 are employed to determine the surface temperature distribution of the heated cylinder. The heated cylinder is described in detail under that title.

---

* Thermanemometer is a name coined to describe the dual use of this instrument as a thermometer and as an anemometer.

Differential electromotive force values existing between the couple involved and a reference couple at 32.00°F (ice point), are measured on a White potentiometer capable of being read to ± 0.2 microvolt. This uncertainty is equivalent to a temperature uncertainty of approximately ± 0.01°F.

b. Pressure measuring instruments

Pressures (with the atmosphere as a reference) are measured in terms of the height differentials produced in a gang-block of single leg manometers (Figure 4) or in a micromanometer (Figure 24). The manometer fluid employed is water-white kerosene the density of which has been carefully measured as a function of temperature. Fluid column heights in the single leg manometers are measurable to ± 0.01 centimeter by means of the cathetometer shown in Figure 4 and in the micromanometer to ± 0.0005 centimeter (or ± 0.0002 inch) by means of the direct reading dial gage. Although there is significant difference in the accuracy obtainable with the two instruments, the micromanometer is ordinarily employed only for pitot impact tube readings because of the time required to change the necessary connections.

Total pressure (dynamic plus static) is measured as a function of position in the working section by means of the traversing pitot impact tube shown in Figure 22. The tube element is stainless steel hypodermic needle stock 0.030 inch outside diameter and 0.020 inch inside diameter. The tube end exposed to the air flow is rounded to approximate the hemispherical form recommended in References 3 and 4. The tube (and the associated hot wire anemometer) is positioned in the channel by means of a traversing unit described under that title.

A second pitot impact tube with 0.026 inch outside diameter and 0.015 inch inside diameter hypodermic tubing element is employed to measure total pressure on the lateral mid-line near the downstream end of the working section. This instrument is permanently mounted on the upper copper plate (Figure 19) and can traverse the working section in a vertical direction only. The tube and tube support are shown extending into the working section in Figure 25. Vertical positioning of the tube is accomplished by means of a micrometer spindle mounted on top of the tube guide shown in Figure 26.

Static pressures are measured as a function of longitudinal position in the working section by the

piezometer bars disposed as shown in Figures 6 and 28. The construction of the piezometer bar and the air connections to the working section are shown in Figure 27. Care was taken to insure that no burrs or projections were left at the opening of the 1/64 inch diameter holes which lead through the copper plate to the piezometer bar.

c. Velocity measuring instruments

A hot-wire anemometer of the form illustrated in Figures 22 and 54 is employed to measure point velocity in the working section. The electrical circuits employed in conjunction with the anemometer are presented in Figure 29. These circuits are adaptable to both the conventional constant current and constant resistance methods of hot wire anemometry. The constant resistance method has the highest average sensitivity over a given range of velocity if the maximum resistance (i.e. temperature) of the wire which is permitted coincides with the constant resistance employed. If no limit is placed on the maximum permissible resistance, the constant current method may be more sensitive. The constant resistance method was chosen for this work because of the desire to avoid overheating the platinum wire which is used to measure temperature as well as velocity. If overheated, this wire might change its resistance characteristics by annealing and provide unreliable temperature data.

In the constant resistance method of operation switches S, S' and S''' are closed (S''' in down position) and the circuit functions essentially as a Mueller bridge in which the anemometer is included with the 0.05 and 0.5 ohm standard (manganin) resistors as one leg. Adjustment of resistances in decade box D, plug box P, and variohm R determines the hot wire resistance (and hence temperature) which is to be employed. Once this resistance is selected, operation of the circuit as a velocity measuring instrument is accomplished by adjusting the resistance values in plug boxes P' and P'' , decade box D', and variohm R' until a balance on galvanometer G is obtained*. Current through the hot wire element for the balance condition is determined by the voltage drop across the 0.05 or 0.5 ohm standard (manganin) resistors whose resistances have been accurately determined by comparison with primary standard resistors furnished by the laboratory.

d. Traversing unit

The traversing unit is illustrated in Figure 18. It provides vertical, lateral, and tilting motion for the thermanemometer and pitot impact tube employed to

---

* Resistances in the bridge circuit, other than that of the hot wire element, are essentially unaffected by variation of bridge current. The hot wire element, however, assumes a resistance (i.e. temperature) determined by a balance of energy input and dissipation to the air. This dissipation is a function of mass velocity and temperature difference between the wire and air. See page 27.

measure point velocity and temperature in the working section. The instruments are mounted on the taut wires held by yoke extension E and a similar extension on the opposite side of the apparatus. The wires, as shown in Figures 18 and 22, enter through slots in the steel backing plates and micarta elements of the specialized sidewall blocks.

The vertical dimensions of the thermanemometer and pitot impact tube bodies limit the closeness of approach of these bodies to either wall of the working section. The tips of the thermanemometer needles and pitot impact tube may be brought as close to the upper or lower wall as desired if the tilt mechanism is employed in conjunction with the vertical drive mechanism.

Counters are associated with each of the three drive mechanisms producing the motions described. The vertical counter reads in 0.0001 inch intervals, the horizontal counter in 0.001 inch intervals and the tilt counter in arbitrary units which may be converted to degrees tilt of the support wire assembly. These counters provide indication of vertical and lateral position of the instruments as long as the support wires move freely in the slots provided. The clearance of the slots was made small to avoid undue

loss of air. Any vertical holdup resulting from friction between the wires and the slot walls may be detected by use of the optical system shown in Figure 18. The telescope, mounted on the same yoke extension as the wire support, may be focussed on the tip of the thermanemometer or pitot impact tube. Before vertical traversing begins, the horizontal cross-hair in the telescope eye-piece is made to "coincide" with an identifiable portion of the instrument. If vertical holdup occurs during the traverse operation, the support wires (and hence thermanemometer and pitot impact tube) move relative to the telescope, and the image is displaced from the cross hair. The holdup may be corrected by lightly tapping the wires to free them.

Longitudinal motion of the thermanemometer and pitot tube in the working section is provided by sliding the traversing unit along the rails shown in Figures 16 and 17. Motive power is provided by the crank assemblies shown in Figures 7 and 9. Longitudinal position of the instruments relative to the centerline of the heated shape is determined, at present, by a steel rule graduated in 0.01 inch intervals.

The pitot impact tube and hot wire element of the thermanemometer are visible through the windows provided in the specialized sidewall blocks associated with the traversing unit (Figures 18 and 23). These windows permit observation of the instruments during operation and also make possible very accurate determination of the distance between the horizontal centerline of either instrument and the upper or lower wall of the working section. The measurement of the distance is carried out with the optical system shown in Figure 18 and, schematically, in Figure 30. The telescope, set at a small (arbitrary) tilt angle, is focussed on the instrument and moved vertically by adjustment of screw S* until an identifiable portion of the (direct) image coincides with the horizontal hair line. Dial gage G is read directly in 0.001 inch intervals and interpolated to the nearest 0.0001 inch. The telescope is then moved vertically until the hair line coincides with the same portion of the (reflected) image visible in the highly polished surface of plate P or P'. Dial gage G is read a second time. The distance between the wall and instrument is then half of the measured vertical separation of the direct and reflected images.

---

* Nomenclature of parts listed in this paragraph is taken from Figure 18.

e. Heated shape

The heated shape employed in this investigation is a 3/16 inch diameter cylinder 12.125 inches long placed normal to the air flow and located at the approximate horizontal centerline of the working section and midway between the entrance and exit to the working section. Investigations reported elsewhere (Reference 15) indicate that stable, two-dimensional flow has been established by the time the air reaches this section, i.e. all entrance effects have died out. A perspective drawing (Figure 32) shows the heated cylinder in place in the working section and indicates the manner of support by two 1/8 inch by 3/4 inch micarta strips. These strips parallel the inner surface of the sidewall blocks and extend upstream to the exit of the convergent section. Grooves milled in the external faces of the strips and in the collars (Figure 32) provide passage for the leads from fourteen thermocouples and a 12 ohm internal heater mounted in the cylinder. The leads are brought out of the working section in this manner to prevent interference with motion of the sidewall blocks and to minimize disturbance of channel flow. Flexible rubber

tubing is used to conduct the leads from the micarta grooves to holes drilled in the low velocity (upstream) portion of the convergent section.

The thermocouples are disposed about the heated shape in the manner indicated in Figure 31 and are intended to permit determination of surface temperature as a function of position on the cylindrical shape. In order to mount the thermocouples in a satisfactory manner, it was found necessary to split the tube in a longitudinal direction. Seven thermocouples and half of the heater element were mounted in each half cylinder. Excess space in the half cylinders was filled with plaster of Paris to prevent dead air zones and to insure thereby uniform transfer of heat to the cylinder surface from the heater element. The half cylinders were then clamped together, soldered along the longitudinal seams and provided with mounting collars to fit holes drilled in the micarta support strips. The junction of each thermocouple was brought flush with the external surface of the cylinder through 0.030 inch diameter holes and cemented in position.

Energy input to the heated shape is measured by the circuit shown in Figure 33. The voltage across the 0.005 ohm, standard (manganin) resistor is used

to calculate current through the heater windings. Voltage drop across the 75 ohm resistor of the voltage divider provides a means of determining voltage across the heater. The voltages in both instances were measured by a K-2 potentiometer.

f. Temperature control circuits

A typical bridge circuit employed to control temperature in the air and oil systems is shown in Figure 34. This circuit provides actuation current for galvanometer G in response to resistance (i.e. temperature) changes experienced by control element R. The magnitude and direction of the actuation current is determined by the magnitude and direction of the unbalance produced in the bridge circuit by variation of control element R and by the sensitivity selected with switch S. In operation the maximum sensitivity provided could be employed without producing hunting or other instability phenomena. The control element is a 20 ohm copper resistance coil mounted on a bakelite form. The coil is provided with four leads (two current leads, two potential leads) and placed in a 3/8 inch outside diameter thin-walled brass tube. This is mounted in the oil bath riser through a fitting which provides closure by compression of a neoprene seal ring.

The deflection produced in the galvanometer by the actuation current is employed to vary the light intensity which is incident upon the photo-cell T (12) of Figure 35. A conventional collimated light shining upon the galvanometer mirror serves as the original light source.

The balance point of the circuit and hence the actuation response which results for a given resistance value of R is determined by the settings made on plug box P, decade box D and variohm R' (Figure 34). These settings are made on the basis of the control temperature desired. In operation, the temperature of the air or oil system concerned is adjusted to the approximate control temperature desired. The control bridge circuit is then balanced at this temperature and the system allowed to operate on automatic control. If, when the system has achieved stable control, the temperature is found to be higher or lower than desired, resistance values of P, D or R' are modified to change the balance point of the bridge and hence the control temperature.

g. Energy supply circuits

A typical circuit* employed to provide electrical energy to the air and oil systems in response to operation of the temperature control circuit is shown in Figures 35 and 36. The light intensity incident upon photo-cell T (12) of this circuit determines the potential on the grids of tube T (6). The plate currents of T (6), passing through R (16) and R (17), establish through associated circuits the phase relationship of the a.c. voltage on the grids to the a.c. voltage on the anodes of the thyratron tubes T (10) and T (11). Thyratron T (11) passes an average current which is a function of the instantaneous light intensity incident upon the photo-cell. Thyratron T (10) passes current which is dependent upon the average intensity of light

* Designed by H. H. Reamer of the Department of Chemical Engineering

incident upon the photo-cell over a preceding time interval. This time interval is determined by condenser C (13), resistor R (23) and the setting of potentiometer R (4), and, in operation, averaged about 20 minutes. Deviations of the light intensity on the photo-cell from a reference intensity, determined by the setting of potentiometer R (4), slowly change the power input from tube T (10) to the oil bath. The rate of change of power input is approximately 10 watts per minute and is determined by the values of R (23) and C (3). When the light intensity is greater than the reference, power input from tube T (10) increases until the response of the oil bath temperature acting through the bridge control circuit has brought the light intensity back to the reference value. When the reference intensity has been reestablished, power input from tube T (10) to the oil bath remains constant. Similarly, a light intensity less than the reference value causes the power input from tube T (10) to the oil bath to decrease until the response of the oil bath temperature has restored the light intensity to the reference value. Because of the amplification in tubes T (5), T (7) and associated circuits, this "droop" correcting circuit can maintain an average light intensity within limits corresponding to $\pm$ 0.003°F temperature change in the oil bath independent of ambient temperature.

C. Calibration of Instruments

1. Platinum Resistance Thermometers

The platinum resistance thermometers employed in this investigation were calibrated by comparison at three temperatures with a

Leeds and Northrup platinum resistance thermometer employed as the laboratory standard. The standard thermometer and one of the thermometers to be calibrated were placed in an agitated bath maintained at the desired temperature. The temperatures used in this comparison were 32.000°F (ice point), 100°F (nominal) and 160°F (nominal). These temperatures cover the interval for which calibration was required. With the exception of the ice point, these temperatures were nominal values since comparative resistances for the standard and experimental thermometers are sufficient to establish calibration curves of the latter. The resistance values of these thermometers were read alternately on the same Mueller bridge and plotted as functions of time to obtain corresponding resistance values. The resistance values of the standard thermometer were converted to temperatures on the basis of the calibration data provided.

Calibration curves for the experimental resistance thermometers were prepared by residual methods from the resistance values corresponding to the bath temperature indicated by the standard thermometer. The average temperature coefficient of resistance was determined for each thermometer in the interval between 32.000°F and 160.00°F. Residual values, obtained as the difference between measured values and values computed from the temperature and average temperature coefficient of resistance, were plotted as functions of temperature for the three thermometers. As this provided only three points for each thermometer, the probable form of the curve between these points

was estimated from a similar residual plot for the more carefully calibrated standard thermometer. A small scale reproduction of the residual plot is presented in Figure 37. The calibration obtained for a typical thermometer is summarized in Table II for 10°F temperature intervals.

2. Thermocouples

a. Heated shape thermocouples

The thermocouples mounted in the heated shape were calibrated by measuring, as a function of heated shape temperature, the electromotive force differentials which exist between heated shape couples and reference couples maintained at 32.000°F (ice point). The calibrations were made at 100.00°F, 120.00°F and 140.00°F. Temperatures in excess of 140°F were not employed because of possible damage to calorimeters mounted on the upper (copper plate) wall of the working section. These calorimeters are described elsewhere (Reference 15). This calibration was conducted with the heated shape installed in the working section in the manner previously described. The oil systems were operated at the desired calibration temperature while air was maintained in a stagnant condition in the working section. Stagnant air was employed to avoid adiabatic compression effects which occur before obstacles in a moving air stream. This phenomena is discussed in more detail in the section describing calibration of the thermanemometer as a hot-wire anemometer. Transfer of thermal energy from the oil baths to the air in the working section gradually brought this air (and the

heated shape) to the calibration temperature. When thermal equilibrium was established throughout the working section, the electromotive force differentials existing between the heated shape couples and the reference couples were measured. Such equilibrium was assumed to exist when the thermocouple in the heated shape gave readings which were constant over a five-minute interval.

The calibration data for the thermocouples were plotted as electromotive force residuals obtained by comparison of measured potentials and potentials listed in (1938 Leeds and Northrup) calibration tables. Calibration data, plotted in terms of these residuals, are shown in Figure 38 for typical thermocouples.

In operation of the heated shape, it was occasionally necessary to employ temperatures greater than the upper limit of the calibration range. In these instances, the residual electromotive force plots were extrapolated to the required temperatures or the (1938 Leeds and Northrup) calibration tables were employed without correction. The residual correction is small, representing less than 0.2°F over the calibration range. This was negligible with respect to the heated shape-air stream temperature differences involved when the correction was omitted.

b. Copper plate thermocouples

The copper plate thermocouples were calibrated in an analogous manner. The oil systems were operated at the desired calibration temperatures, and, when thermal equilibrium was established between the plates and the oil systems, electromotive force differentials between the

plate thermocouples and reference couples at 32.00°F (ice point) were measured.

The calibration data were plotted as residuals in the same manner as employed for the heated shape thermocouples. In this instance, the calibration range (100° F to 140°F) was not exceeded in operation of the apparatus and the calibration data did not require extrapolation.

3. Thermanemometer

The thermanemometer was employed to measure both point velocity and point temperature. The point velocity measured by this instrument is a function of the temperature difference existing between the hot wire element and the air to which it is exposed. This functional relationship may be expressed (References 3, 4 and 12) in the following manner:

$$i^2 R = (A + B\sqrt{V_p})(\theta - \theta_a)$$

The symbols employed are explained in the Nomenclature. The point temperature measured by this instrument does not correspond to the free stream temperature but rather to some value between the free stream and the stagnation temperature (References 9-11). This requires calibration for temperature in terms of velocity in that the "adiabatic recovery factor" must be determined as a function of point velocity for the particular physical situation. Inasmuch as temperature measured by this instrument is a function of velocity (and vice versa),

the calibration procedures for velocity and temperature were conducted concurrently. This dual calibration is somewhat involved, however, and will be described as two distinct operations.

a. Temperature calibration

Temperature calibration of the thermanemometer as a resistance thermometer was accomplished by measuring the resistance of the platinum wire element (Figures 22 and 54) as a function of temperature and velocity in the air stream to which it was exposed. This was achieved in a series of two-step measurements:

(i) The oil systems were brought exactly and the air system approximately to a desired calibration temperature. The temperatures employed for this purpose were 100.00°F, 110.00°F, 120.00°F and 140.00°F. Mean air velocity (bulk volumetric flow per unit area) through the working section was measured in terms of Venturi meter differential. If this flow rate was satisfactory, the point velocity on the horizontal centerline of the working section was measured by the fixed pitot impact tube* and used, in conjunction with the mean velocity, to determine the control temperature for the air which

---

* A pitot impact tube measures total pressure head (static plus dynamic). Static pressures required to correct the pitot impact readings to dynamic pressures were obtained from piezometer bar readings corrected to the proper longitudinal position in the working section.

would compensate for the adiabatic decrease in free stream temperature between the control thermometer position and the working section. Appendix A contains a description of the method employed in computing this adiabatic temperature change. The correction (i.e. temperature change) obtained was added to the desired calibration temperature to obtain the control temperature which was employed.

(ii) The pitot impact tube was withdrawn to a position near the upper wall and the thermanemometer platinum element moved to the exact position previously occupied by the tip of the tube. The temperature of the air was adjusted to the control temperature determined in step (i) and the system allowed to approach equilibrium. Switch S''' of Figure 29 was thrown to the Mueller bridge and resistance of the platinum wire element was measured in conventional manner as a function of time. Thermal equilibrium was assumed to exist when no change in resistance was observed over a five-minute interval, and the final resistance was recorded as the calibration value.

The two typical steps outlined above were conducted for air velocities of approximately 0, 30, 60 and 90 feet per second at

each of the four calibration temperatures. The zero velocity measurement required no adjustment of air control temperature, the stagnant air simply being allowed to attain the temperature of the oil systems.

The resistances obtained in step (ii) were plotted against point velocities* obtained in step (i) for each calibration temperature. It was observed that the resistance differential produced by a given change of velocity was independent of air temperature. This differential, converted to the corresponding temperature differential, was plotted as a function of point velocity (Figure 39). It was further observed that the temperature coefficient of resistance (at a given point velocity) was independent of both temperature and velocity, and essentially equal to that of pure platinum. A plot of wire element resistance (at zero velocity) was prepared on the basis of the observed temperature coefficient of resistance (Figure 40).

Resistance measurements made in experimental work were converted to free stream temperatures by use of Figures 39 and 40. The measured resistance was first converted to apparent temperature by means of the zero velocity resistance plot (Figure 40). This apparent temperature was then corrected to the free stream temperature by subtracting the adiabatic recovery differential which was obtained as a function of point velocity from Figure 39.

---

* This procedure tacitly assumes that point (rather than mean) velocities govern temperature recovery in adiabatic compression before the wire. This is in distinction to the assumption employed in step (ii) that mean velocities govern temperature drop in adiabatic expansion through the convergent section.

b. Velocity calibration

Velocity calibration of the thermanemometer was also conducted as a series of two step measurements.

(i) The air and oil systems were brought to the desired calibration conditions and allowed to attain stable temperature distribution. Stable thermal gradients were present in many of the calibration measurements. These do not interfere with the velocity calibration inasmuch as the point temperature involved was measured. The point velocity was then measured at a particular position in the air stream through use of either the traversing or fixed pitot impact tube. The static pressure for correction of total to dynamic head was obtained in the manner previously described.

(ii) The pitot impact tube was moved away from the point of measurement and the wire element of the thermanometer positioned at the point previously occupied by the tip of the tube. The temperature of the air stream was measured in terms of resistance of the wire element by the method described previously. When this was completed, switch S''' (Figure 29) was thrown to the anemometer circuit and a balance obtained on galvanometer G by variation of the resistance

values of P', P'', D'and R' (Figure 32). The resistance (and hence temperature) of the hot wire was selected through trial. A resistance corresponding approximately to 150°F was found to be satisfactory, both in terms of velocity sensitivity and stability of wire resistance for temperature measurement. The current through the hot wire for this balance was determined by the voltage drop across the 0.05 ohm resistor in series with the wire.

Steps (i) and (ii) were repeated until a sufficient spread in data was obtained to provide a reliable calibration curve. This curve was obtained by plotting $\frac{I^2}{(R-R_a)^{0.8}}$* as a function of $\sqrt{V}$. Data for a typical calibration are presented in Figure 41. The mass velocity $V\rho$ rather than V actually should be employed. The changes in density encountered in this experimental investigation were too small to modify the calibration curve. Omission of ρ greatly simplifies the application of the curve.

It was observed that the calibration characteristics of the hot wire changed from day to day. It was thought that part of this difficulty, at least, resulted from accumulation of very fine lint or dust on the wire, for the heat transfer coefficient

---

* The factor 0.8 differs from the theoretically derived factor 1.0 (References 9-12). The data for another experimental program (Reference 15) were found, empirically, to require the 0.8 factor for satisfactory correlation. Calibration data for the experimental program reported in this thesis, which do not cover as wide a range of velocity or temperature as that of Corcoran, correlate equally well with the factors 0.8 and 1.0. The factor 0.8 was employed because of the weight of experimental evidence in its favor.

appeared to decrease consistently with time (i.e. smaller current was required to bring the wire to the selected resistance when exposed to air streams of the same velocity and temperature). An impingement-type coated filter was employed in the air system as designed. It was felt that insertion of additional filters would succeed only in impeding flow to an undesirable extent.

4. Standard Resistances

The (secondary) standard resistances employed to measure current and to serve as voltage dividers in the thermanemometer and heated shape circuits were calibrated by direct comparison with primary standard resistors provided by the laboratory.

The resistors to be calibrated were placed in series with a primary standard resistor of approximately the same resistance value. Current was passed through both resistors and the relative voltage drop across the resistors determined*. These data, and absolute resistance values of the standard, sufficed to determine the resistance of the secondary standard resistors.

IV. Experimental procedure

The experimental investigation described in this thesis may be divided into two distinct parts: These are:

(i) Measurement of the transfer of thermal energy from a heated cylinder to a turbulent gas stream.

(ii) The diffusion of thermal energy in the wake of the heated cylinder.

---

* A K-2 or White potentiometer was employed for the comparison, the choice depending upon the magnitude of the voltage drops involved.

In each part of this investigation the air and oil systems were operated at 100.00°F, the control temperature of the air being adjusted, as a function of mean velocity in the working section, to produce air at 100.00°F in the working section. Electrical energy was added to the cylinder in such amount that the surface temperature assumed a value which was deemed satisfactory for the test to be conducted. This temperature was measured by thermocouples imbedded in the cylinder surface as previously described.

In part (i), the electrical energy input required to maintain the surface of the cylinder at a given temperature was measured as a function of this surface temperature and the mass velocity past the cylinder. This mass velocity was measured in terms of Venturi meter differential pressures. These were supplemented by measurements of air pressure and temperature at the entrance to the Venturi meter and temperature (hence density) of the manometric fluid. Measurements were made at six surface temperatures for each of two mass velocity rates. The data obtained are summarized in Table III and Figure 42.

In part (ii), the surface temperature of the heated cylinder was maintained at a constant value while (point) velocity, temperature and total head traverses were made between the upper and lower walls of the working section. These traverses were made on the lateral midline of the working section at various distances downstream from

the centerline of the heated cylinder. The distances of the traverses downstream from the centerline of the heated cylinder varied between 0.21 inch and 62.5 inches. The preponderance of data was taken at distances less than 1 inch from the cylinder since the most marked velocity and temperature gradients were encountered in this region. Five velocity and seven temperature traverses were made for each of two mass velocity rates. The data obtained are summarized in Tables V and VI and Figures 43-48.

V. Experimental Results

Table IV summarizes the experimental conditions employed in this investigation while Tables III, V and VI present the unsmoothed experimental data. Such unsmoothed data are presented rather than smoothed data to avoid bias in interpretation which might vitiate usefulness of the data.

The data obtained in part (i) of the experimental investigation were analyzed in terms of the conventional dimensionless quantities $\frac{hD_o}{k_f}$ (Nusselt number) and $\frac{D_o \bar{V} \rho}{\mu_f}$ (Reynolds number). It was found that an empirical relation of the form

$$\frac{hD_o}{k_f} = 0.615 \left(\frac{D_o \bar{V} \rho}{\mu_f} \right)^{0.471}$$

correlates the data within a probable error (50 per cent zone) less than 1 per cent and a maximum error of 3 per cent. It was also found that the influence of the temperature difference between the cylinder

and the air stream may be represented by an expression of the form

$$\frac{h D_o}{k_f} = 0.545 \left[\frac{D_o \bar{V} \rho}{\mu_f} \left(\frac{\Theta_{surface}}{\Theta_{air}} \right)^{\frac{1}{4}} \right]^{0.485}$$

with a probable error less than 1 per cent and a maximum error of 2 per cent.

The data correlate very satisfactorily with the data presented in McAdams (Reference 13) and Goldstein (Reference 4) for gases flowing normal to a single heated cylinder. The experimental data are presented in Figure 47 in comparison with data from these sources.

The data obtained in part (ii) of the experimental investigation were cross-plotted from Figures 43-46 to obtain lines of constant velocity and temperature as functions of distance downstream from the heated cylinder. The data obtained from these cross plots are shown in Figures 48-53.

The velocities employed in the two runs for part (ii) were sufficiently similar (see Table IV) to permit comparison of details. It may be observed that:

(a) Velocity and temperature wakes extended somewhat further downstream for the run at higher mass velocity (Test 2).

(b) Turbulent mixing in the wake of the cylinder was somewhat greater for the run at higher mass velocity. This is evidenced by the more uniform distribution of isotherms through the wake.

(c) The bouyant rise of heated air in the wake of the cylinder is evident in both runs but is more pronounced in the case of the run at lower mass velocity (Figures 50-53).

The high temperature protuberances which extend downstream from the heated cylinder are characteristic phenomena associated with natural or forced convection past such an object. These characteristics result from the separation of flow from the cylinder wall. Hot air, which was in the laminar or near-laminar layers, is carried away from the cylinder and, following the lines of flow, skirts the double vortex zone downstream of the cylinder. This double vortex (see Plate 7, Reference 4) produces back flow in the region where the flow lines rejoin behind the cylinder. This back flow prevents the protuberances from joining to enclose a high temperature zone and helps to disperse energy in the protuberance tips by carrying the hot air into the vortex zone. Photographic evidence for the existence of such protuberances behind heated cylinders is presented in both Reference 4 and Reference 13.

The increase in air velocity which occurs in the working section at the cylinder position because of the decrease in free area produces adiabatic cooling of the air. This is evident in Figures 45 and 46, and in the data of Table VI. The amount of cooling is small and does not modify the temperature structure produced by the heated cylinder to a significant extent.

The performance of the apparatus was quite satisfactory. The thermanemometer, under adverse conditions of high turbulence, gave

consistent values for both temperature and velocity. The reading reproduced much of the detail of the turbulence passing the wire, but reasonable mean values with respect to time were obtained.

It is felt that temperatures measured by the thermanemometer are accurate to $\pm$ 0.05°F even under conditions in the highly turbulent wake. The reproducibility of data is shown by the traverse at 0.82 inch downstream of the cylinder centerline in Test 1. The expected behavior did not appear in the traverse made initially so additional points were taken as a check. One of these additional points was taken at the exact position of an earlier point and was found to agree within 0.0001 ohm or approximately 0.03°F.

The velocities measured by the thermanemometer are believed to be accurate to within $\pm$ 0.5 foot per second over the range of velocity encountered. The data were internally consistent and checked quite closely with values obtained through use of the pitot impact tubes. The primary source of error in velocity measurement appeared to be the gradual accumulation of lint and dust on the hot wire element. The most satisfactory solution to this unfortunate characteristic was found to be repeated calibration during the conduct of the investigation.

The data for velocity and temperature distributions in the wake of the cylinder are intended primarily to indicate the qualitative nature of such distributions. The spacing of the traverses downstream of the shape is somewhat too great to fix the exact form of the lines of constant velocity and constant temperature, particularly in the regions

where such curves close. The tips of the closed curves are shown to be quite pointed for both temperature and velocity. This pointed form of curve fits the data more readily than a rounded form, and is, furthermore, similar to the form of lines of constant composition and constant velocity in mass diffusion processes such as the diffusion flame (Reference 16).

Equations are derived in Appendix B for eddy viscosity and eddy conductivity in compressible fluid media which are accelerated or decelerated as they pass through the region of interest. It is apparent from these equations that knowledge of the variation of V_x, V_y and θ with x and y (See Nomenclature of Appendix B) is required. Inasmuch as uncertainties exist in the exact manner of variation of these variables between traverse stations, it is believed that calculation of eddy conductivity and eddy viscosity as functions of position in the wake should be deferred until additional data are obtained.

VI. Conclusions

The data presented in this thesis agree with the empirical correlations which are available in the literature for transfer of energy to air streams from heated cylinders. The apparatus thus provides a satisfactory means of further investigating such correlations based upon dimensionless parameters.

The velocity and temperature distribution data for traverses in the wake of the heated cylinder are consistent with those described in the literature. Additional traverses to fill in the unexplored regions are necessary before the data are employed to determine eddy viscosity and eddy conductivity as functions of position in the wake.

Nomenclature

A	Constant for hot wire anemometer
B	Constant for hot wire anemometer
β	Ratio of upstream area to throat area in Venturi meter
C_p	Isobaric specific heat, B.t.u./lb ^{o}F
D_o	Outside diameter of cylinder, ft
d	Outside diameter of hot wire for anemometer, ft
F	Force, lb
g	Acceleration due to gravity, ft^2/sec
h	Heat transfer coefficient, B.t.u./ft^2 sec ^{o}F
K	Thermometric conductivity, ft^2/sec
k_f	Thermal conductivity at arithmetic mean of wall and fluid temperature, B.t.u. ft/sec ft^2 ^{o}F
P	Static pressure in fluid, lb/ft^2
$\overset{*}{Q}$	Rate of thermal energy transfer per unit area, B.t.u./sec ft^2
R	Resistance, ohms
t	Time, sec
$\overline{V}$	Bulk velocity, ft/sec
V	Point velocity, ft/sec
x	Longitudinal coordinate in working section, ft
y	Vertical coordinate in working section, ft
z	Lateral coordinate in working section, ft
ϵ_m	Eddy viscosity, ft^2/sec
ϵ_c	Eddy conductivity, ft^2/sec
θ	Absolute Temperature, ^{o}R
μ_f	Molecular viscosity at arithmetic mean of wall and fluid temperature, lb sec/ft^2
ν	Kinematic viscosity, ft^2/sec

Nomenclature (continued)

ρ	Density or specific mass, lb sec^2/ft^4
σ	Specific weight, lb/ft^3
τ_{yx}	Stress acting over element of surface perpendicular to the y-axis and in the positive x-direction, lb/ft^2
τ_{zx}	Stress acting over element of surface perpendicular to the z-axis and in the positive x-direction, lb/ft^2

Subscripts

a	Air
x	Value in the positive x-direction
y	Value in the positive y-direction
z	Value in the positive z-direction
o	Value at the wall of the conduit

Mathematical Symbols

D	Total differential of quantity indicated
d	Differential of quantity indicated
δ	Increment of quantity indicated
$\frac{\partial A}{\partial B}$	Partial derivative of A with respect to B under conditions wherein all other independent variables remain constant

References

1. A.S.M.E. Committee on Fluid Meters, Fluid Meters Their Theory and Application, American Society of Mechanical Engineers (1937).

2. Patterson, G. N., Aircraft Engineering (Aug. 1937) 9, 205-208.

3. Ower, E., Measurement of Air Flow, Chapman-Hall (1933).

4. Goldstein, S., Modern Developments in Fluid Dynamics, Oxford University Press (1938).

5. Reynolds, O. S., Proc. Manchester Literary and Philosophical Society, (1874) 14, 7; Collected Papers, I, 81.

6. Taylor, G. I., Great Britain Advisory Committee for Aeronautics, Reports and Memoranda, No. 272 (1916-1917) 2, 423.

7. von Karman, Th., Trans. Amer. Soc. Mech. Engrs., (1939) 61, 705.

8. Prandtl, L., Physicalische Zeitschrift, (1928) 29, 487.

9. Liepmann, H. W., and Puckett, A. E., Introduction to Aerodynamics of a Compressible Fluid, John Wiley & Sons, Inc. (1947).

10. Eckert, E., Temperature Recording in High Speed Gases, Nat. Advis. Comm. for Aero. Tech. Mem. No. 983 (1941).

11. Wimmer, W., Stagnation Temperature Recording, Nat. Advis. Comm. for Aero. Tech. Mem. No. 967 (1941).

12. Willis, J. B., Review of Hot Wire Anemometry, Australian Council for Aeronautics, Report ACA-19 (1945).

13. McAdams, W. N., Heat Transmission, McGraw-Hill (1933).

14. Lacey, W. N., and Sage, B. H., Thermodynamics of One-Component Systems, California Institute of Technology (1940).

15. Corcoran, W. H., Ph.D. Thesis, California Institute of Technology (1948).

16. Jost, W., Explosion and Combustion Processes in Gases, McGraw-Hill Book Co., Inc. (1946).

LIST OF FIGURES

LIST OF FIGURES (CONT.)

LIST OF FIGURES (CONT.)

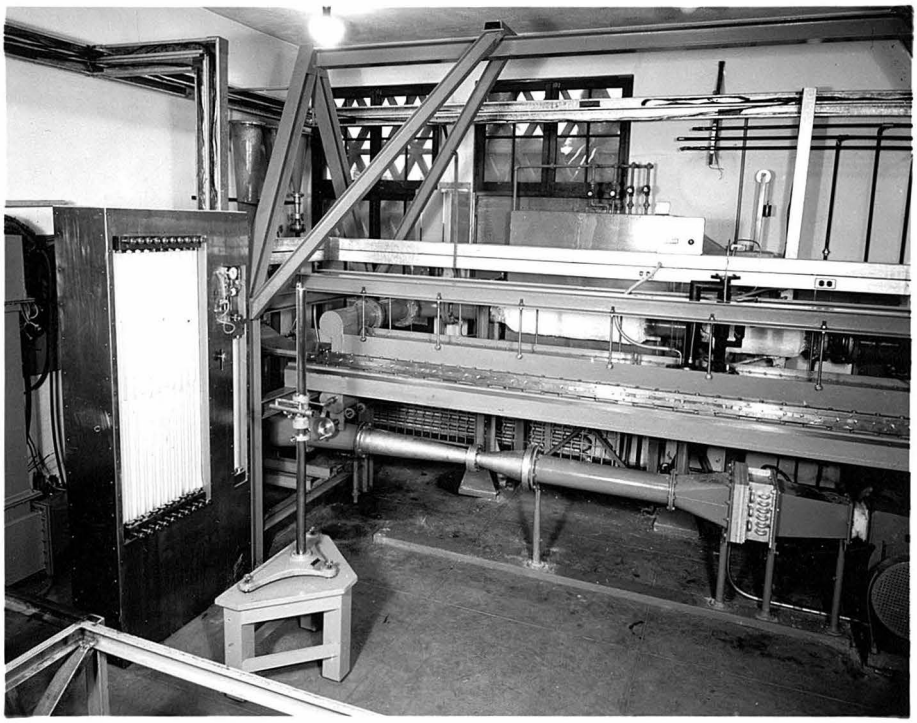

Figure 1

General View, West End of Apparatus

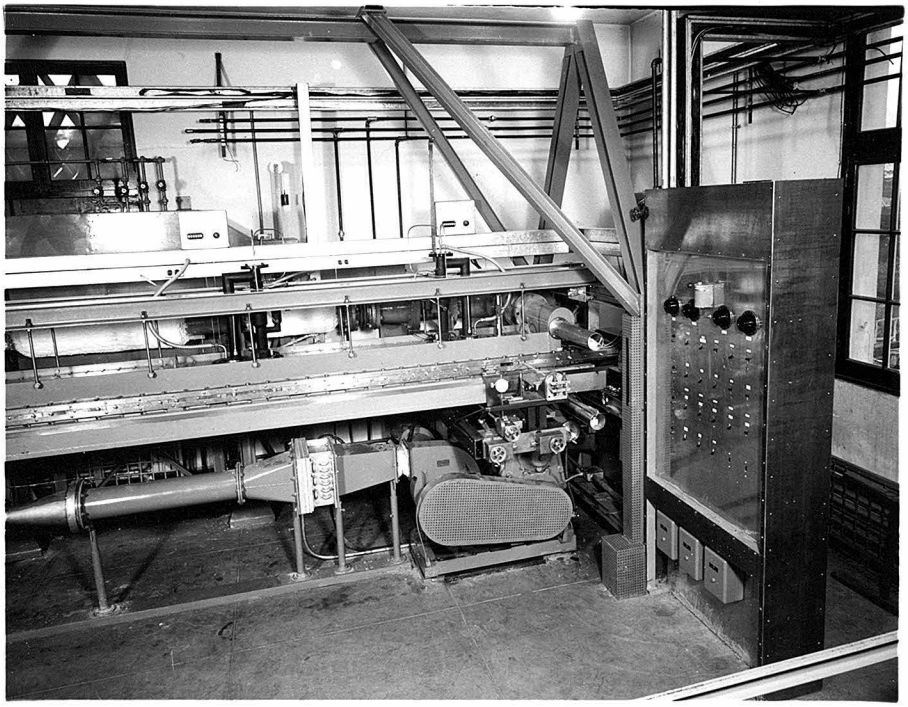

Figure 2

General View, East End of Apparatus

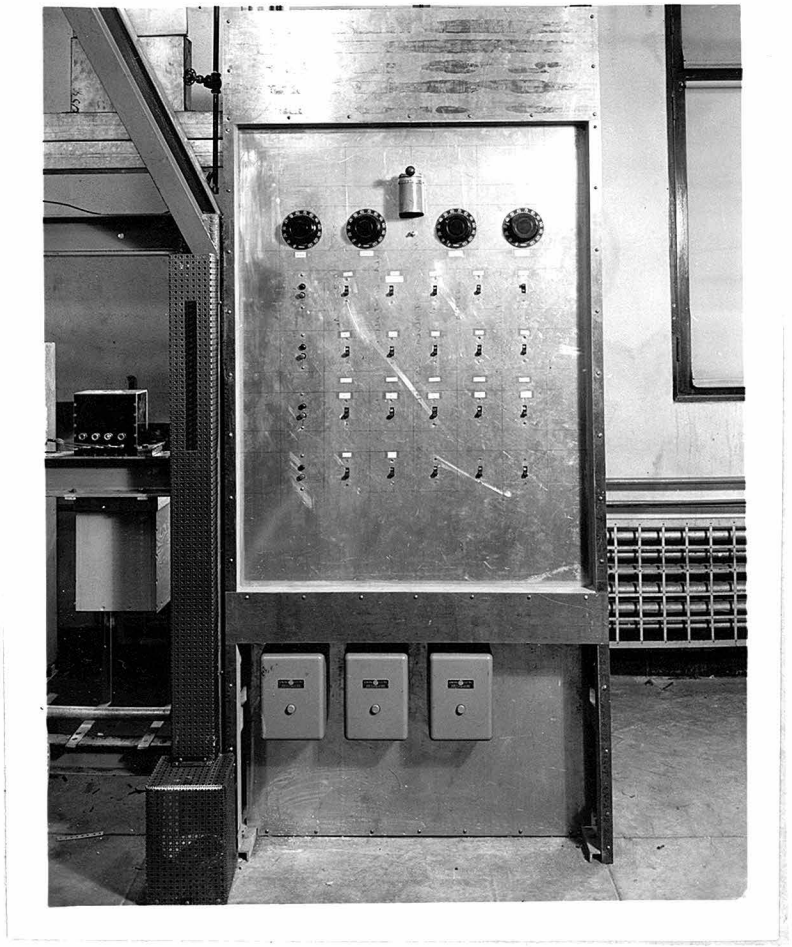

Figure 3

Electrical Power Panel for Motors, Pumps and Heaters

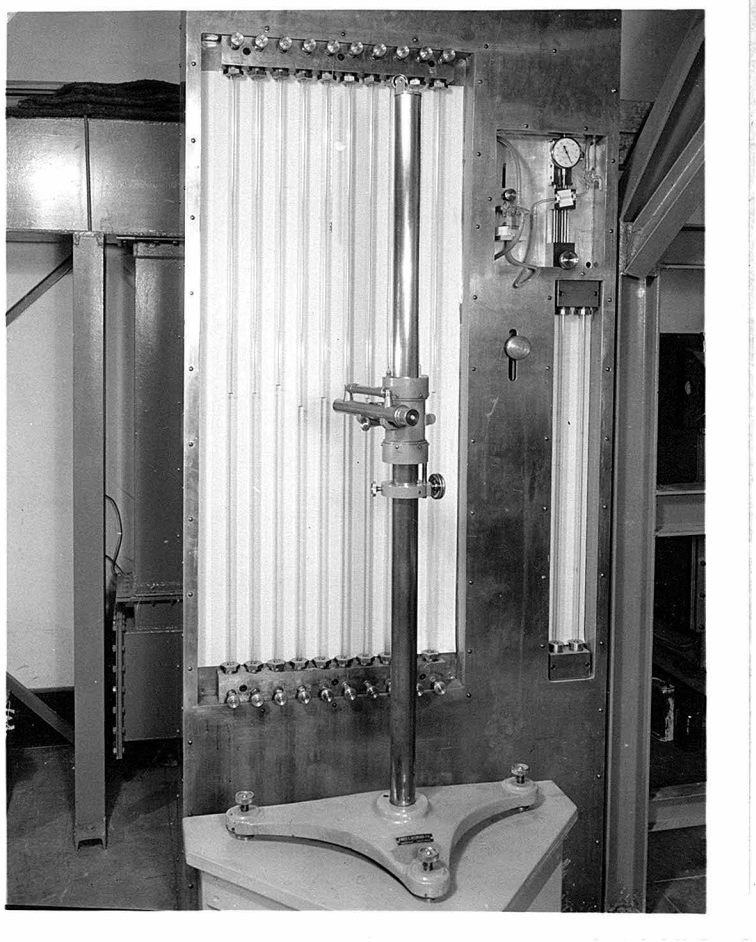

Figure 4

Manometer Panel for Gang Manometer and Micromanometer

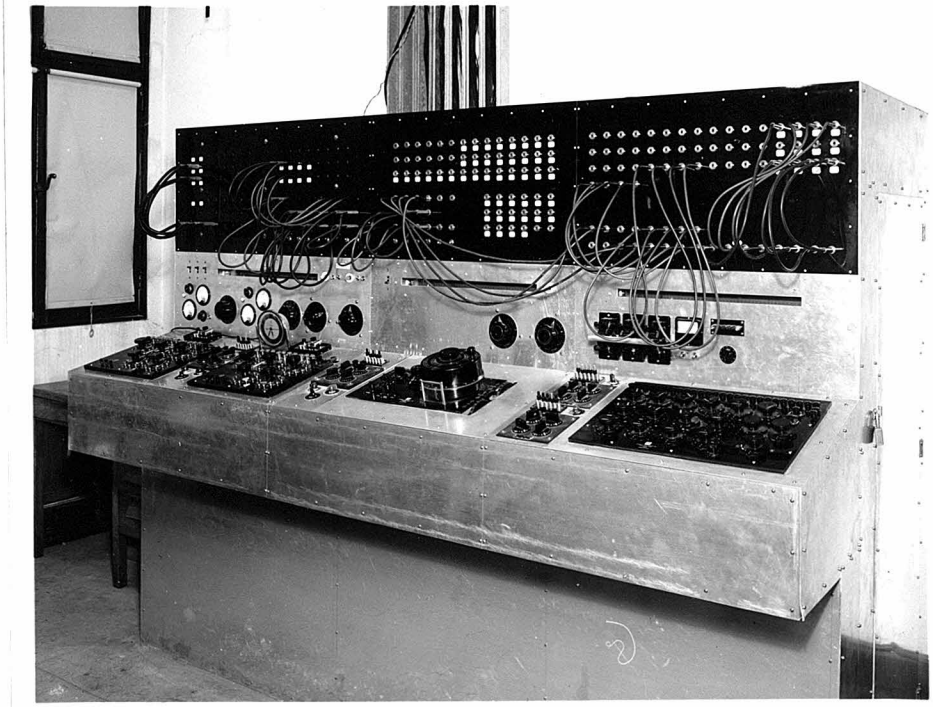

Figure 5

Instrument Bench

Legend for Figure 6

(a) Air Measurement Thermometer

(b) Air Control Element

(c) Thermocouple (Typical)

(d) Piezometer Bar (Typical)

(e) Oil Control Element (Typical)

(f) Oil Measurement Thermometer (Typical)

(g) Pitot Impact Tube Mounted on Upper Copper Plate

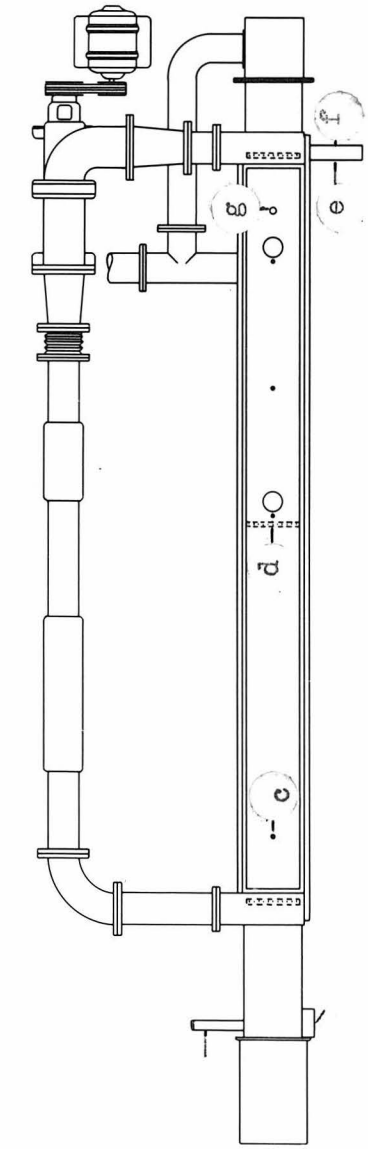

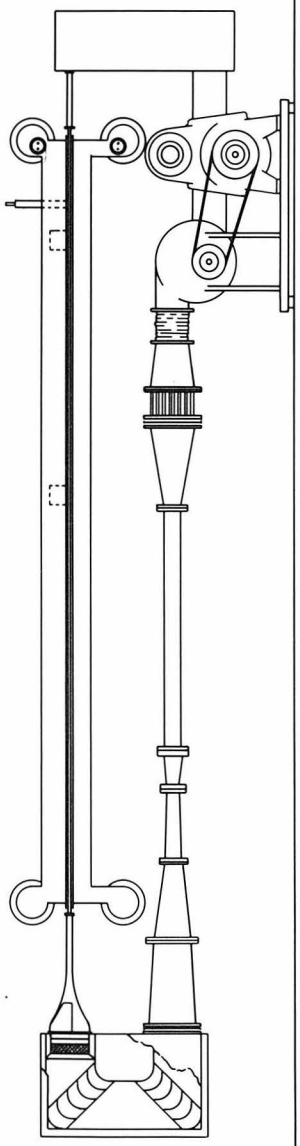

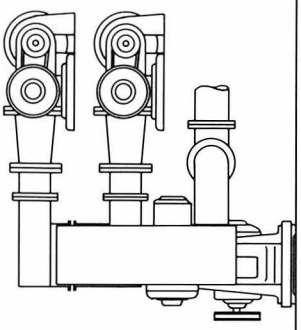

Figure 6

Orthogonal Projection of Apparatus

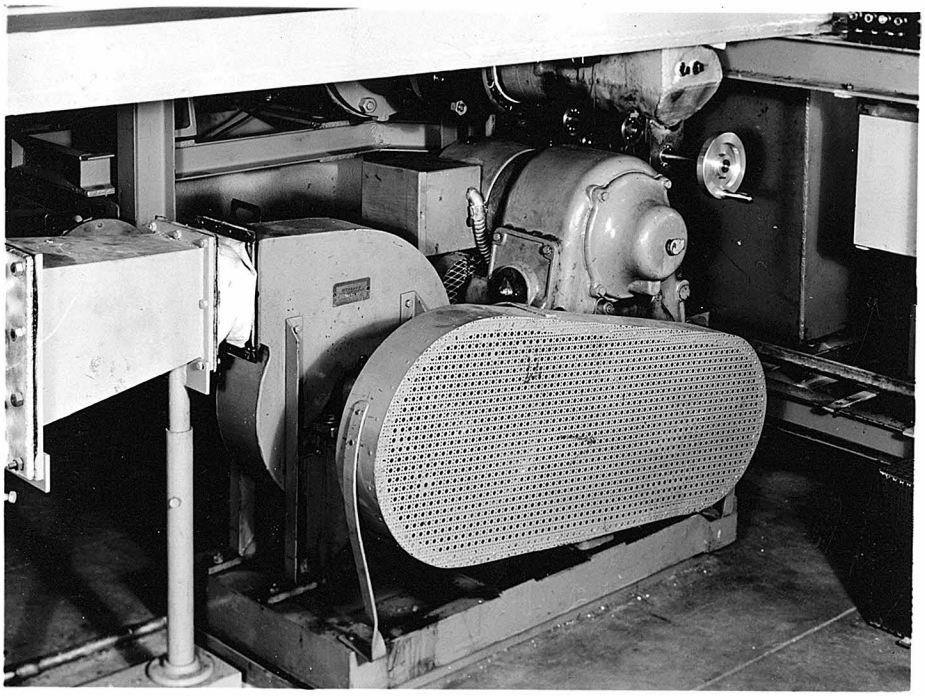

Figure 7

Motor-Blower Unit

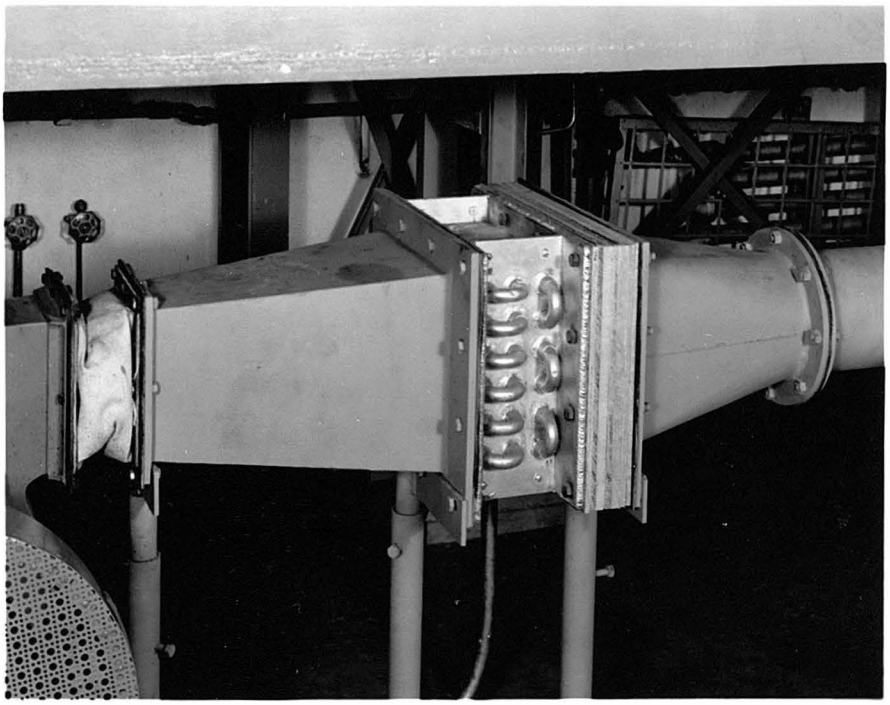

Figure 8

Air System (Manual Control) Heater and Cooler Unit

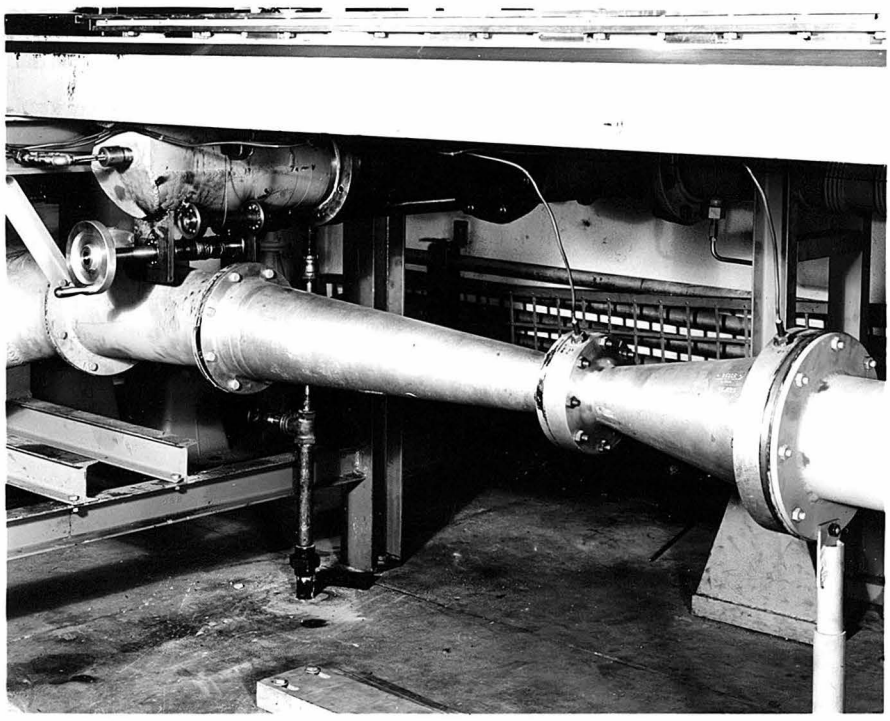

Figure 9

Typical Venturi Meter

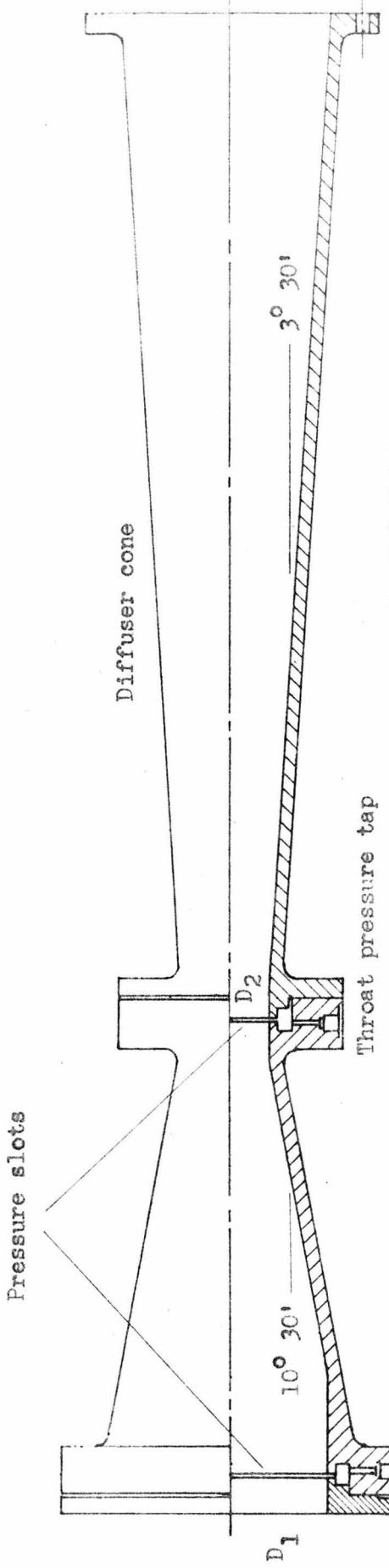

Material: Alcoa alloy 43

Finish: Smooth machine after casting

Figure 10 6-inch Venturi meter cross-section

MANOMETER DIFFERENTIAL vs. WORKING SECTION REYNOLD'S NUMBER

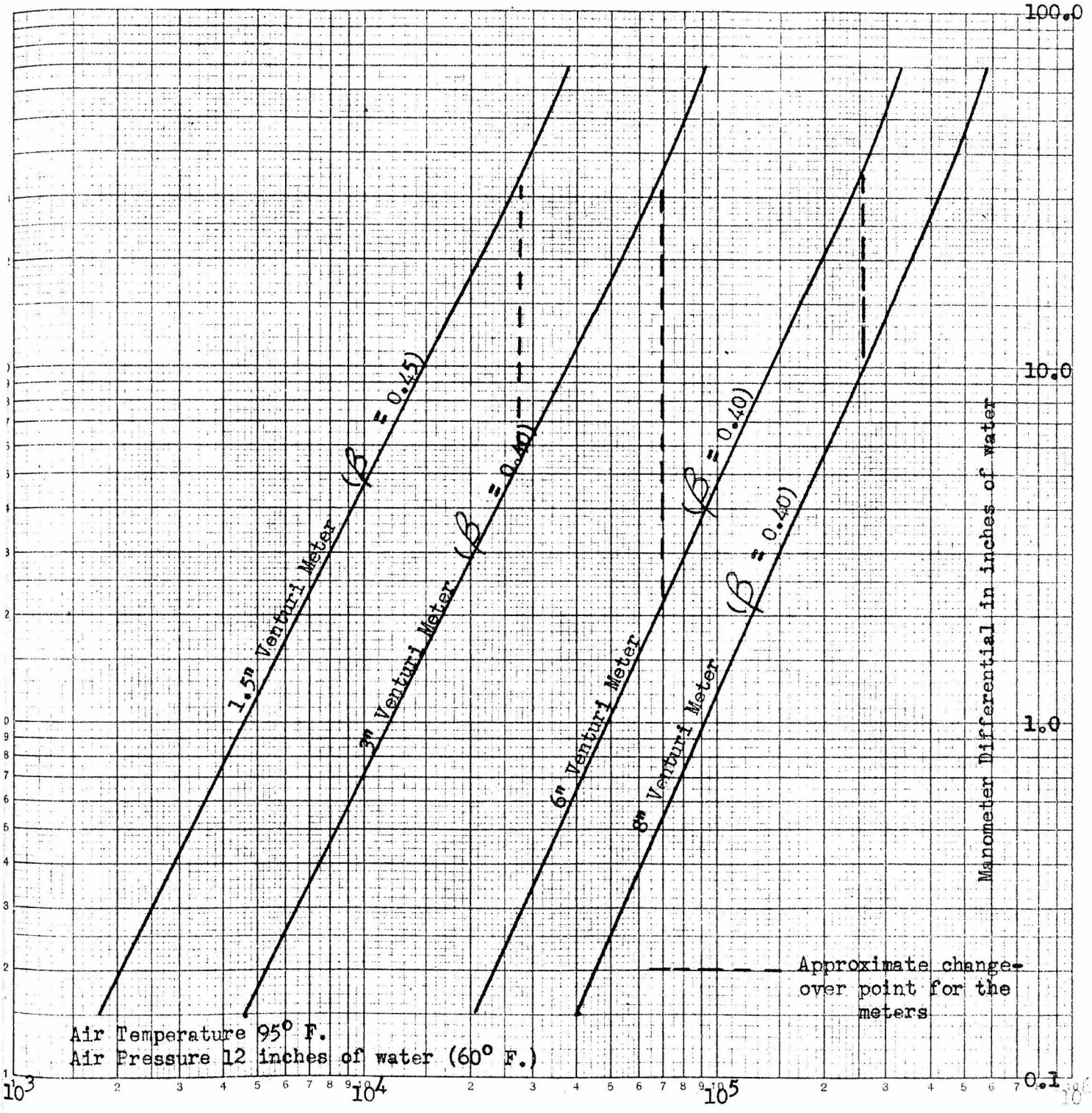

Figure 11

Venturi Meter Differentials as Functions of Working Section Reynolds Number

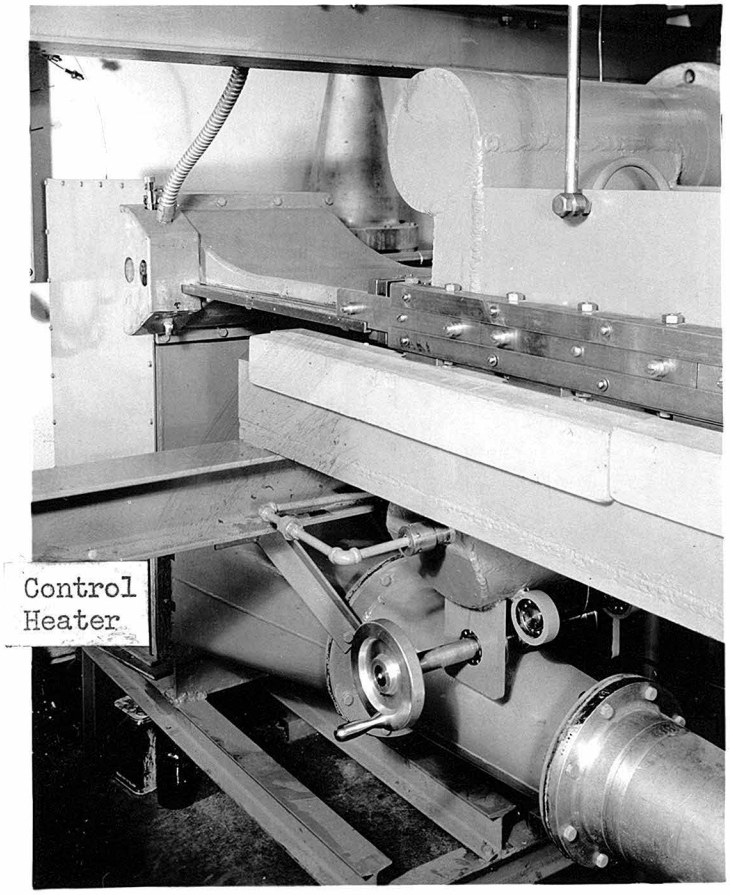

Figure 12

Venturi Meter Diffuser, Expansion Sections, Plenum Chamber and Convergent Section

Figure 13

Details of Plenum Chamber

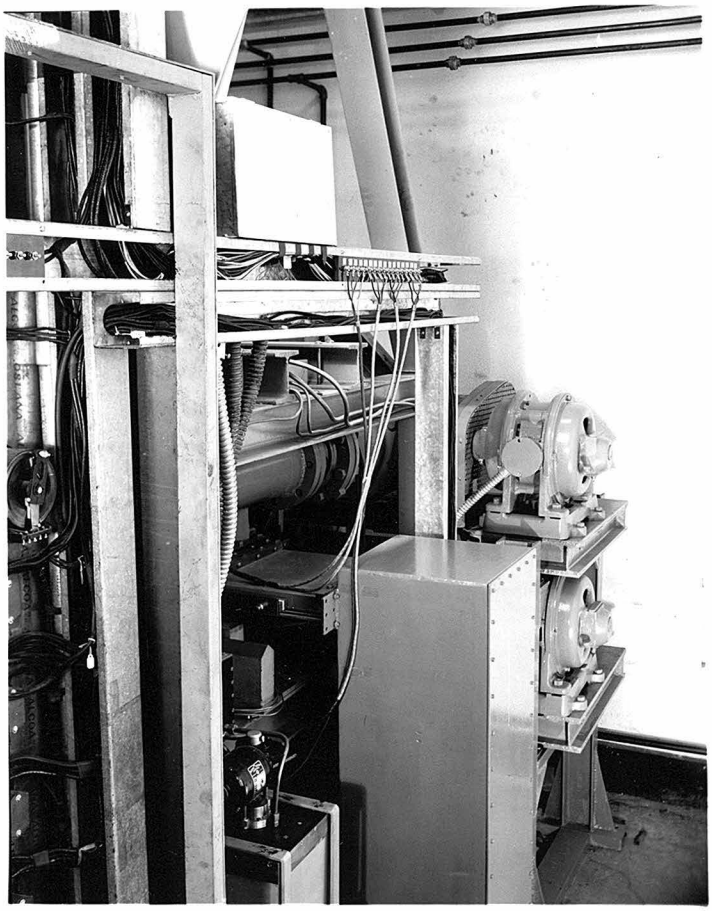

Figure 14

Downstream End Box, Pump Motors, and Thermocouple Ice Bath

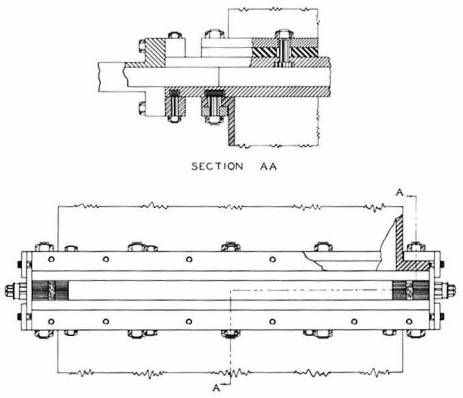

Figure 15

Cross-Section of Wind Tunnel Working Section

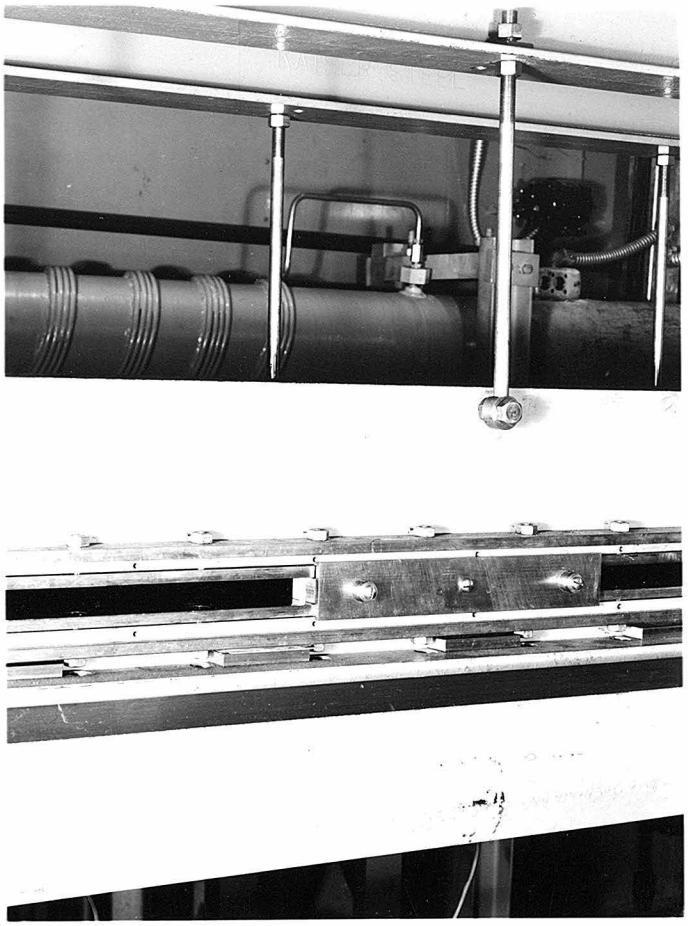

Figure 16

Standard Sidewall Block in Position between Upper and Lower Walls of Tunnel Working Section

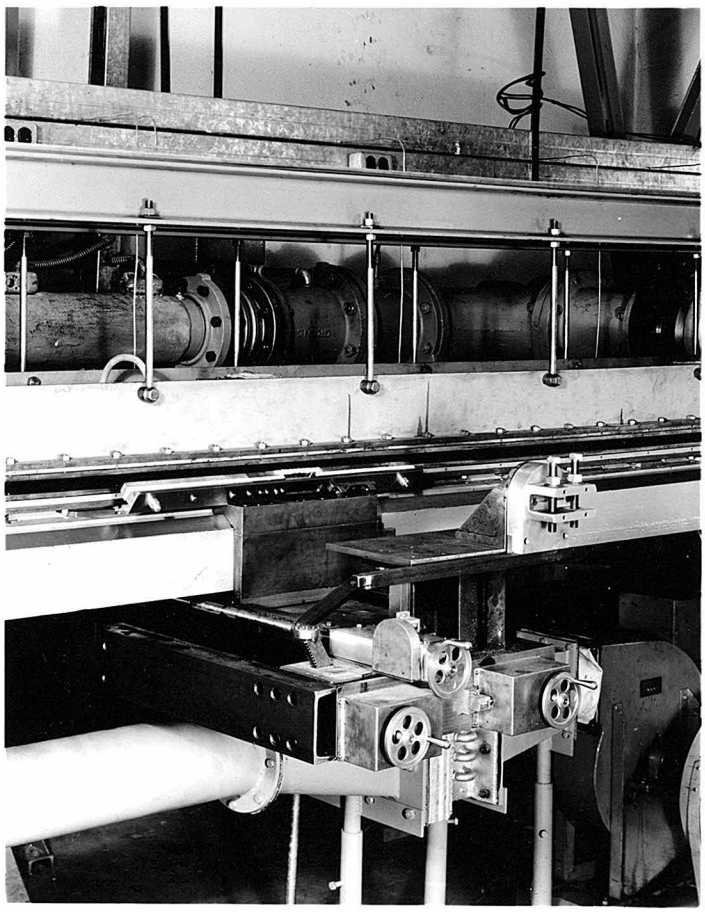

Figure 17

Special Sidewall Block Associated with Traverse Unit

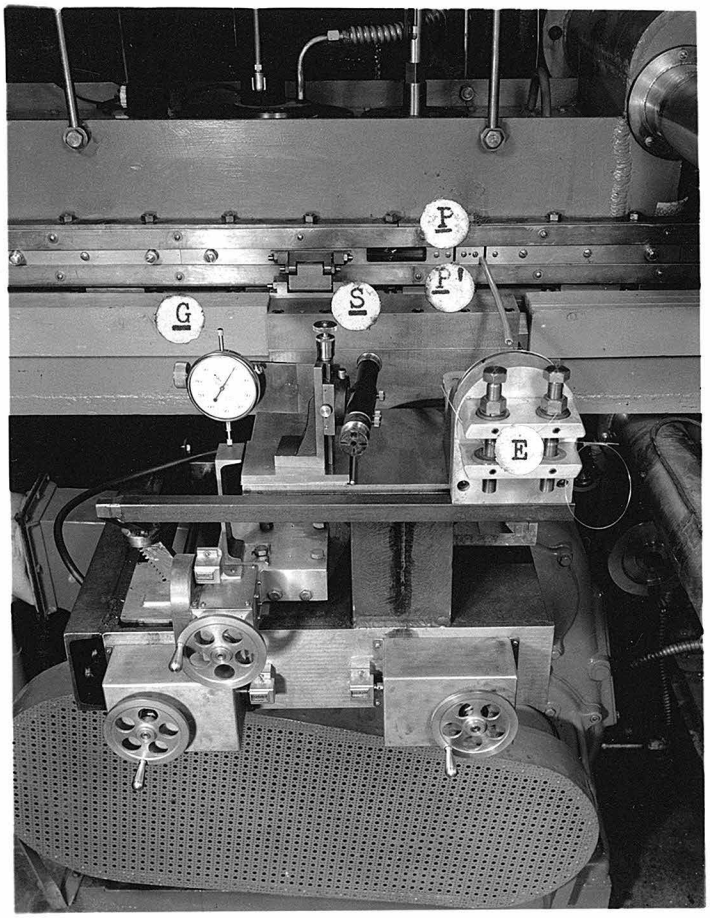

Figure 18

Traverse Unit and Optical System

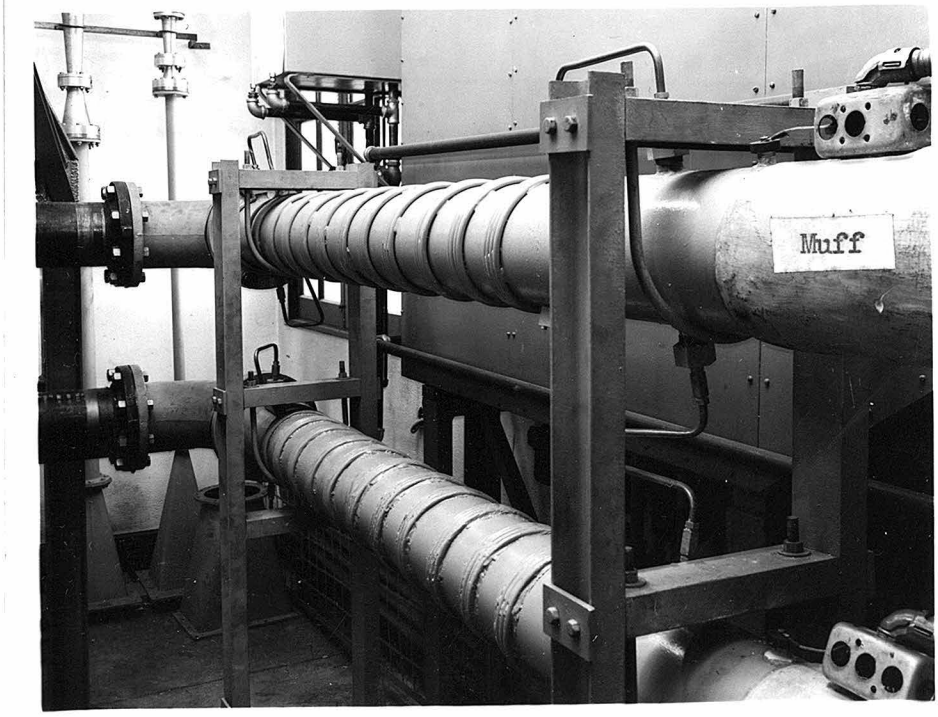

Figure 19

Oil Bath Exit Sections and Cooler-Heater Sections of Oil Bath Return Lines

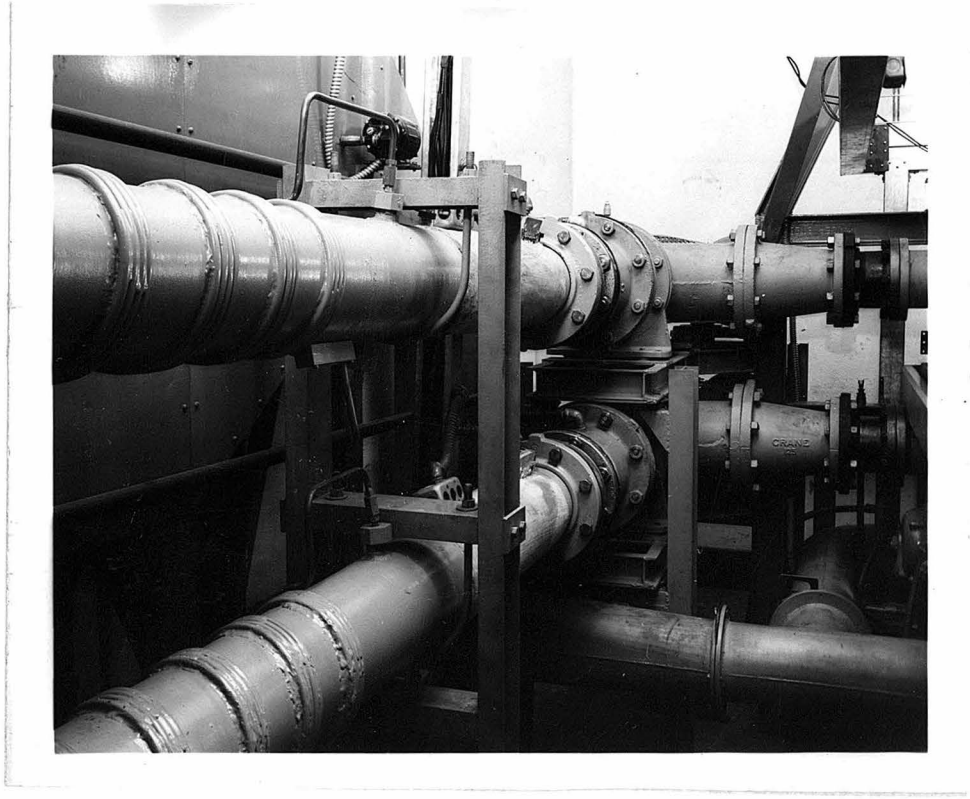

Figure 20

Cooler-Heater Sections of Oil Bath Return Lines, Axial Flow Pumps, and Oil Bath Engrance Sections

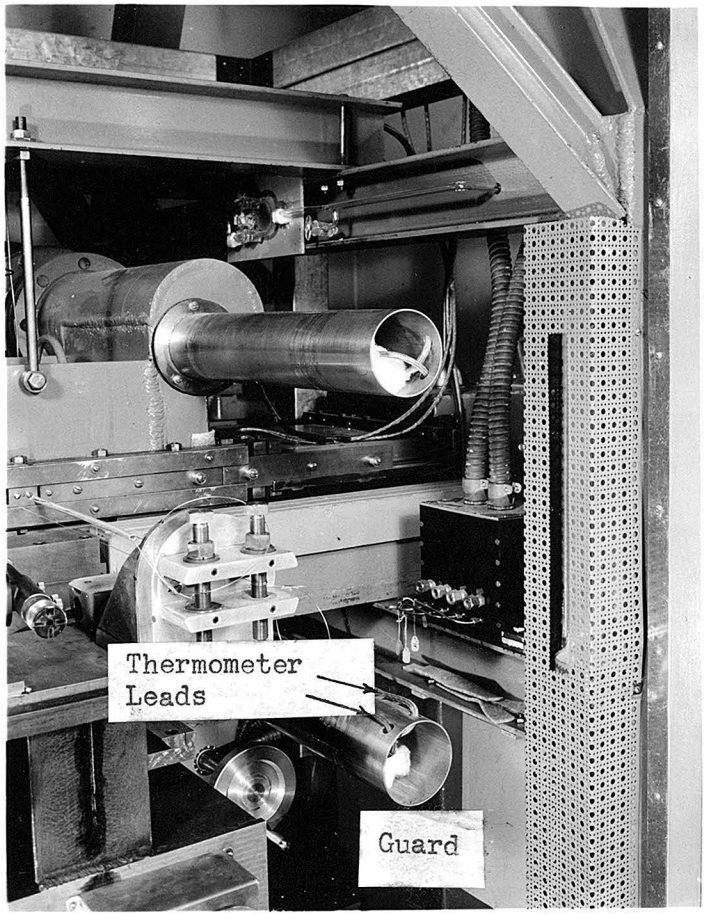

Figure 21

Guards for Platinum Resistance Thermometers and Temperature Control Elements

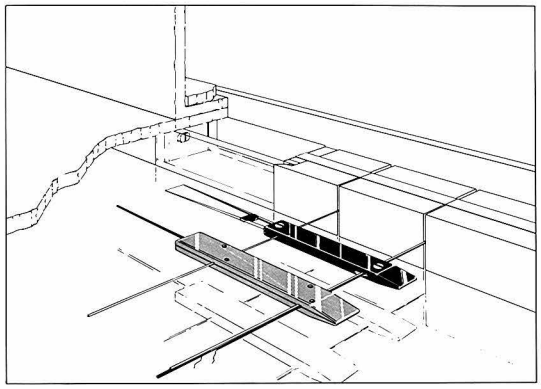

Figure 22

Pitot Impact Tube and Thermanemometer in Working Section

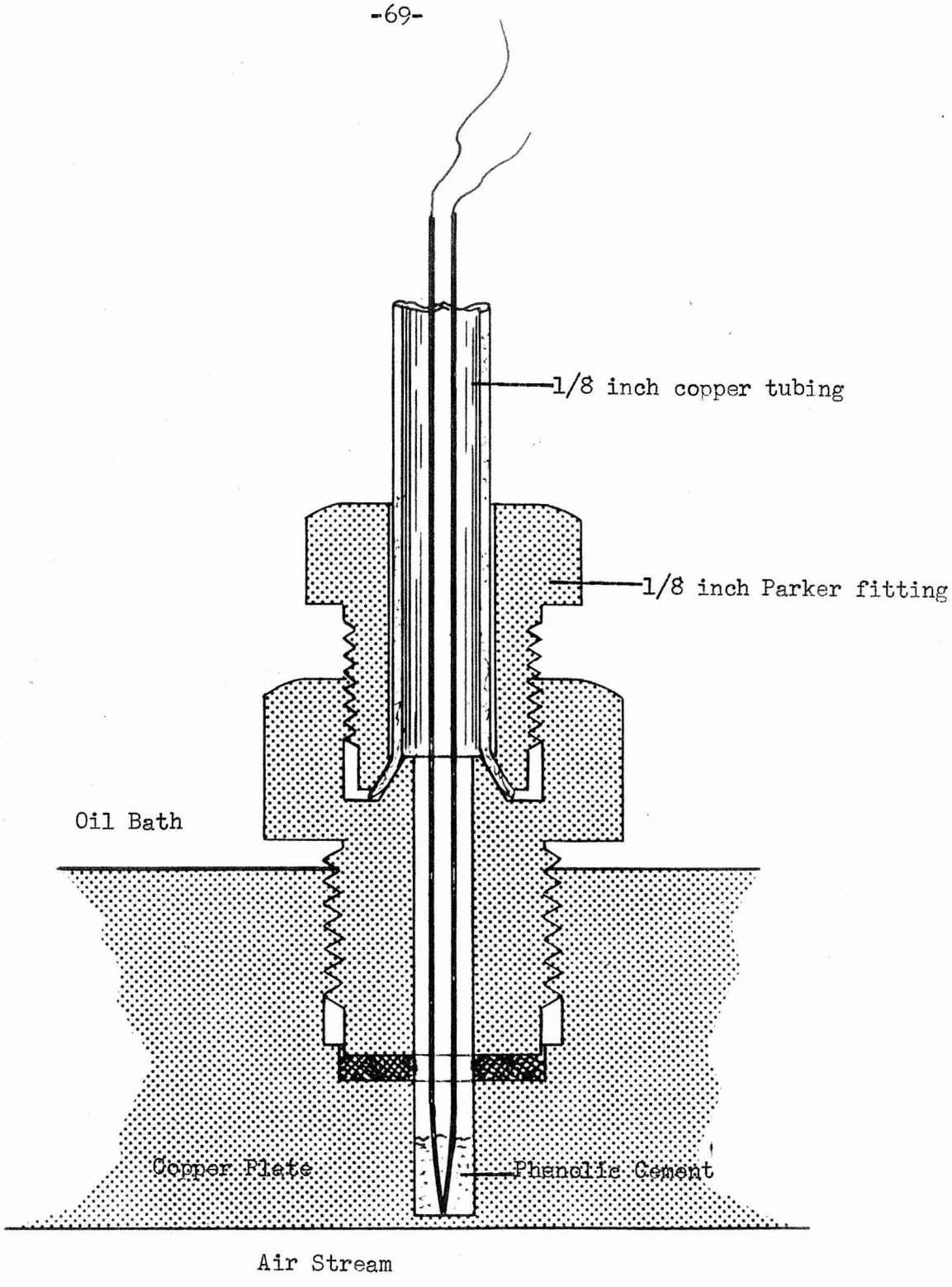

Figure 23

Thermocouple Mounting in Walls of Working Section

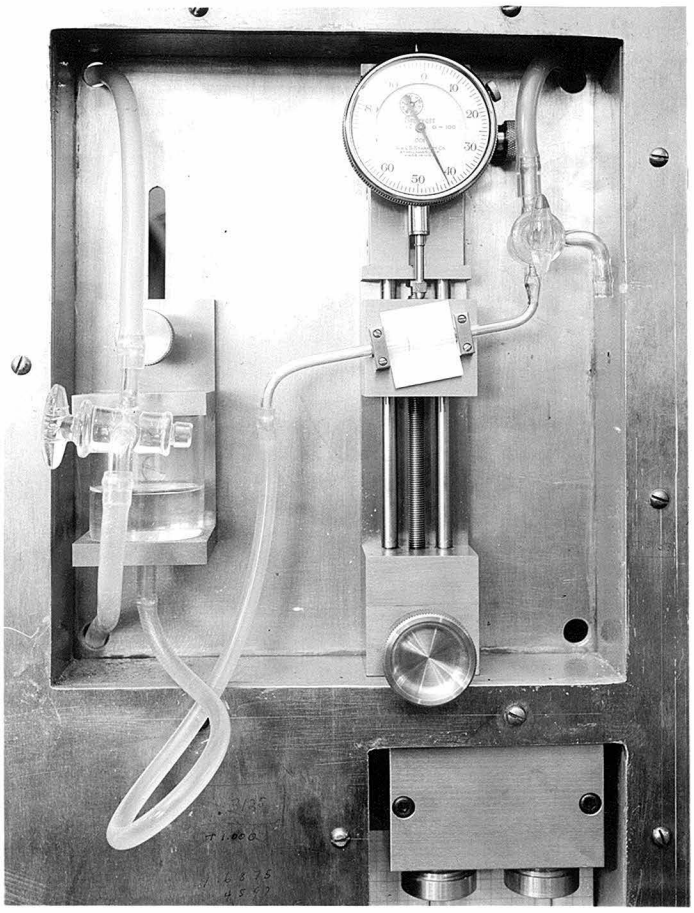

Figure 24

Micromanometer, Adjustable Reservoir and Gage

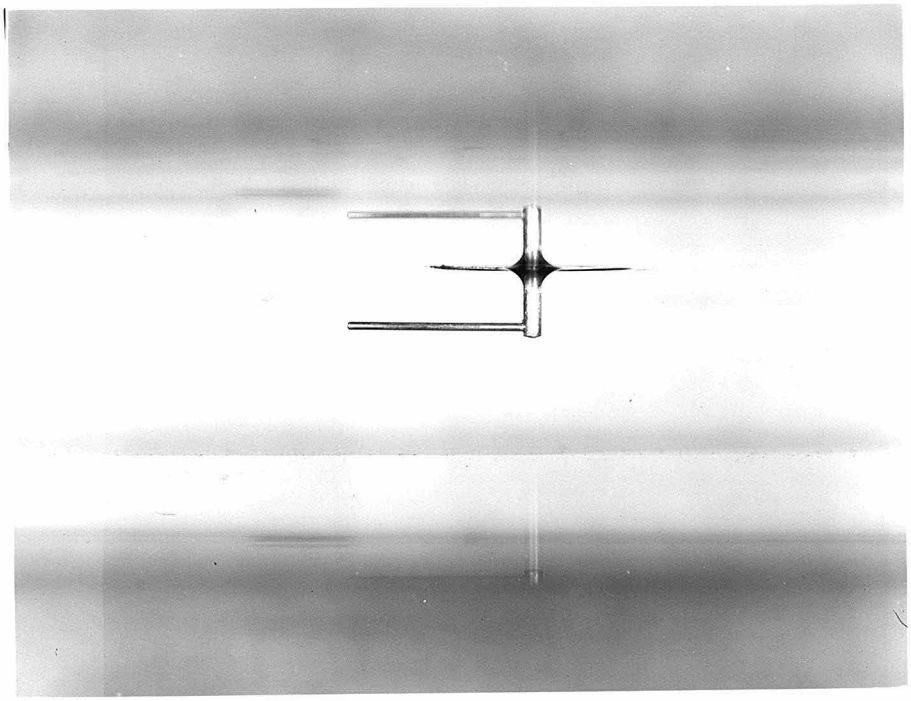

Figure 25

Fixed Pitot Impact Tube and Reflection in Upper Wall of Working Section

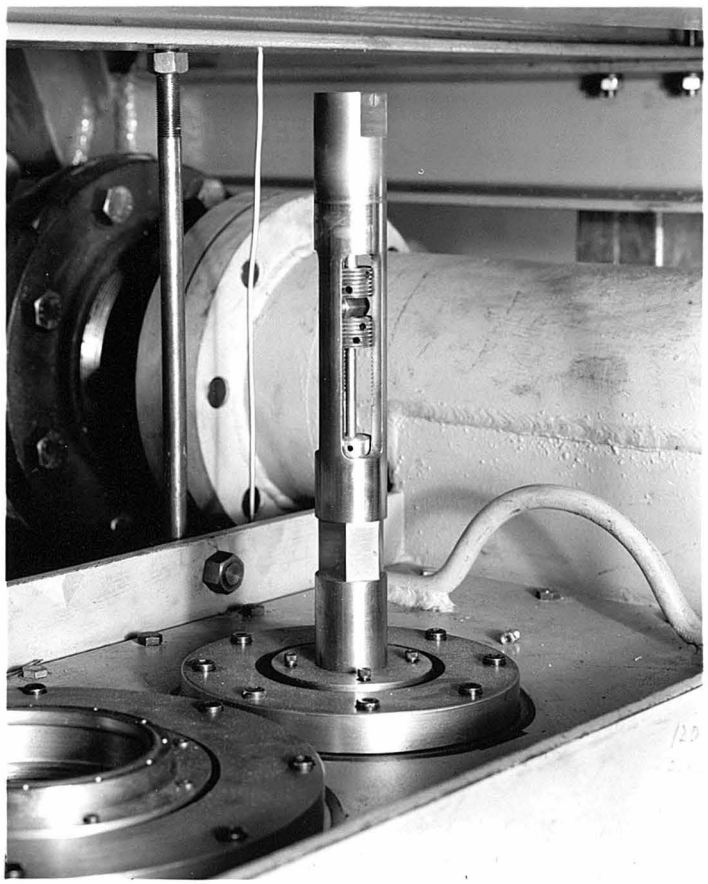

Figure 26

Guide Assembly for Fixed Pitot Impact Tube

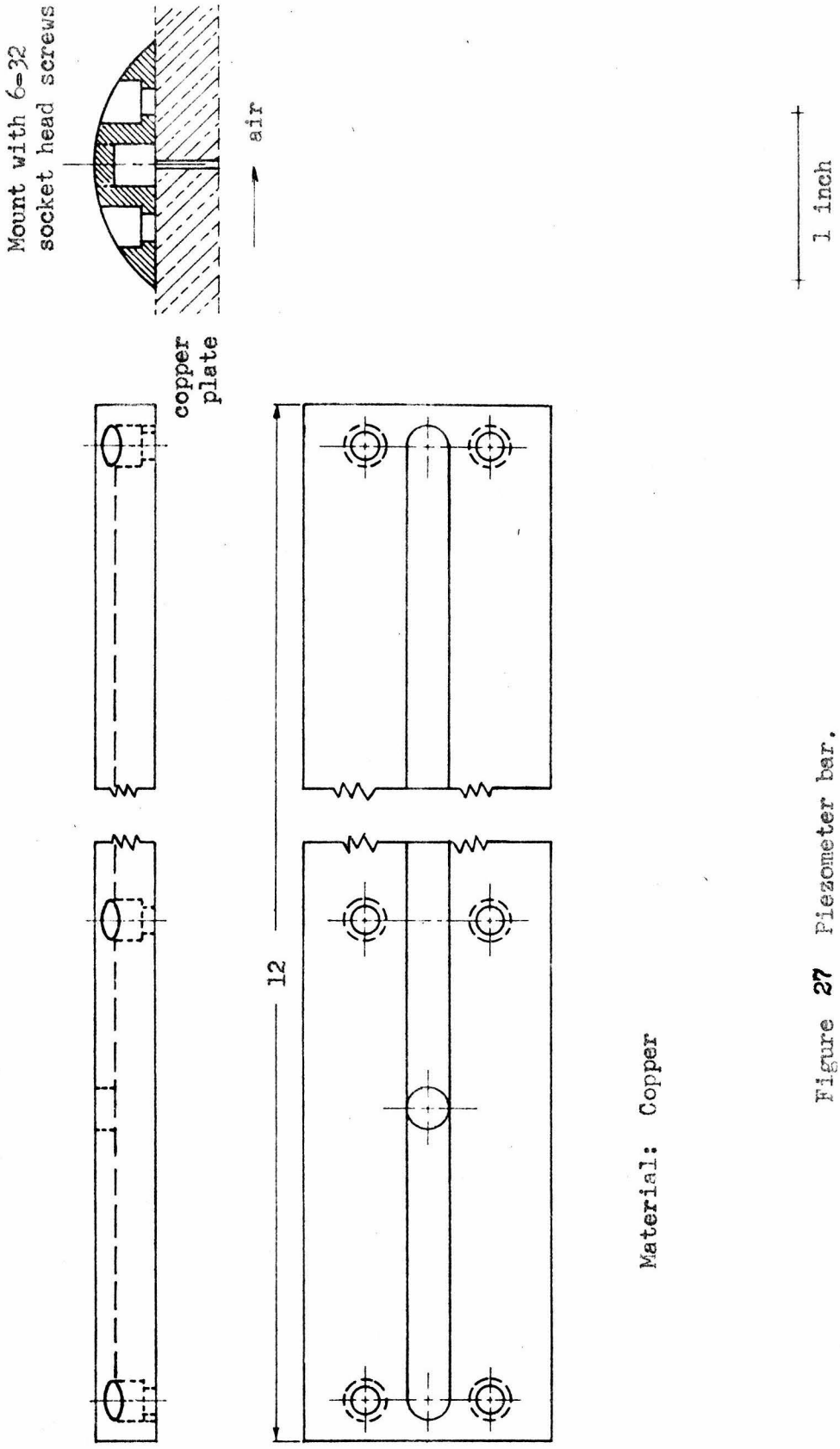

Material: Copper

Figure 27 Piezometer bar.

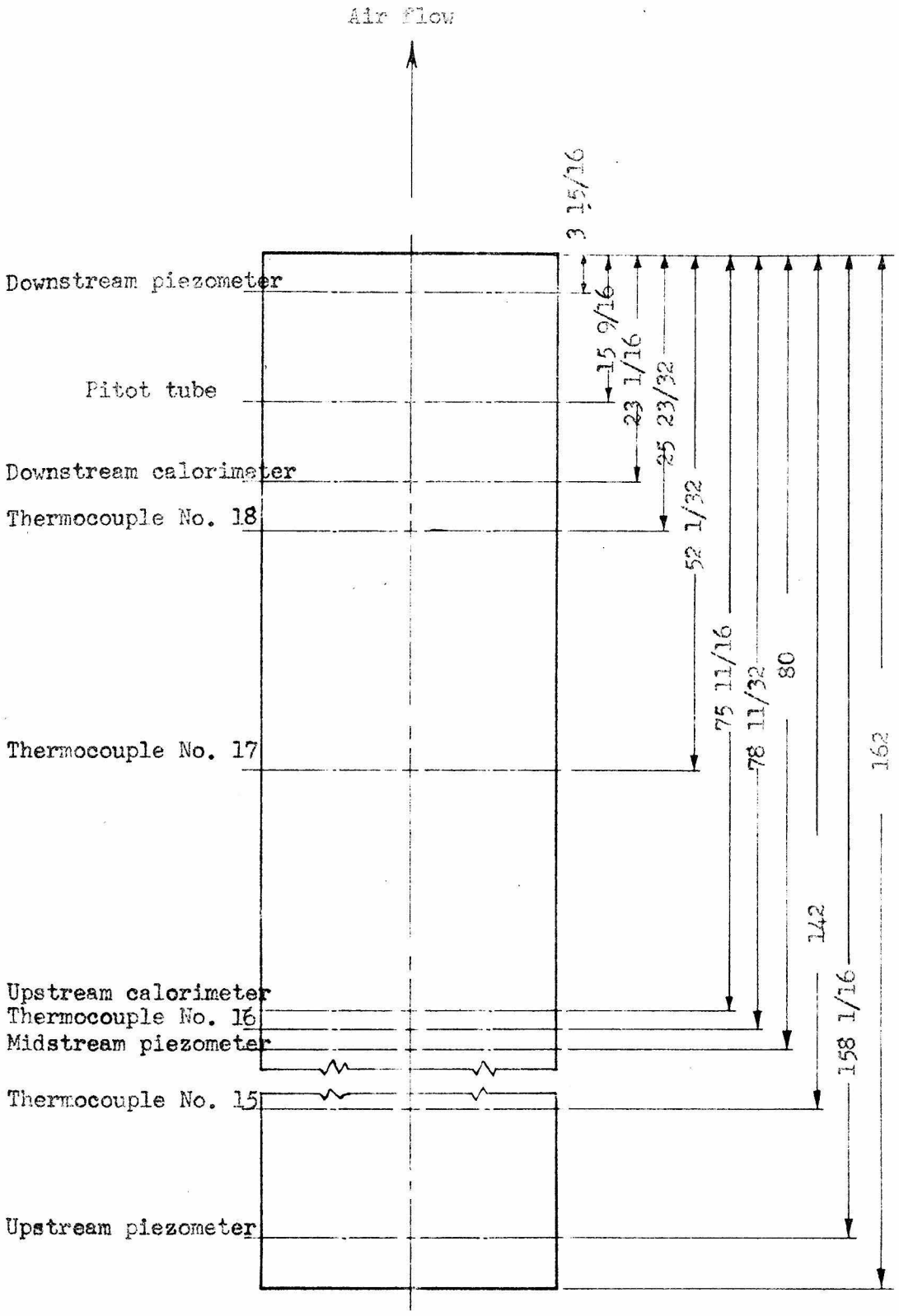

Figure 28 Instrument positions in upper copper plate.

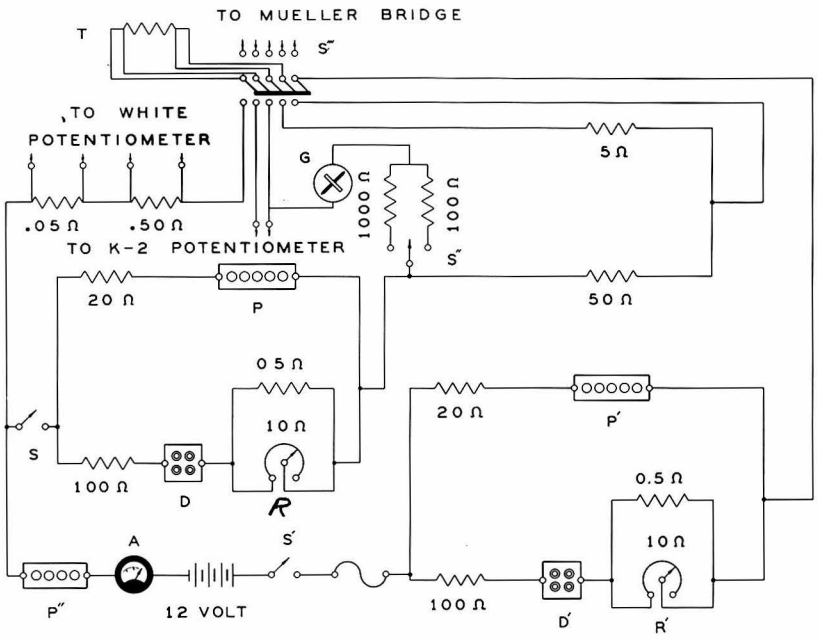

Figure 29

Thermanemometer Circuit

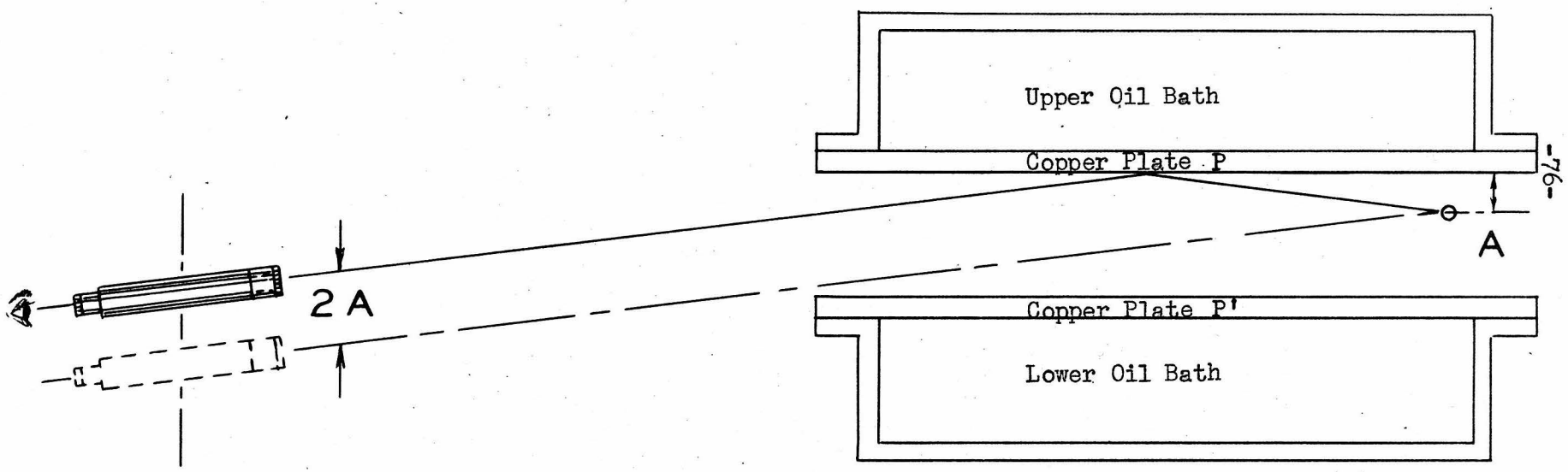

Figure 30

Schematic of Optical System Associated with Traverse Unit

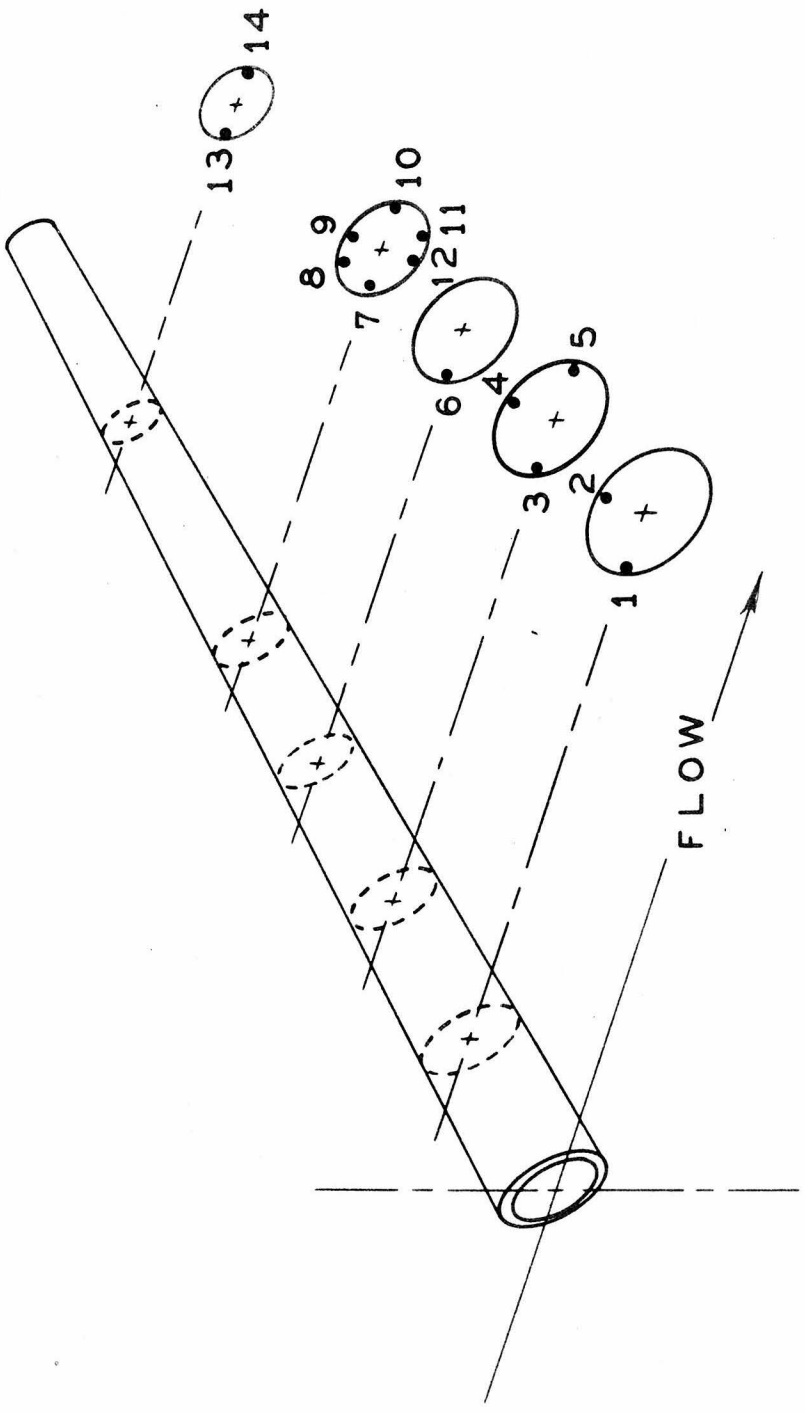

Figure 31

Thermocouple Location in Heated Cylinder

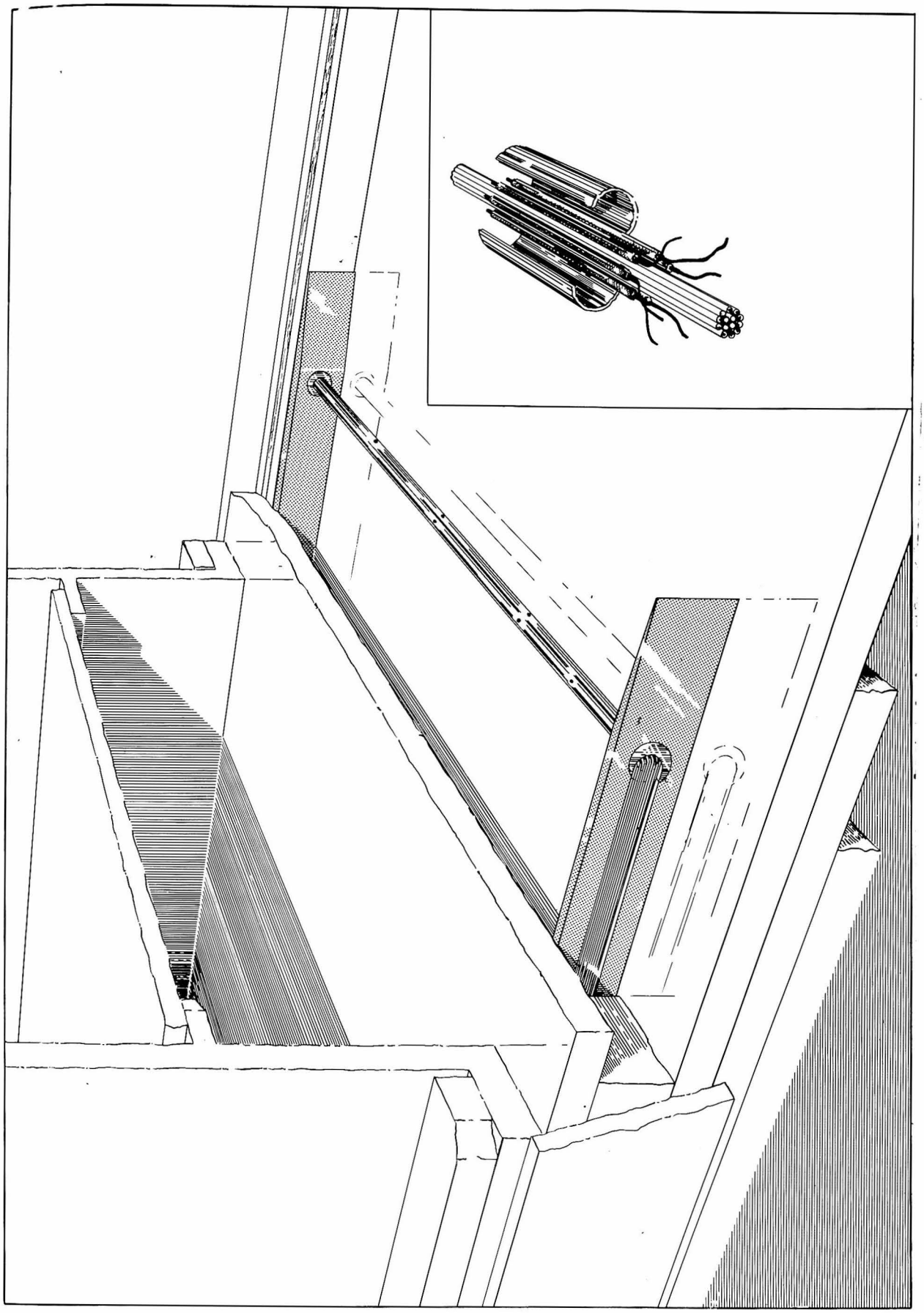

Figure 32

Heated Cylinder Mounted in the Working Section

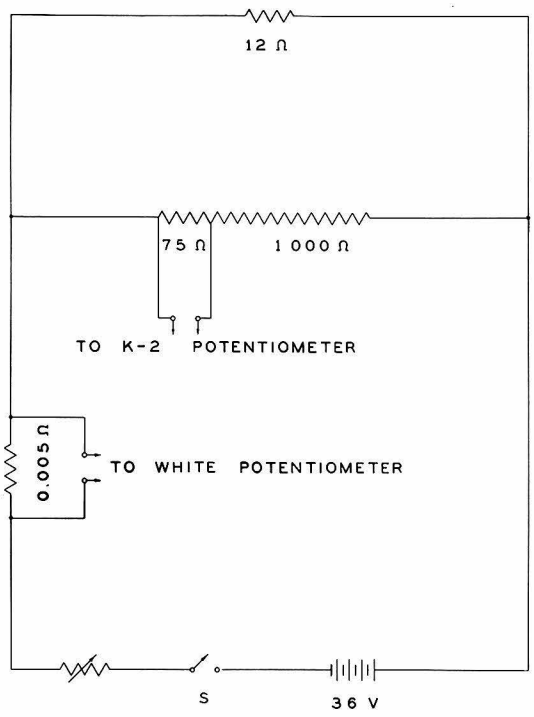

Figure 33

Energy Input Circuit for Heated Cylinder

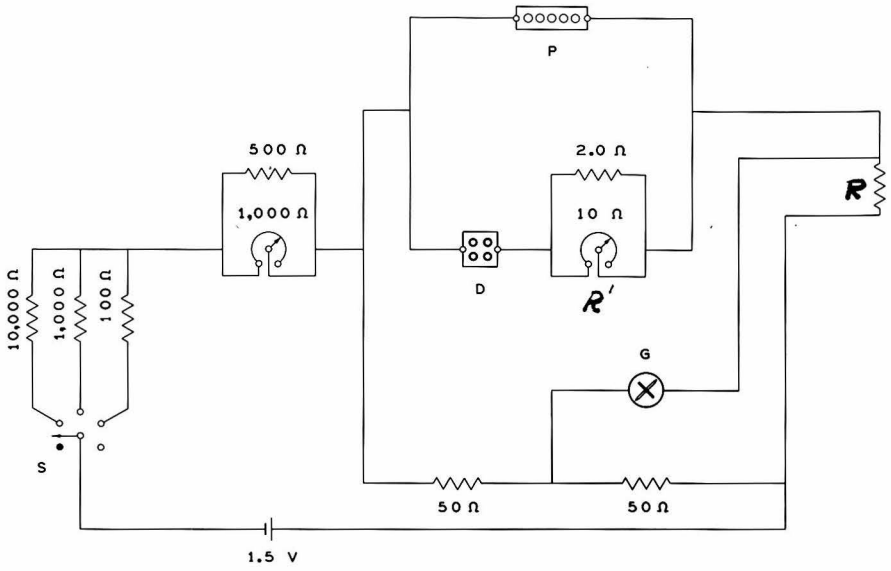

Figure 34

Temperature Control Bridge Circuit

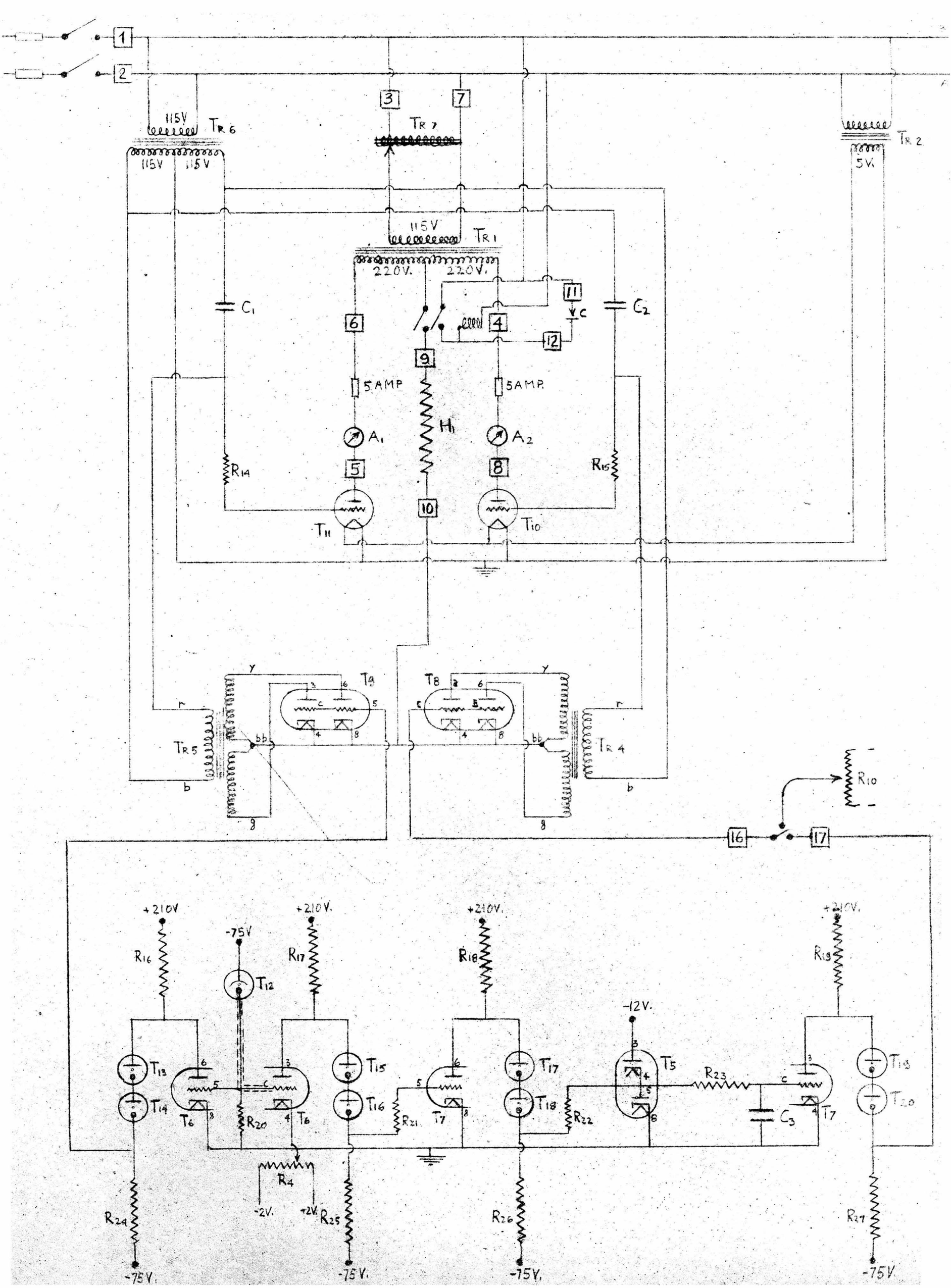
1
2
3
7
115V
TR 6
115V
115V
TR 7
TR 2
5V.
115V
TR 1
220V.
220V.
C1
C2
11
C
6
4
12
9
5AMP
5AMP
A1
H1
A2
R14
R15
5
8
10
T11
T10
TR 5
TR 4
T9
T8
bb
16
17
R10
+210V
+210V.
+210V.
+210V.
-75V
R16
R17
R18
R19
T12
T13
T14
T15
T16
T17
T18
T5
T6
T7
T19
T20
R20
R21
R22
R23
C3
-12V.
R4
-2V.
+2V.
R24
R25
R26
R27
-75V.
-75V.
-75V.
-75V.

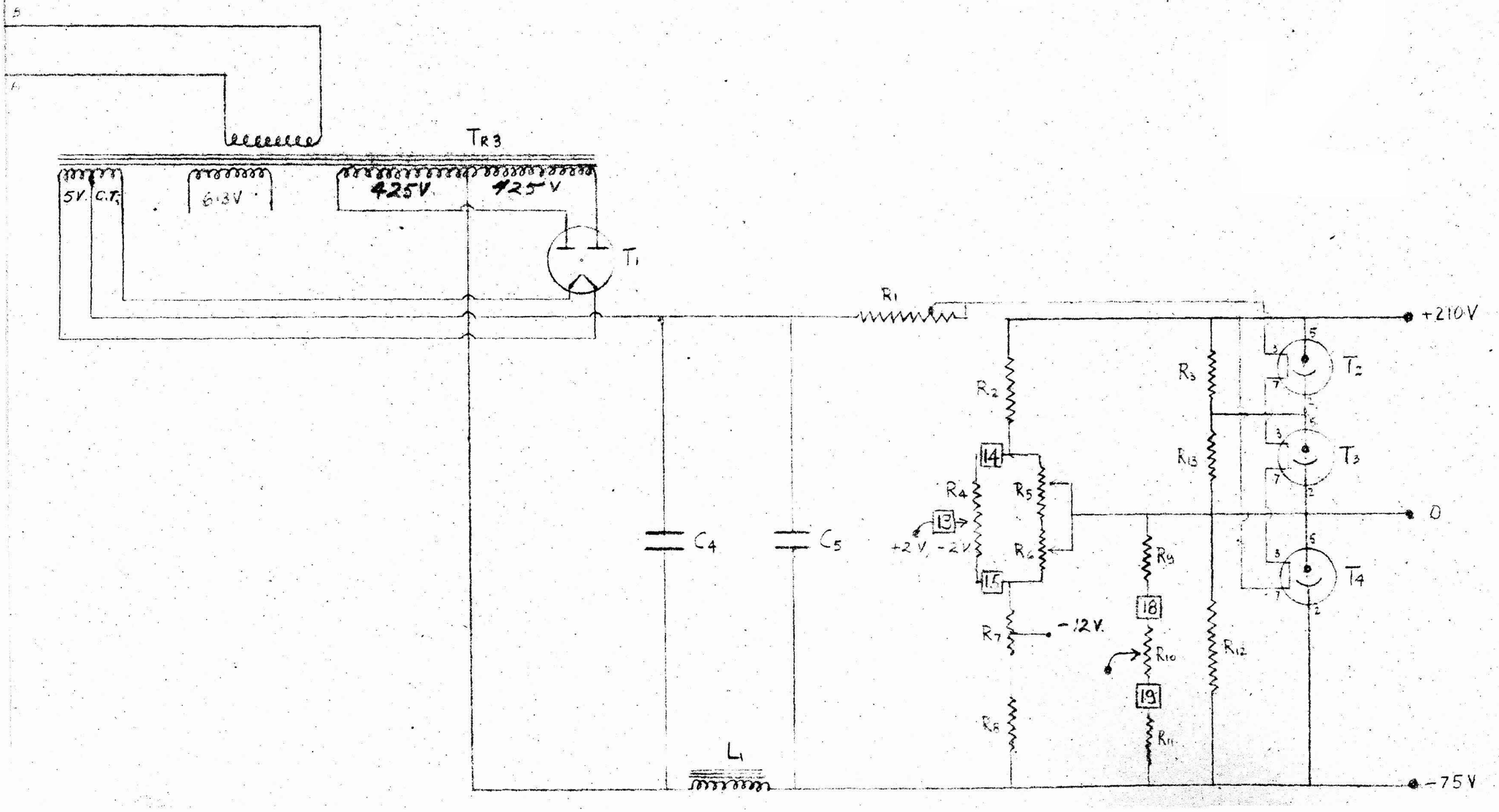

Figure 36

Power Supply Circuits for Thyratron Control Circuit

Figure 37

CALIBRATION OF PLATINUM RESISTANCE THERMOMETERS

RESIDUAL RESISTANCE RATIO vs. TEMPERATURE (° F.)

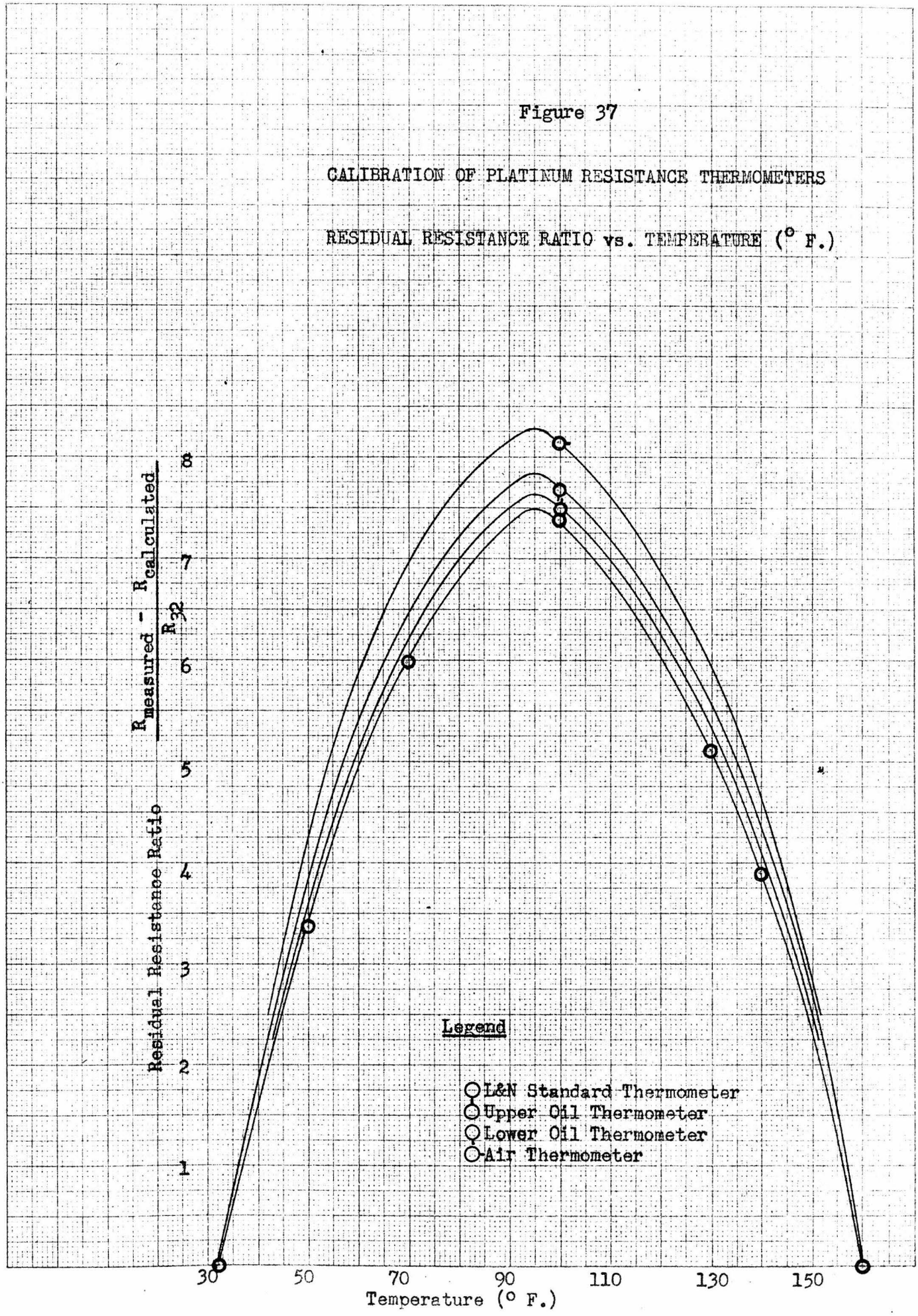

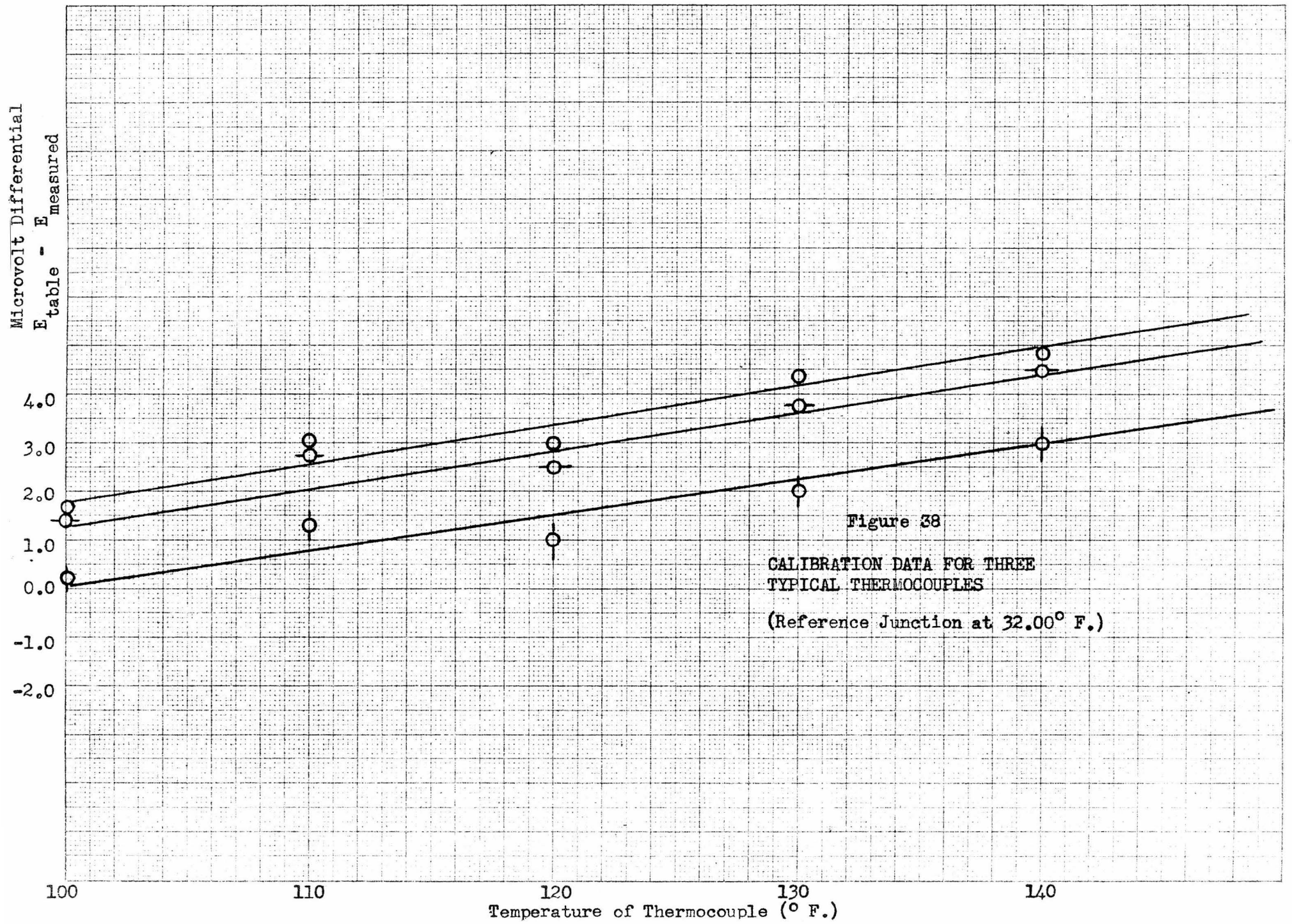

Figure 38

CALIBRATION DATA FOR THREE TYPICAL THERMOCOUPLES

(Reference Junction at 32.00° F.)

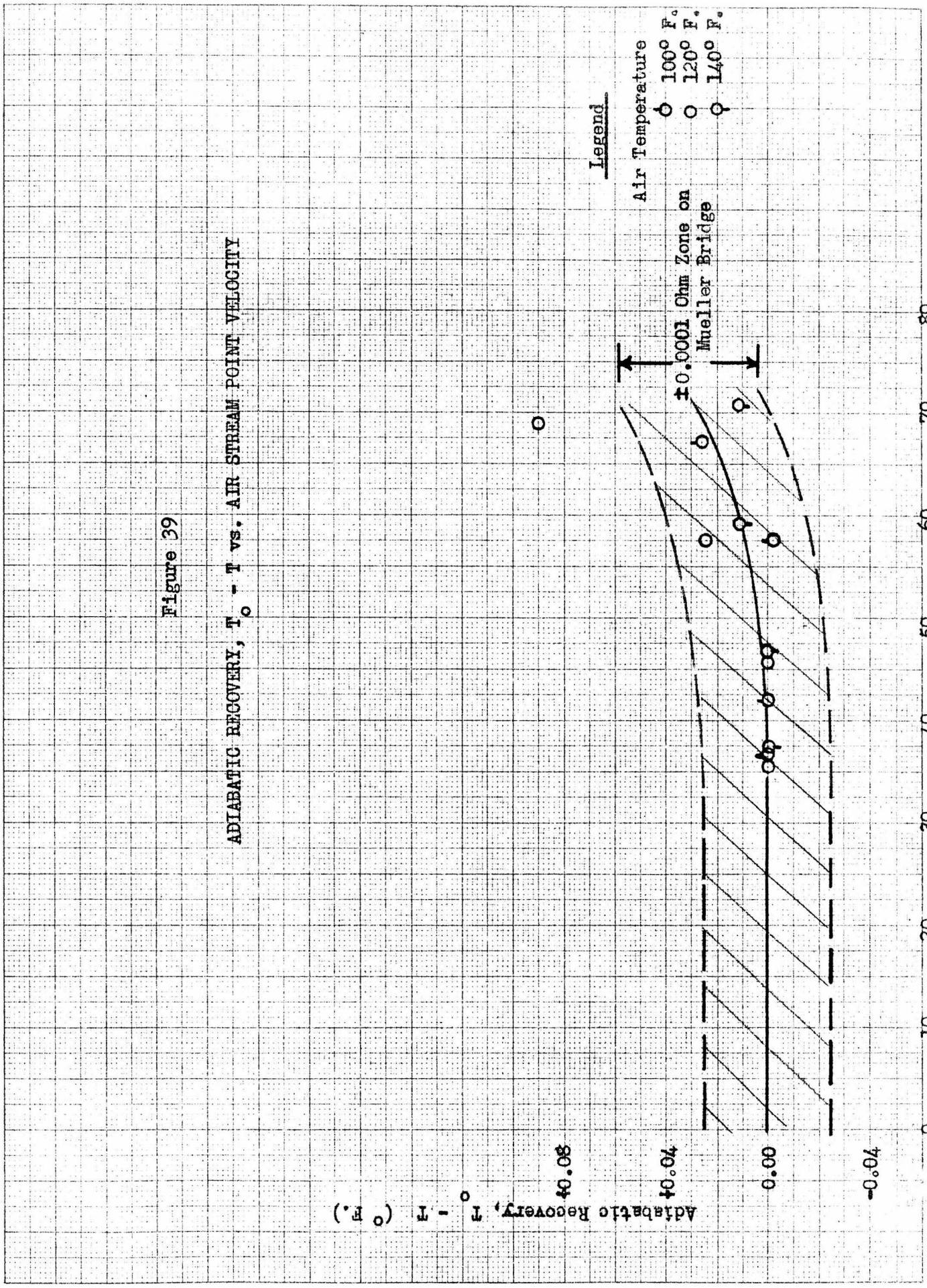

Figure 39

ADIABATIC RECOVERY, $T_o - T$ vs. AIR STREAM POINT VELOCITY

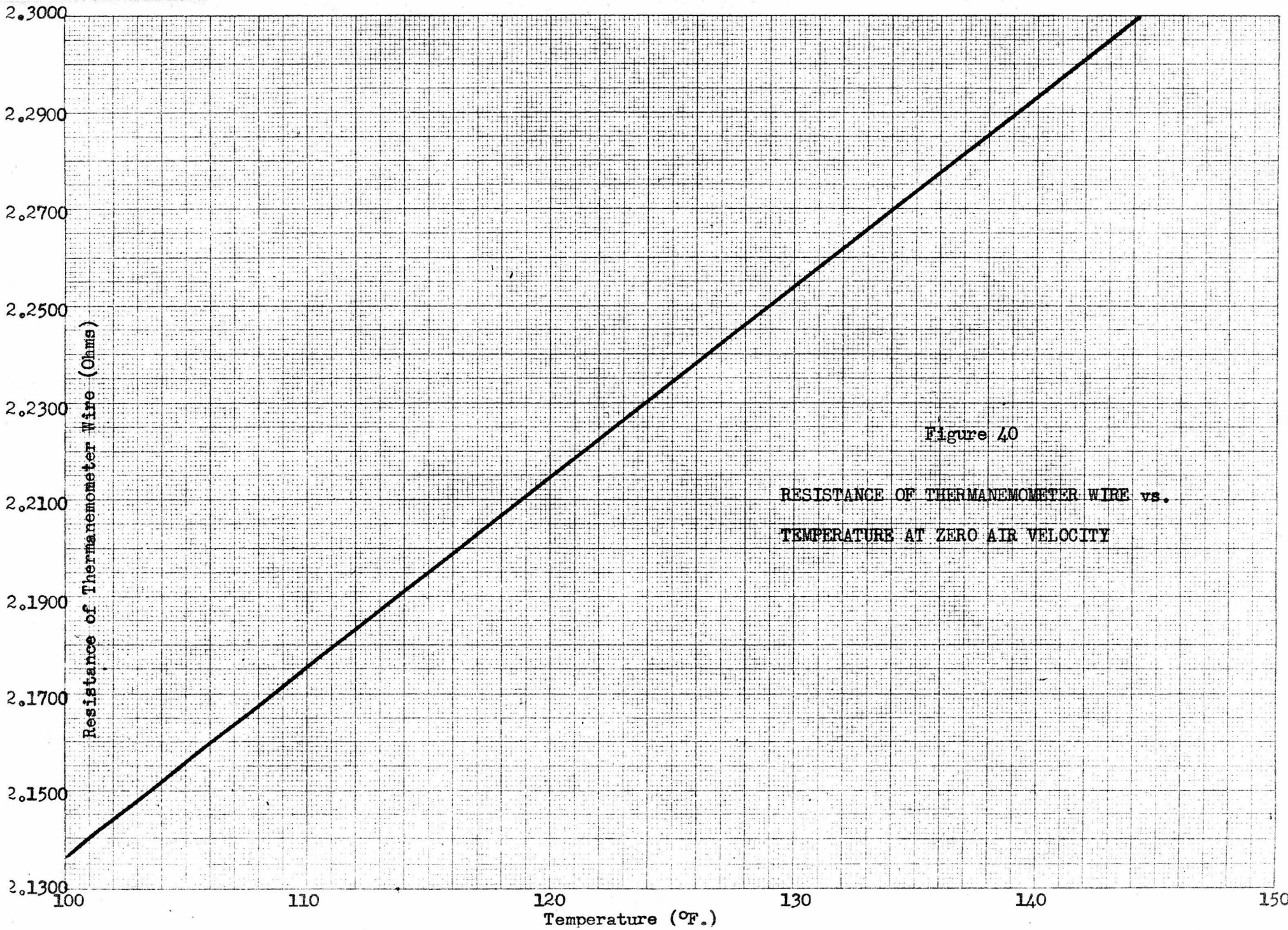

Figure 40

RESISTANCE OF THERMANEMOMETER WIRE vs.

TEMPERATURE AT ZERO AIR VELOCITY

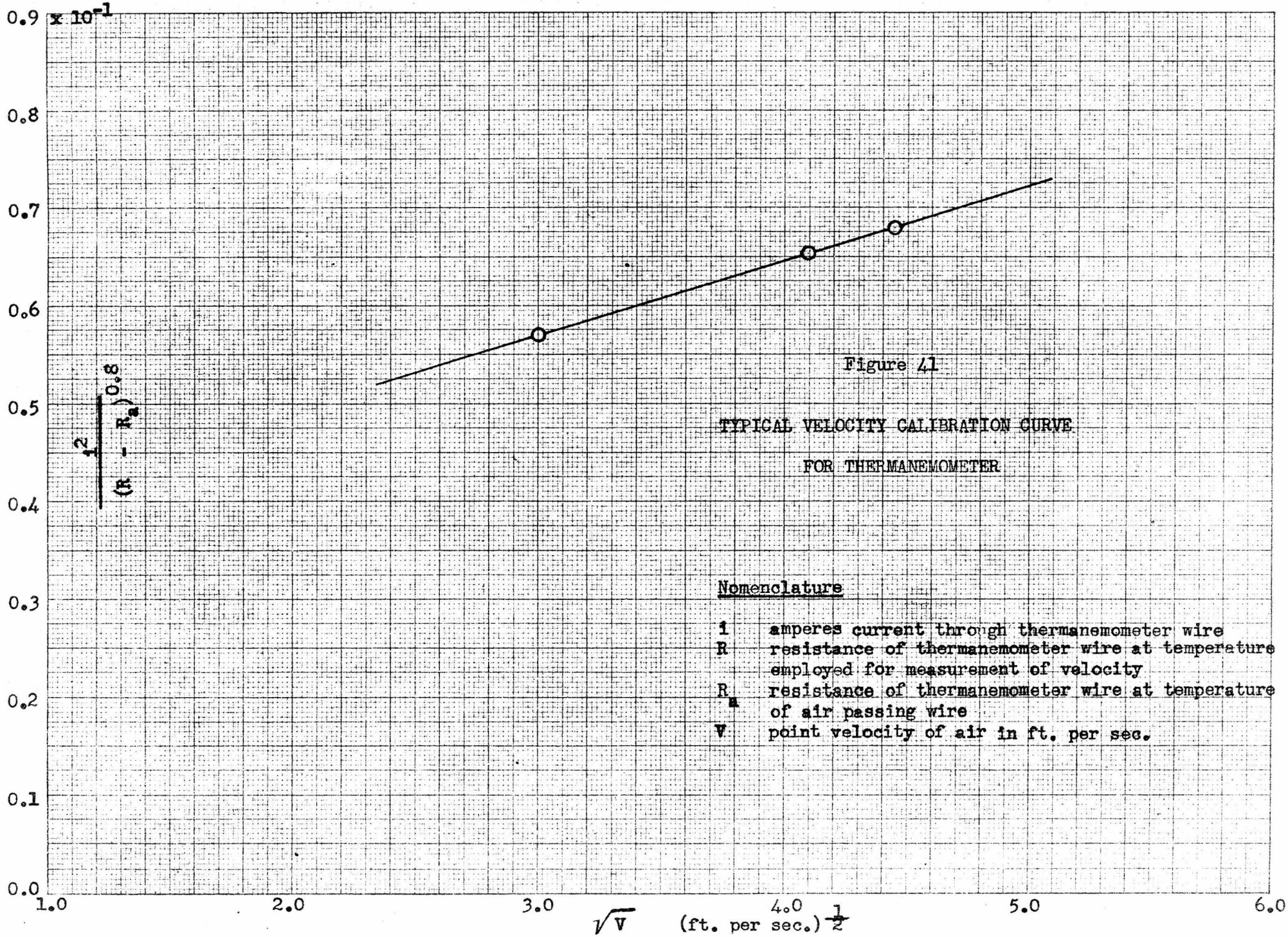

Figure 41

TYPICAL VELOCITY CALIBRATION CURVE

FOR THERMANEMOMETER

Nomenclature

i	amperes current through thermanemometer wire
R	resistance of thermanemometer wire at temperature employed for measurement of velocity
R_a	resistance of thermanemometer wire at temperature of air passing wire
V	point velocity of air in ft. per sec.

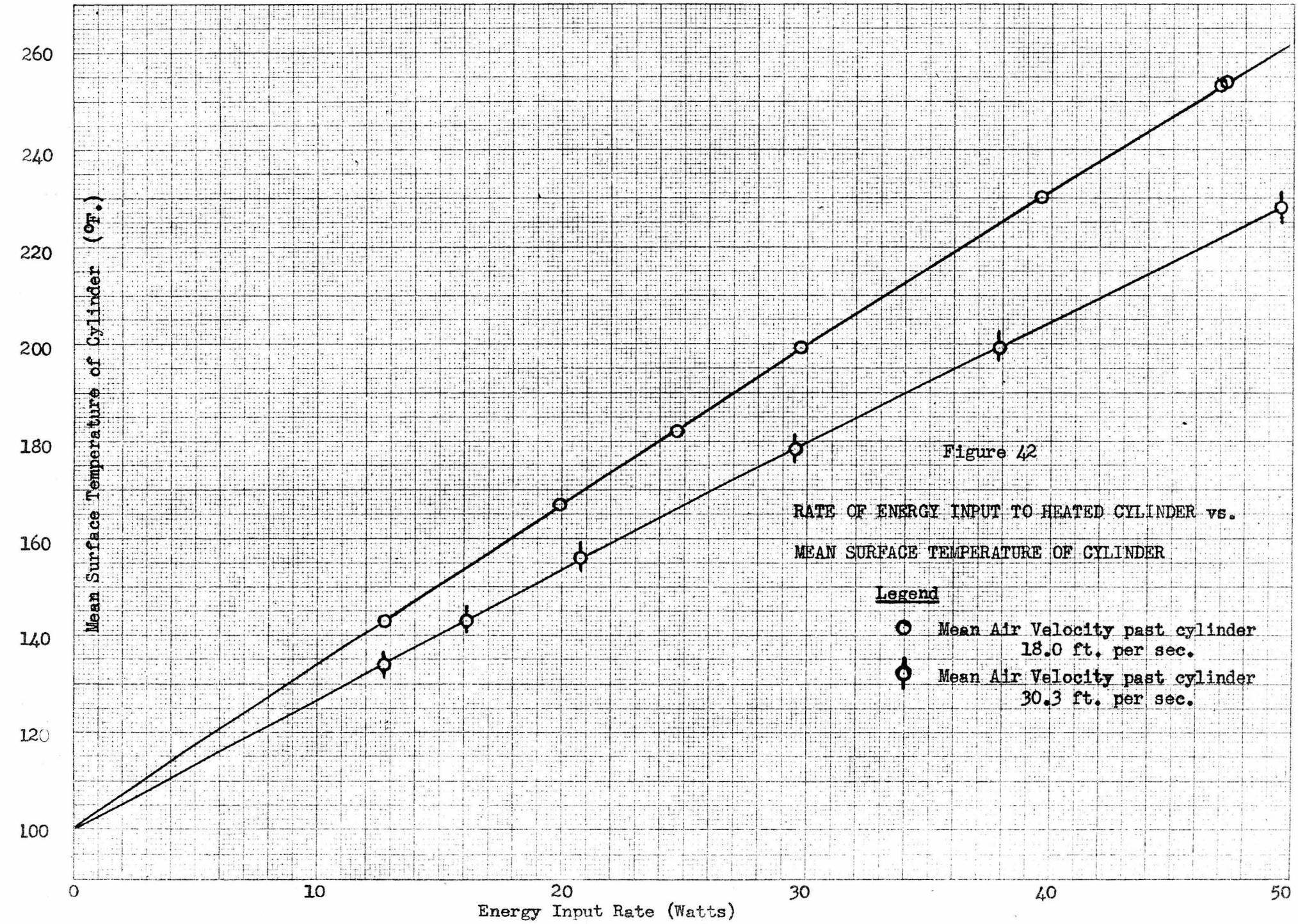

Figure 42

RATE OF ENERGY INPUT TO HEATED CYLINDER vs.

MEAN SURFACE TEMPERATURE OF CYLINDER

Legend

Mean Air Velocity past cylinder 18.0 ft. per sec.

Mean Air Velocity past cylinder 30.3 ft. per sec.

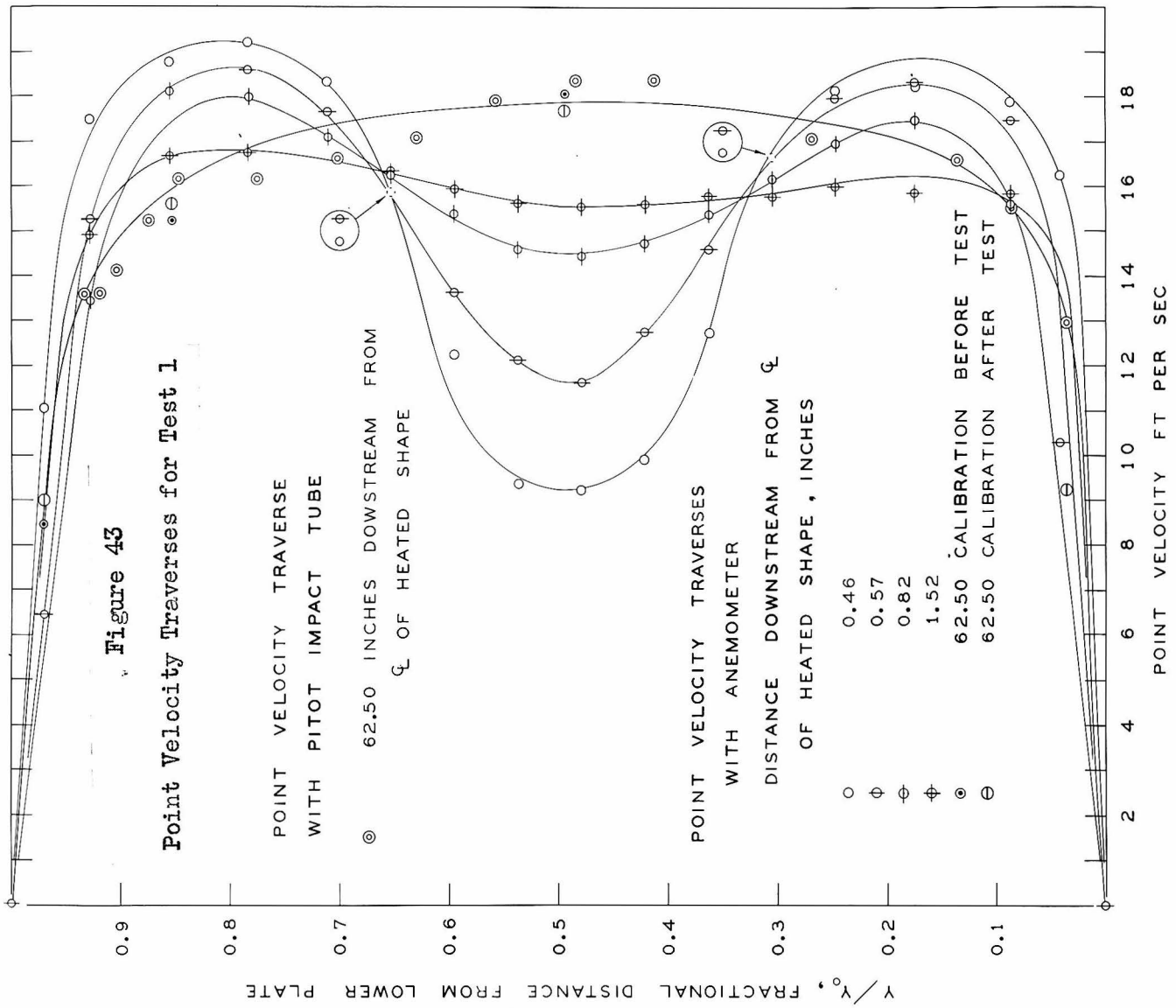
Figure 43
Point Velocity Traverses for Test 1
POINT VELOCITY TRAVERSE
WITH PITOT IMPACT TUBE
62.50 INCHES DOWSTREAM FROM
℄ OF HEATED SHAPE
POINT VELOCITY TRAVERSES
WITH ANEMOMETER
DISTANCE DOWNSTREAM FROM ℄
OF HEATED SHAPE, INCHES
0.46
0.57
0.82
1.52
62.50 CALIBRATION BEFORE TEST
62.50 CALIBRATION AFTER TEST
y/y₀, FRACTIONAL DISTANCE FROM LOWER PLATE
POINT VELOCITY FT PER SEC

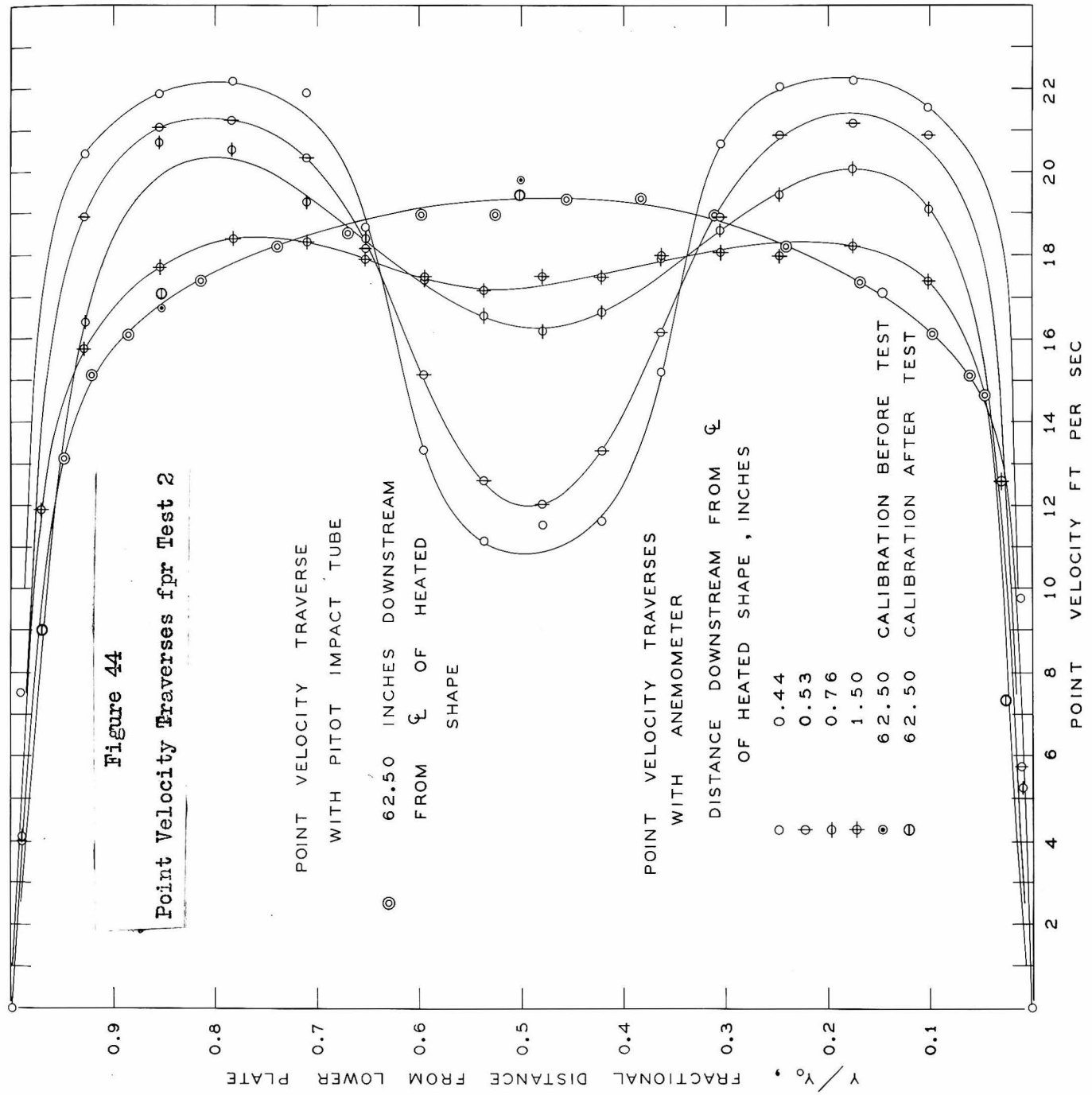
Figure 44
Point Velocity Traverses for Test 2
POINT VELOCITY TRAVERSE WITH PITOT IMPACT TUBE
62.50 INCHES DOWNSTREAM FROM ℄ OF HEATED SHAPE
POINT VELOCITY TRAVERSES WITH ANEMOMETER
DISTANCE DOWNSTREAM FROM ℄ OF HEATED SHAPE, INCHES
0.44
0.53
0.76
1.50
62.50 CALIBRATION BEFORE TEST
62.50 CALIBRATION AFTER TEST
y / y₀ , FRACTIONAL DISTANCE FROM LOWER PLATE
0.9
0.8
0.7
0.6
0.5
0.4
0.3
0.2
0.1
2
4
6
8
10
12
14
16
18
20
22
POINT VELOCITY FT PER SEC

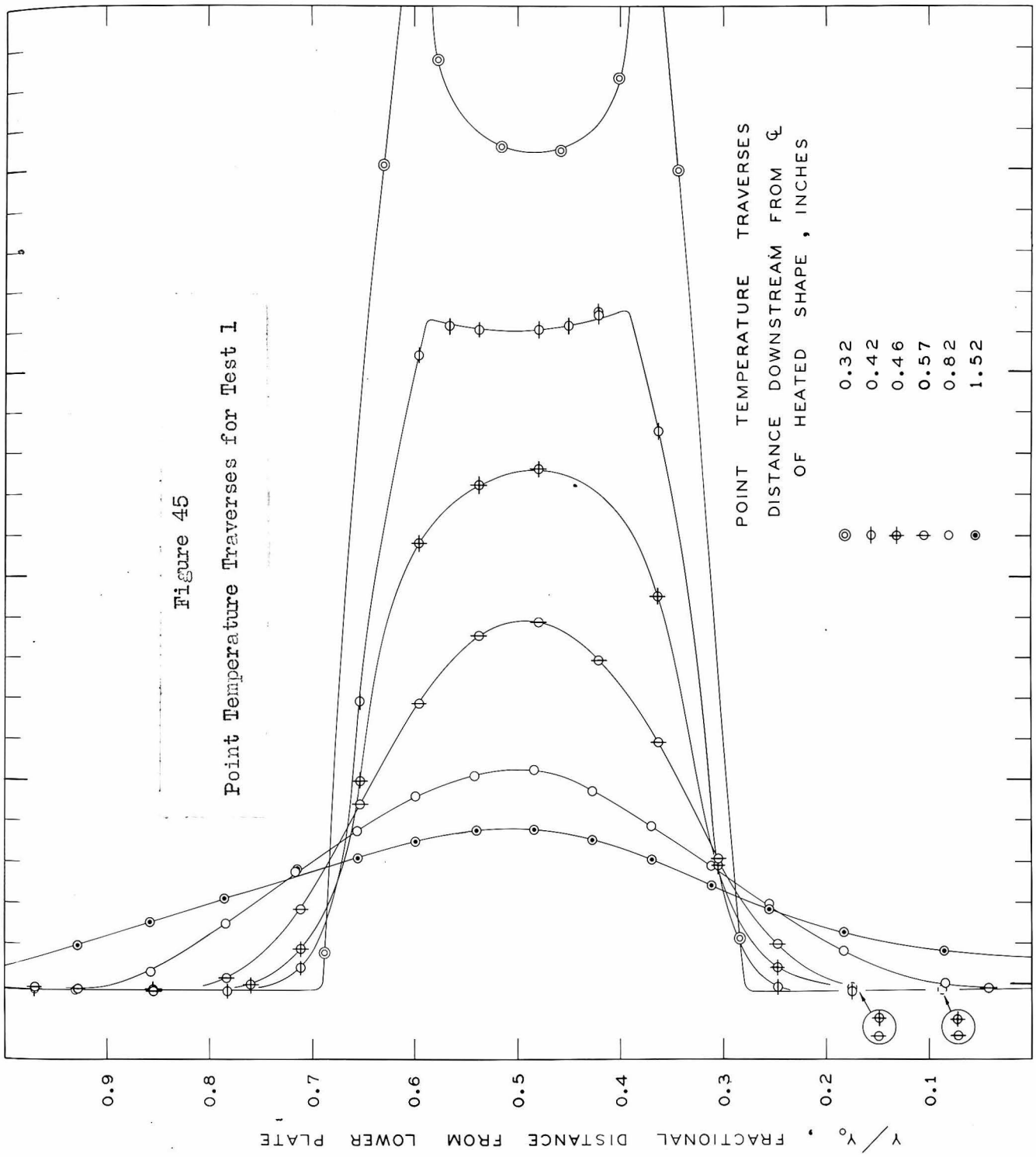
Figure 45
Point Temperature Traverses for Test 1
POINT TEMPERATURE TRAVERSES
DISTANCE DOWNSTREAM FROM ℄
OF HEATED SHAPE, INCHES
0.32
0.42
0.46
0.57
0.82
1.52
POINT TEMPERATURE °F
100
105
110
115
120
y / y₀ , FRACTIONAL DISTANCE FROM LOWER PLATE
0.9
0.8
0.7
0.6
0.5
0.4
0.3
0.2
0.1

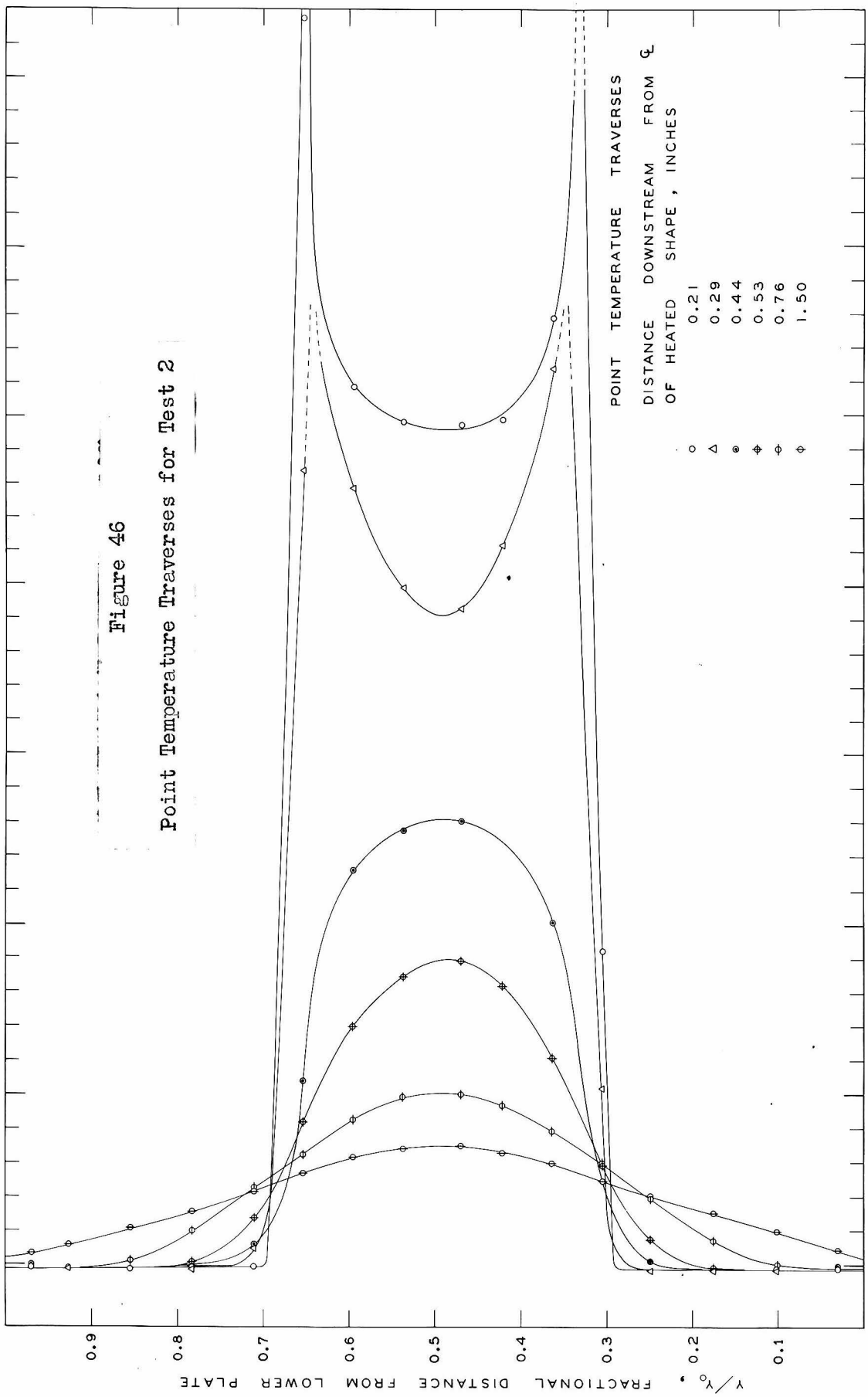

Figure 46

Point Temperature Traverses for Test 2

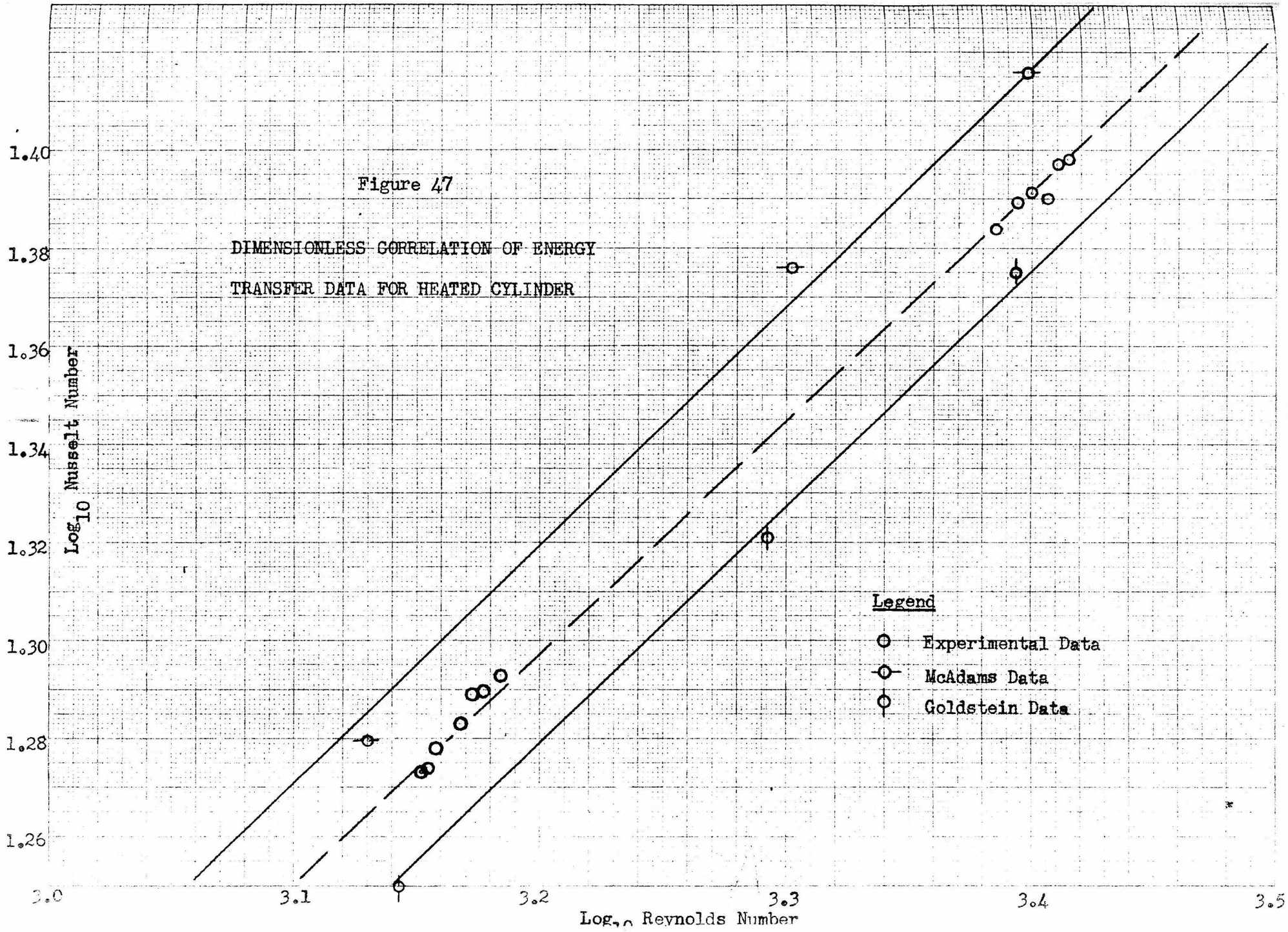
Figure 47
DIMENSIONLESS CORRELATION OF ENERGY
TRANSFER DATA FOR HEATED CYLINDER
Log10 Nusselt Number
1.40
1.38
1.36
1.34
1.32
1.30
1.28
1.26
3.0
3.1
3.2
3.3
3.4
3.5
Log10 Reynolds Number
Legend
Experimental Data
McAdams Data
Goldstein Data

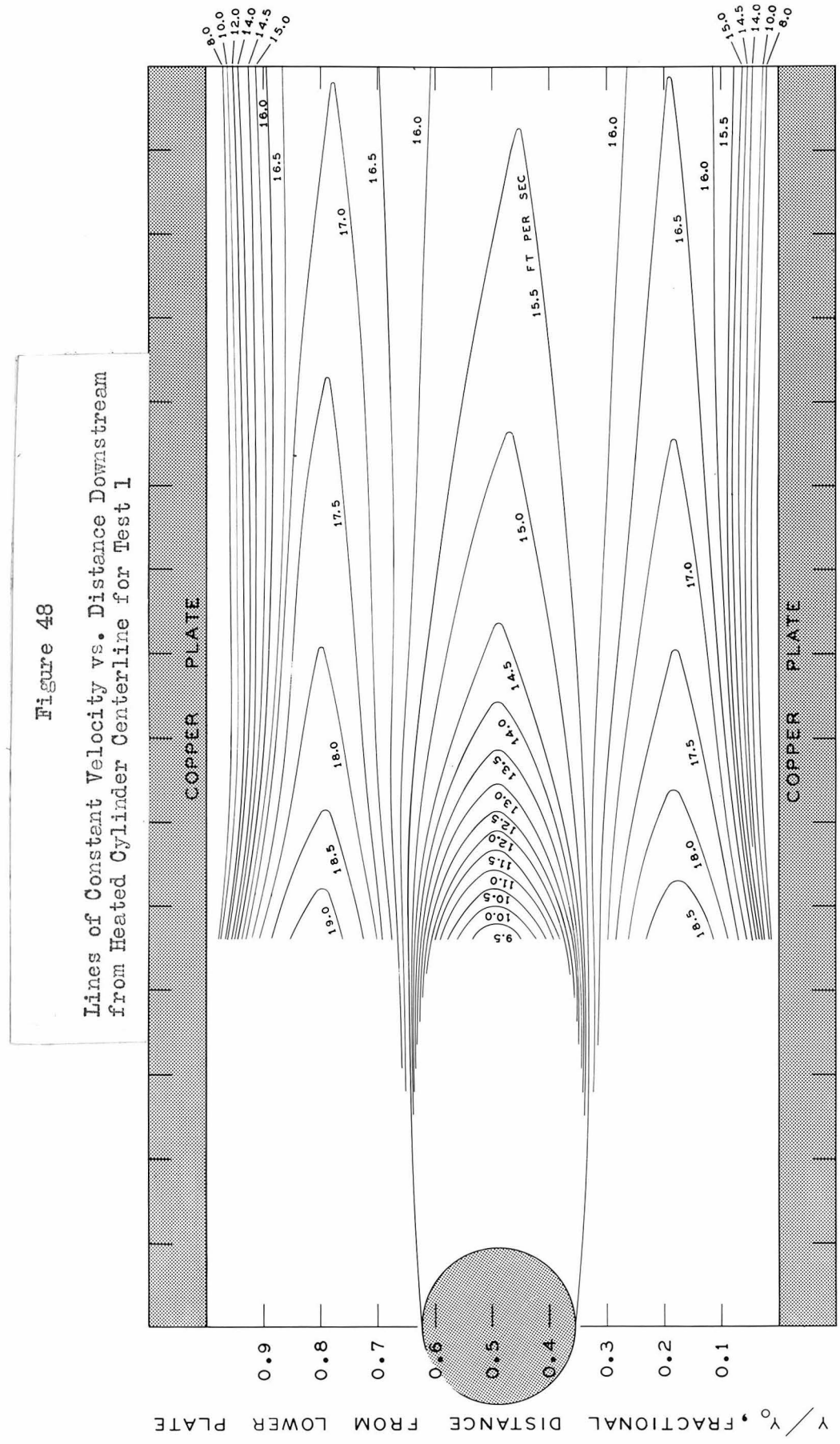

Figure 48

Lines of Constant Velocity vs. Distance Downstream from Heated Cylinder Centerline for Test 1

Figure 49

Lines of Constant Velocity vs. Distance Downstream from Heated Cylinder Centerline for Test 2

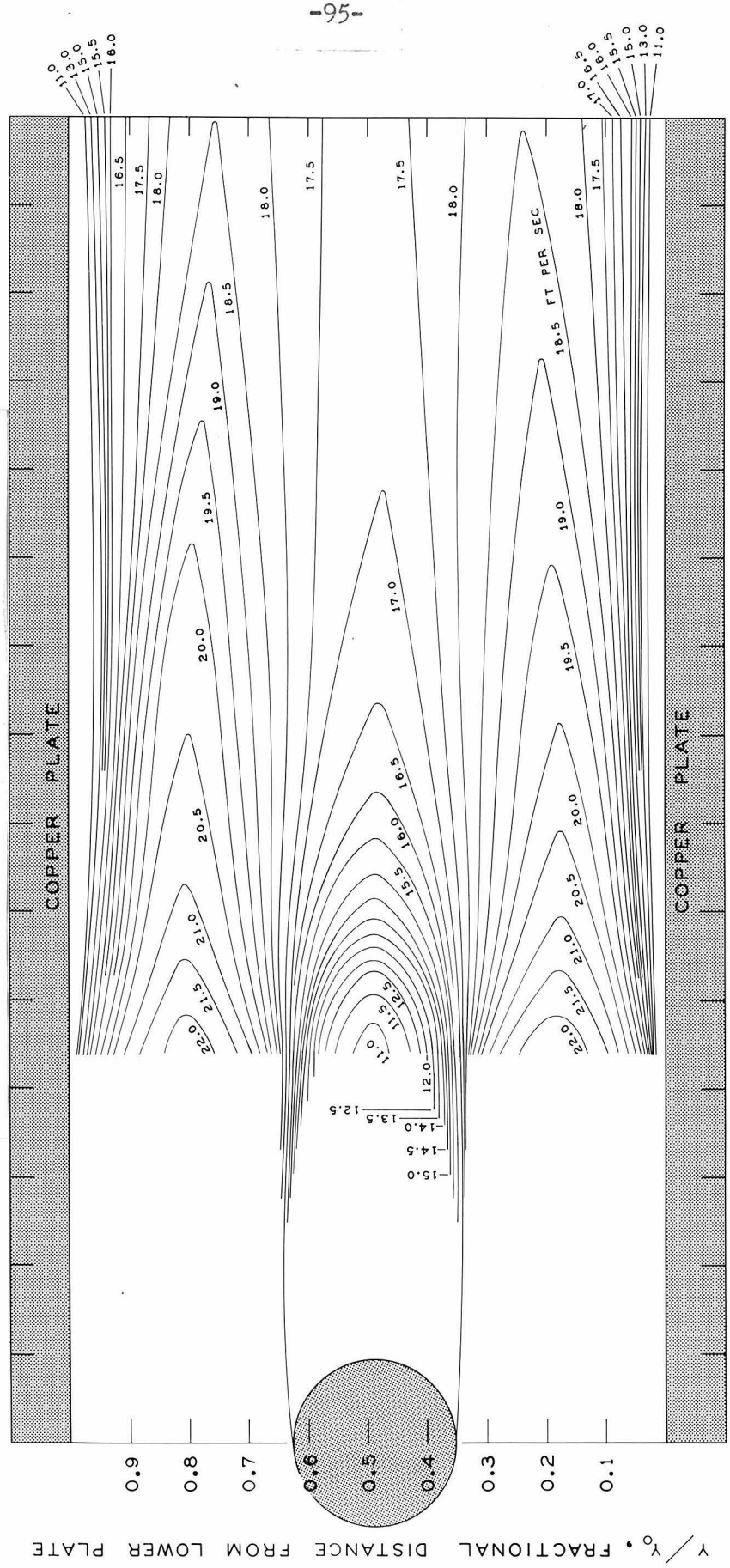

Figure 50

Lines of Constant Temperature vs. Distance Downstream from Heated Cylinder Centerline for Test 1

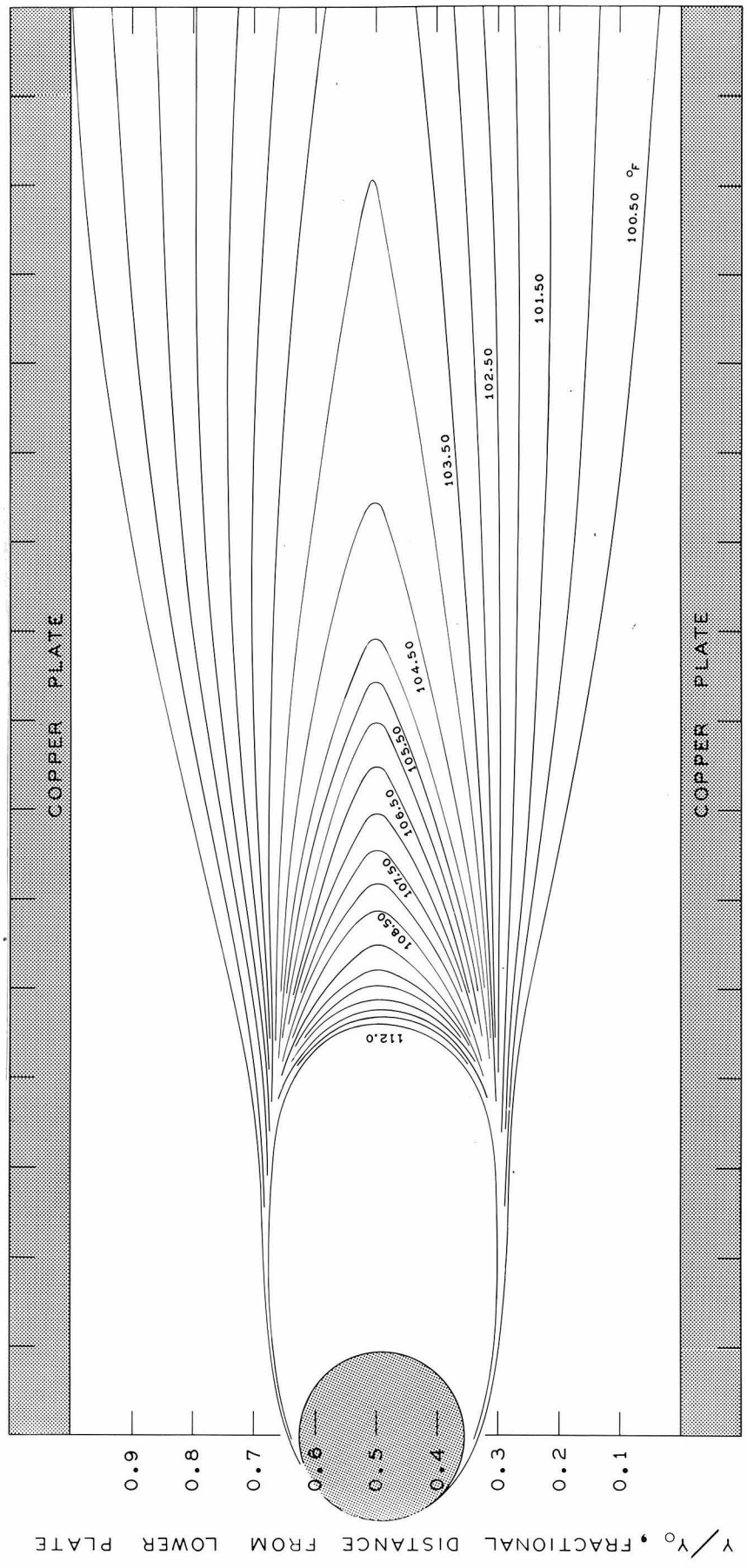

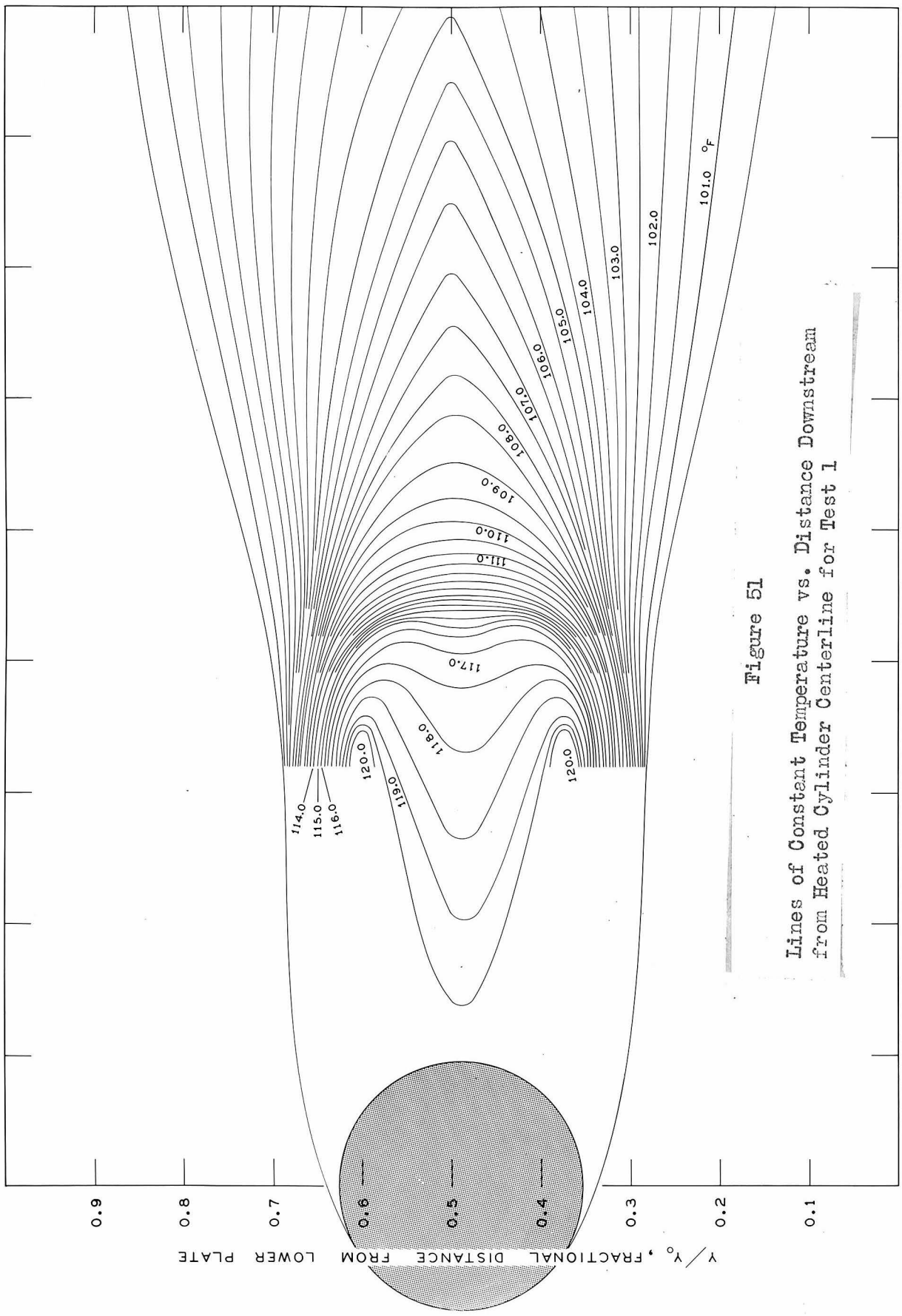

Figure 51

Lines of Constant Temperature vs. Distance Downstream from Heated Cylinder Centerline for Test 1

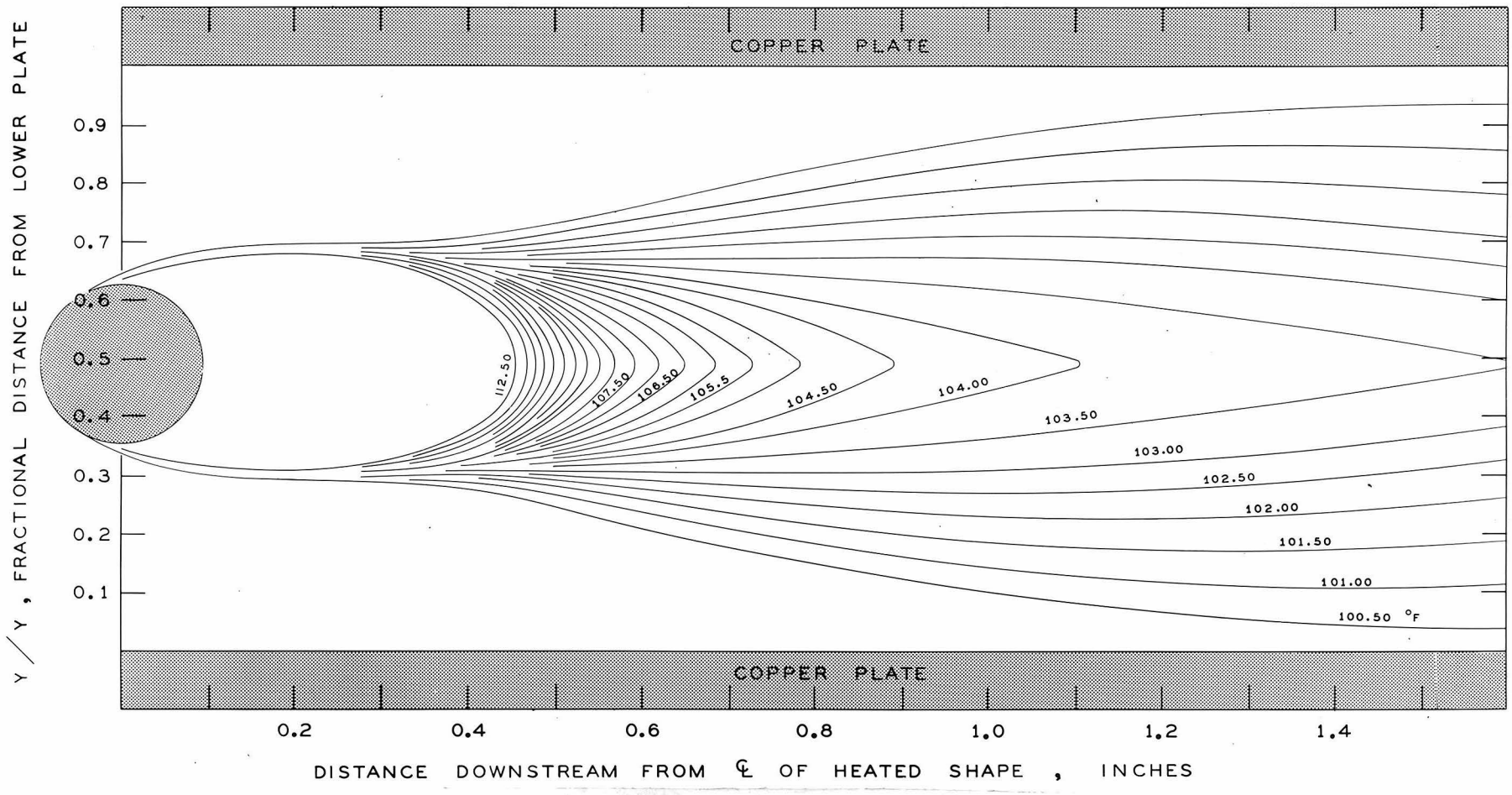

Figure 52

Lines of Constant Temperature vs. Distance Downstream from Heated Cylinder Centerline for Test 2

Figure 53

Lines of Constant Temperature vs. Distance Downstream from Heated Cylinder Centerline for Test 2

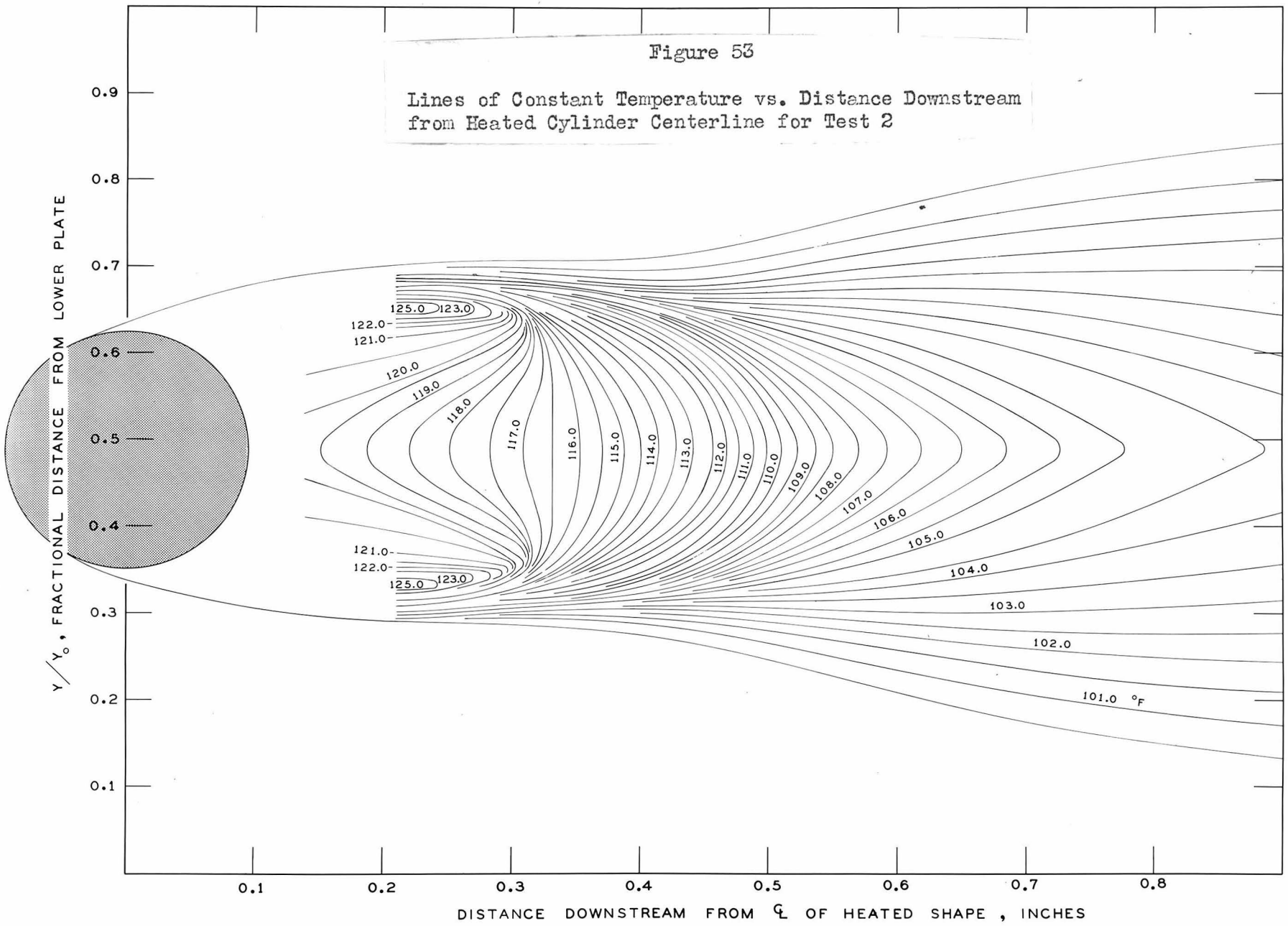

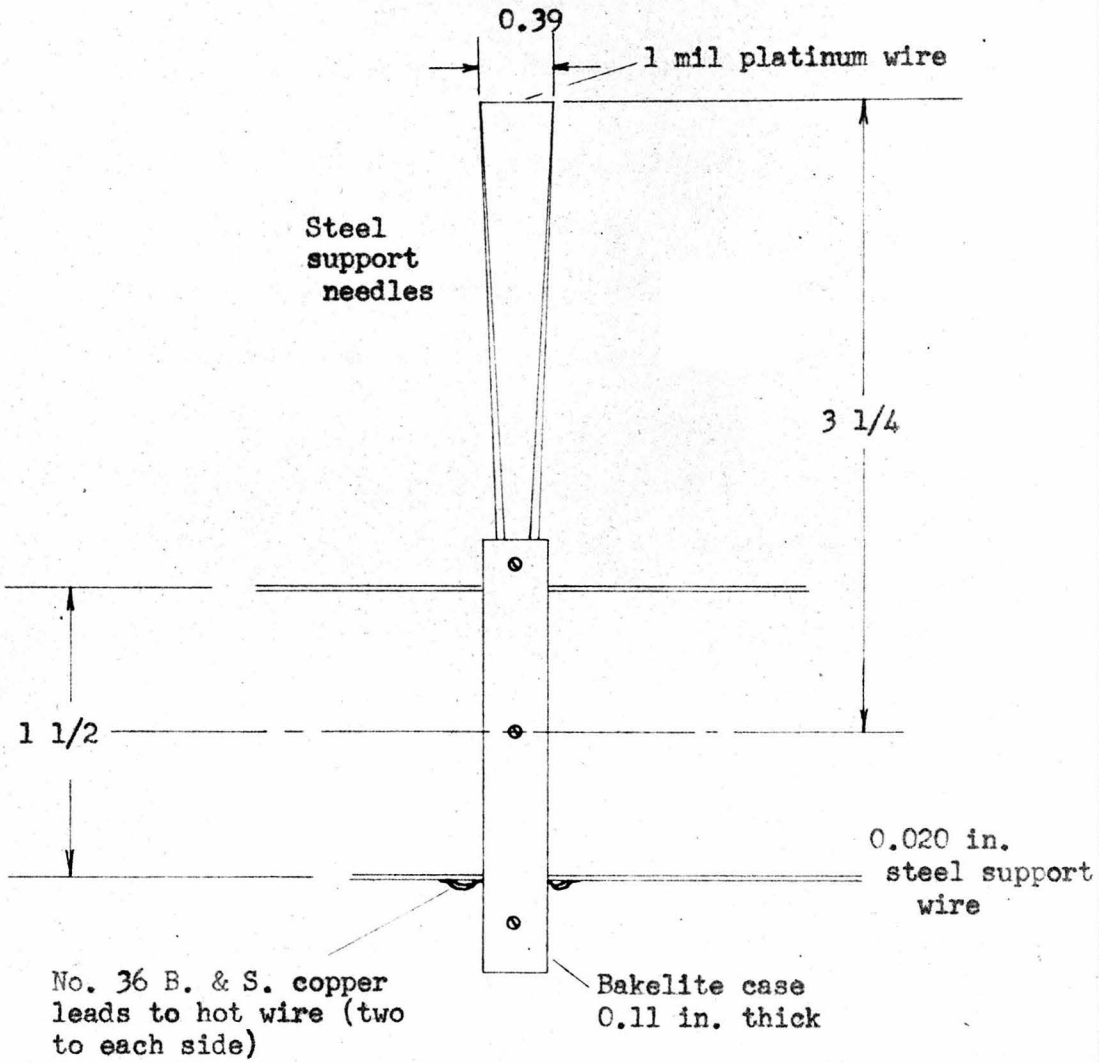

Figure 54 Schematic sketch of hot wire anemometer.

LIST OF TABLES

TABLE I

VENTURI METER CHARACTERISTICS

Meter No.	Entrance and Exit Diameter (in.)	Throat Diameter (in.)	Over-all Length (in.)
1	1.495	0.673	11.408
2	2.995	1.198	23.289
3	6.010	2.404	45.773
4	8.000	3.200	60.930

All meters have contraction sections with 10° $30'$ angle of convergence and diffuser sections with 3° $30'$ angle of divergence.

TABLE II

CALIBRATION DATA FOR AIR SYSTEM PLATINUM RESISTANCE THERMOMETER

Temperature of Thermometer (°F)	Thermometer Resistance (Ohms)	Ten Degree Resistance Difference (Ohms)
60.00	20.6641	
		0.4162
70.00	21.0803	
		0.4154
80.00	21.4957	
		0.4146
90.00	21.9103	
		0.4139
100.00	22.3242	
		0.4131
110.00	22.7373	
		0.4123
120.00	23.1496	
		0.4115
130.00	23.5611	
		0.4108
140.00	23.9719	
		0.4100
150.00	24.3819	
		0.4092
160.00	24.7911	

TABLE III

RATE OF ENERGY INPUT TO HEATED CYLINDER

Mean Surface Temperature of Cylinder (°F)	Energy Input Rate (Watts)	Mean Air Velocity Past Cylinder (Ft. per Sec.)
253	46.95	18.0
254	47.33	18.0
230	39.54	18.0
199	29.76	18.0
182	24.67	18.0
167	19.94	18.0
143	12.66	18.0
134	12.64	30.3
143	16.07	30.3
156	20.77	30.3
178	29.56	30.3
199	37.92	30.3
228	49.50	30.3

TABLE IV

COMPARISON OF EXPERIMENTAL TESTS

Test Number	Working Section Reynolds Number	Air Stream Bulk Temperature ($^{o}F.$)	Purpose of Test
1	6,600	100.00	Measurement of Diffusion of Energy in Wake of Heated Cylinder
2	7,600	100.00	Measurement of Diffusion of Energy in Wake of Heated Cylinder
3	7,600	100.00	Measurement of Energy Transfer Rate from Heated Cylinder to Air Stream
4	12,900	100.00	Measurement of Energy Transfer Rate from Heated Cylinder to Air Stream

TABLE V

VELOCITY TRAVERSES DOWNSTREAM FROM HEATED CYLINDER

Test 1

Traverse at 0.46 in. Downstream		Traverse at 0.57 in. Downstream	
y/y_o*	Point Velocity (Ft. per Sec.)	y/y_o	Point Velocity (Ft. per Sec.)
0.970	11.02	0.970	6.45
0.928	17.47	0.928	15.84
0.855	18.75	0.855	18.06
0.783	19.18	0.783	18.57
0.711	18.31	0.711	17.64
0.653	15.84	0.653	15.84
0.595	12.25	0.595	13.62
0.537	9.36	0.537	12.11
0.479	9.24	0.479	11.62
0.421	9.92	0.421	12.75
0.363	12.74	0.363	14.59
0.305	16.65	0.305	16.65
0.247	18.15	0.247	17.98
0.175	18.23	0.175	18.32
0.087	17.89	0.087	17.47
0.042	16.24	0.042	10.30

* Fractional distance from lower plate

TABLE V (CONT.)

VELOCITY TRAVERSES DOWNSTREAM FROM HEATED CYLINDER

Test 1

Traverse at 0.82 in. Downstream		Traverse at 1.52 in. Downstream	
y/y_o*	Point Velocity (Ft. per Sec.)	y/y_o	Point Velocity (Ft. Per Sec.)
0.928	13.40	0.928	14.90
0.855	17.56	0.855	16.40
0.783	17.97	0.783	16.73
0.711	17.06	0.711	17.22
0.653	16.24	0.653	16.32
0.595	15.37	0.595	15.92
0.537	14.59	0.537	15.60
0.479	14.44	0.479	15.52
0.421	14.74	0.421	15.60
0.363	15.37	0.363	15.76
0.305	16.16	0.305	15.76
0.247	16.97	0.247	16.00
0.175	17.47	0.175	15.84
0.087	15.60	0.087	15.84

* Fractional distance from lower plate

TABLE V (CONT.)

VELOCITY TRAVERSES DOWNSTREAM FROM HEATED CYLINDER

Test 1

Traverse at 62.5
in. Downstream

y/y_o*	Point Velocity (Ft. per Sec.)
0.934	13.58
0.919	13.57
0.905	14.11
0.876	15.24
0.847	16.14
0.775	16.14
0.702	16.60
0.630	17.07
0.558	17.97
0.486	18.36
0.413	18.36
0.269	17.05
0.197	16.59
0.124	15.63

* Fractional distance from lower plate

TABLE V (CONT.)

VELOCITY TRAVERSES DOWNSTREAM FROM HEATED CYLINDER

Test 2

Traverse at 0.44 in. Downstream		Traverse at 0.53 in. Downstream	
y/y_o*	Point Velocity (Ft. per Sec.)	y/y_o*	Point Velocity (Ft. per Sec.)
0.971	7.51	0.971	4.00
0.928	20.43	0.928	18.92
0.855	21.90	0.855	21.07
0.783	22.18	0.783	21.25
0.711	21.90	0.711	20.34
0.653	18.66	0.653	18.15
0.596	13.32	0.595	15.13
0.537	11.15	0.537	12.60
0.479	11.56	0.479	12.04
0.421	11.63	0.421	13.32
0.363	15.21	0.363	16.16
0.305	20.70	0.305	18.92
0.247	22.09	0.247	20.79
0.175	22.18	0.175	21.16
0.101	21.53	0.101	20.88
0.029	9.80	0.029	5.76

* Fractional distance from lower plate

TABLE V (CONT.)

VELOCITY TRAVERSES DOWNSTREAM FROM HEATED CYLINDER

Test 2

Traverse at 0.76 in. Downstream		Traverse at 1.50 in. Downstream	
y/y_o*	Point Velocity (Ft. per Sec.)	y/y_o	Point Velocity (Ft. per Sec.)
0.971	4.08	0.971	11.90
0.928	16.40	0.928	15.76
0.855	20.70	0.855	17.72
0.783	20.52	0.783	18.40
0.711	19.27	0.711	18.32
0.653	18.40	0.653	17.89
0.595	17.39	0.595	17.47
0.537	16.56	0.537	17.14
0.479	16.16	0.479	17.47
0.421	16.65	0.421	17.47
0.363	17.89	0.363	17.98
0.305	18.57	0.305	18.06
0.247	19.45	0.247	17.98
0.175	20.07	0.175	18.23
0.101	19.10	0.101	17.39
0.029	5.29	0.029	12.60

* Fractional distance from lower plate

TABLE V (CONT.)

VELOCITY TRAVERSES DOWNSTREAM FROM HEATED CYLINDER

Test 2

Traverse at 62.5 in. Downstream

y/y_o*	Point Velocity (Ft. per Sec.)
0.950	13.15
0.921	15.14
0.885	16.08
0.814	17.37
0.742	18.22
0.670	18.53
0.598	18.99
0.527	18.99
0.455	19.35
0.383	19.35
0.311	18.99
0.240	18.24
0.168	17.37
0.096	16.11
0.060	15.17
0.045	14.67

* Fractional distance from lower plate

TABLE VI

TEMPERATURE TRAVERSES DOWNSTREAM FROM HEATED CYLINDER

Test 1

Traverse at 0.32 in. Downstream		Traverse at 0.42 in. Downstream	
y/y_o*	Point Temperature (°F)	y/y_o	Point Temperature (°F)
0.916	99.85	0.970	99.95
0.817	99.82	0.928	99.90
0.745	99.93	0.855	99.87
0.688	100.77	0.783	99.85
0.630	120.10	0.711	100.42
0.573	122.68	0.653	106.93
0.516	120.57	0.595	115.39
0.458	120.44	0.566	116.12
0.401	122.26	0.537	116.01
0.344	119.95	0.479	116.01
0.284	101.11	0.450	116.12
0.216	100.00	0.421	116.38
0.143	100.00	0.363	113.51
0.070	100.02	0.305	103.58
		0.247	99.93
		0.175	99.83
		0.087	99.83
		0.042	99.87

* Fractional distance from lower plate

TABLE VI (CONT.)

TEMPERATURE TRAVERSES DOWNSTREAM FROM HEATED CYLINDER

Test 1

Traverse at 0.46 in. Downstream		Traverse at 0.57 in. Downstream	
y/y_o*	Point Temperature (°F)	y/y_o	Point Temperature (°F)
0.970	99.93	0.970	99.95
0.928	99.87	0.928	99.90
0.855	99.87	0.855	99.85
0.783	99.98	0.783	100.16
0.711	100.87	0.711	101.84
0.653	105.21	0.653	104.39
0.595	110.78	0.595	106.88
0.537	112.20	0.537	108.52
0.479	112.58	0.479	108.85
0.421	112.33	0.421	107.92
0.363	109.50	0.363	105.92
0.305	102.92	0.305	103.07
0.248	100.42	0.248	100.99
0.1751	99.93	0.175	99.95
0.087	99.90	0.087	99.85
0.042	99.90	0.042	99.90

* Fractional distance from lower plate

TABLE VI (CONT.)

TEMPERATURE TRAVERSES DOWNSTREAM FROM HEATED CYLINDER

Test 1

Traverse at 0.82 in. Downstream		Traverse at 1.52 in. Downstream	
y/y_o*	Point Temperature (°F)	y/y_o	Point Temperature (°F)
0.930	99.87	0.928	100.98
0.857	100.31	0.858	101.53
0.784	101.50	0.785	102.10
0.716	102.76	0.715	102.82
0.656	103.75	0.655	103.07
0.599	104.60	0.599	103.49
0.542	105.09	0.530	103.78
0.484	105.24	0.484	103.78
0.427	104.73	0.427	103.54
0.370	103.88	0.370	103.07
0.312	102.92	0.312	102.43
0.255	101.97	0.255	101.84
0.183	100.80	0.183	101.27
0.084	100.03	0.085	101.06

* Fractional distance from lower plate

TABLE VI (CONT.)

TEMPERATURE TRAVERSES DOWNSTREAM FROM HEATED CYLINDER

Test 1

Traverse at 62.5 in. Downstream

y/y_o*	Point Temperature (°F)
0.971	100.41
0.853	100.99
0.494	101.16
0.129	100.93
0.037	100.44

* Fractional distance from lower plate

TABLE VI (CONT.)

TEMPERATURE TRAVERSES DOWNSTREAM FROM HEATED CYLINDER

Test 2

Traverse at 0.21 in. Downstream		Traverse at 0.29 in. Downstream	
y/y_o*	Point Temperature (°F)	y/y_o	Point Temperature (°F)
0.971	99.90	0.971	99.90
0.928	99.87	0.928	99.85
0.855	99.85	0.855	99.85
0.783	99.90	0.783	99.85
0.711	99.93	0.711	100.47
0.653	136.72	0.653	123.35
0.595	125.80	0.595	122.83
0.537	124.76	0.537	119.90
0.479	124.69	0.479	119.30
0.421	124.84	0.421	121.15
0.363	127.85	0.363	126.34
0.305	109.27	0.305	105.16
0.248	99.87	0.248	99.82
0.175	99.85	0.175	99.82
0.101	99.85	0.101	99.82
0.029	99.87	0.029	99.87

* Fractional distance from lower plate

TABLE VI (CONT.)

TEMPERATURE TRAVERSES DOWNSTREAM FROM HEATED CYLINDER

Test 2

Traverse at 0.44 in. Downstream		Traverse at 0.53 in. Downstream	
y/y_o*	Point Temperature (^oF)	y/y_o	Point Temperature (^oF)
0.971	99.98	0.971	99.98
0.928	99.87	0.928	99.93
0.855	99.87	0.855	99.93
0.783	99.87	0.783	100.08
0.711	100.60	0.711	101.37
0.653	105.40	0.653	104.21
0.595	111.58	0.595	107.01
0.537	112.74	0.537	108.49
0.479	113.02	0.479	108.93
0.421	112.92	0.421	108.20
0.363	110.05	0.363	106.08
0.305	103.22	0.305	102.92
0.247	100.10	0.248	100.75
0.175	99.85	0.175	99.93
0.101	99.82	0.101	99.82
0.029	99.98	0.029	99.95

* Fractional distance from lower plate

TABLE VI (CONT.)

TEMPERATURE TRAVERSES DOWNSTREAM FROM HEATED CYLINDER

Test 2

Traverse at 0.76 in. Downstream		Traverse at 1.50 in. Downstream	
y/y_o*	Point Temperature (^oF)	y/y_o	Point Temperature (^oF)
0.971	99.93	0.971	100.34
0.928	99.90	0.928	100.57
0.855	100.10	0.855	101.06
0.783	100.99	0.783	101.55
0.711	102.28	0.711	102.15
0.653	103.23	0.653	102.69
0.595	104.26	0.595	103.18
0.537	104.93	0.537	103.41
0.479	105.01	0.479	103.49
0.421	104.68	0.421	103.28
0.363	103.93	0.363	102.97
0.305	102.97	0.305	102.46
0.248	101.94	0.248	102.05
0.175	100.70	0.175	101.53
0.101	100.00	0.101	100.99
0.029	99.95	0.029	100.47

* Fractional distance from lower plate

TABLE VI (CONT.)

TEMPERATURE TRAVERSES DOWNSTREAM FROM HEATED CYLINDER

Test 2

Traverse at 62.5 in. Downstream

y/y_o*	Point Temperature (^oF)
0.971	100.41
0.853	100.88
0.502	101.09
0.147	100.88
0.026	100.21

* Fractional distance from lower plate

Appendix A

Computation of Control Temperature for Air System

The control temperature for the air system (which is required to provide air at a specified temperature in the working section of the tunnel) is computed by reference to Figures 11, A-1 and A-2. Figure 11, as previously described, is a plot of Venturi meter differential as a function of channel (working section) Reynolds number. Figure A-1 is a plot of average channel velocity as a function of channel Reynolds number. Figure A-2 is a plot of adiabatic temperature decrease associated with acceleration to a particular channel velocity as a function of that velocity.

The adiabatic temperature decrease for Figure A-2 is computed from the area and pressure ratios involved by use of the total energy flow equation discussed in Reference 14. The cross-sections chosen for this balance are:

(1) The entrance to the convergent section

(2) The entrance to the working section

In the balance, kinetic energy at section (1) is neglected with respect to that at section (2) because of the large change of velocity between the sections.

The figures are applied in computation of the adiabatic temperature decrease by measuring the Venturi differential associated with the desired flow. The differential is converted by Figure 11 to channel Reynolds number. Figure A-1 provides conversion of Reynolds

number to average channel velocity which, by appropriate use of Figure A-2 is converted to adiabatic temperature decrease. The temperature decrease obtained is added, as a positive value, to the desired operating temperature to obtain the control temperature.

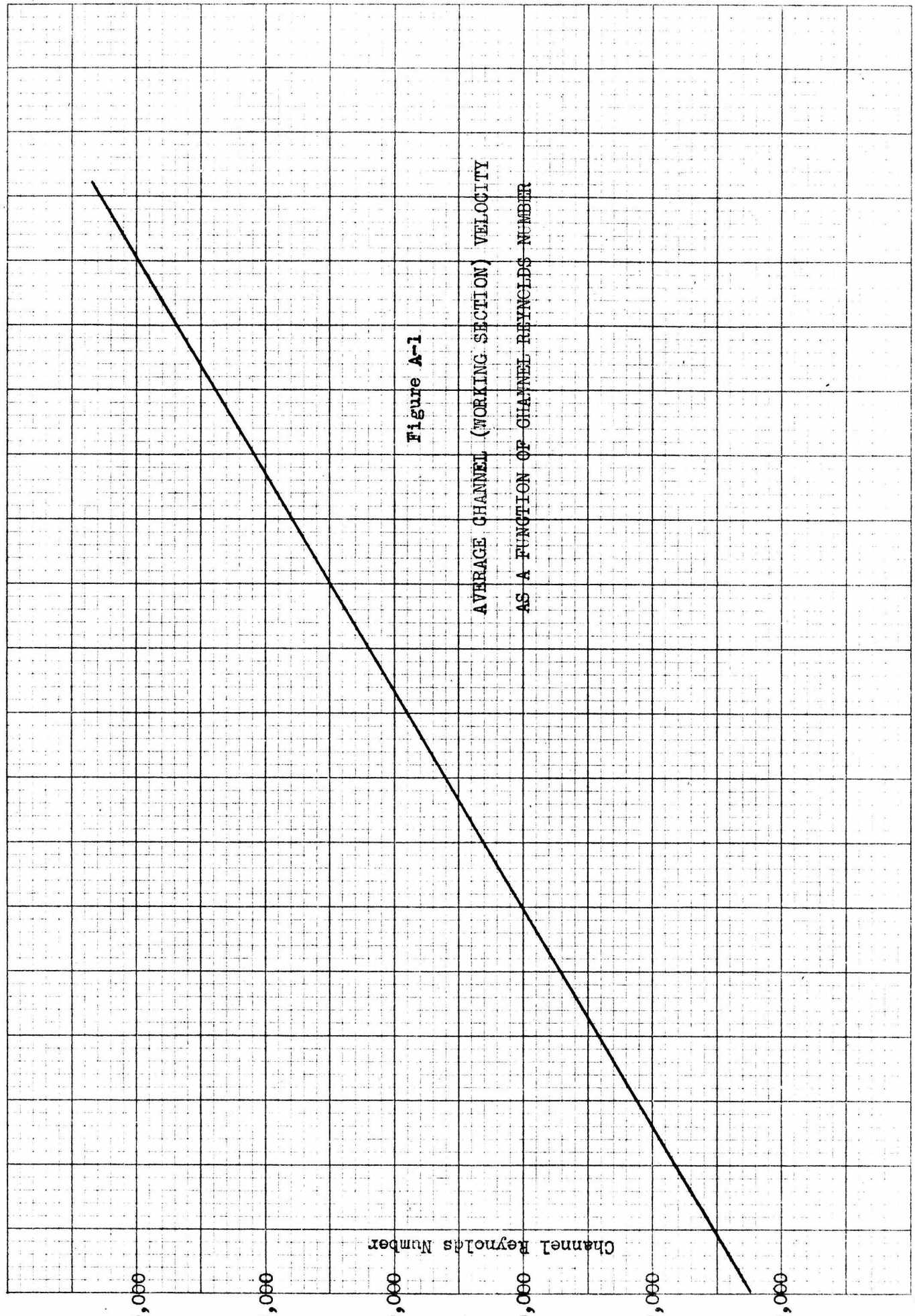

Figure A-1

AVERAGE CHANNEL (WORKING SECTION) VELOCITY
AS A FUNCTION OF CHANNEL REYNOLDS NUMBER

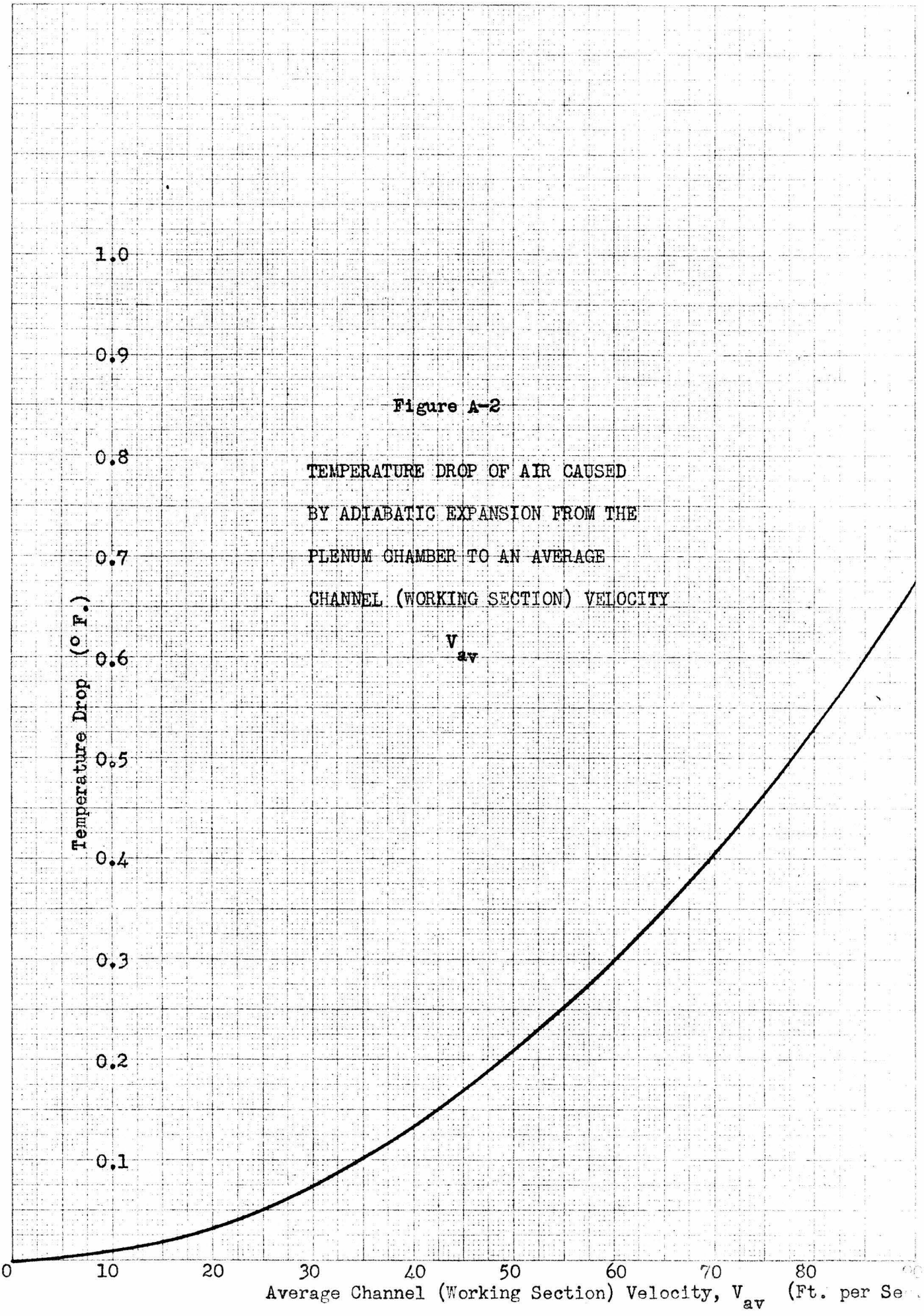

Figure A-2

TEMPERATURE DROP OF AIR CAUSED BY ADIABATIC EXPANSION FROM THE PLENUM CHAMBER TO AN AVERAGE CHANNEL (WORKING SECTION) VELOCITY V_{av}

Appendix B

Derivation of Equations for Eddy Viscosity and Eddy Conductivity

The equation which may be employed to compute eddy viscosity as a function of position in the wake is obtained from a force balance on a volume element. A rectangular coordinate system may be established in the fluid media and a volume element, centered at point (x, y, z) and with elemental dimensions δx , δy and δz* , may be isolated for consideration as in the following sketch:

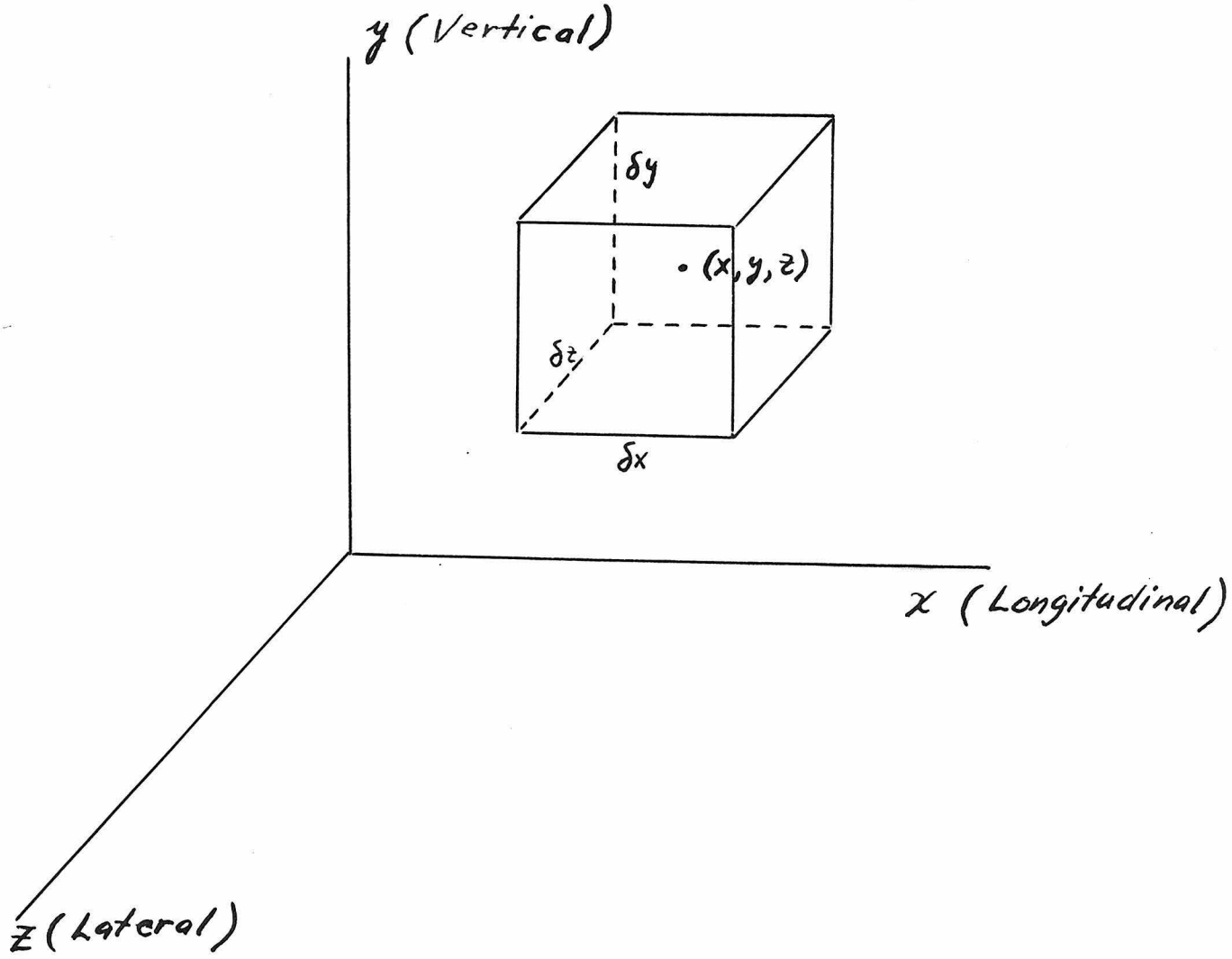

---

* The nomenclature for this Appendix is the same as that employed in the text of the thesis.

The force balance of interest is made in the x-direction which corresponds to the longitudinal direction in the working section. This may be expressed as

$$\begin{aligned}\Sigma F_x = &- \rho\,\delta x\,\delta y\,\delta z\,\frac{DV_x}{Dt} + \left[P-\left(\frac{\partial P}{\partial x}\right)\frac{\delta x}{2}\right]\delta y\,\delta z \\ &- \left[P+\left(\frac{\partial P}{\partial x}\right)\frac{\delta x}{2}\right]\delta y\,\delta z + \left[-\tau_{yx}-\left(\frac{\partial -\tau_{yx}}{\partial y}\right)\frac{\delta y}{2}\right]\delta x\,\delta z \\ &+ \left[\tau_{yx}+\left(\frac{\partial \tau_{yx}}{\partial y}\right)\frac{\delta y}{2}\right]\delta x\,\delta z + \left[-\tau_{zx}-\left(\frac{\partial -\tau_{zx}}{\partial z}\right)\frac{\delta z}{2}\right]\delta x\,\delta y \\ &+ \left[\tau_{zx}+\left(\frac{\partial \tau_{zx}}{\partial z}\right)\frac{\delta z}{2}\right]\delta x\,\delta y = 0\end{aligned} \tag{1}$$

where $\frac{DV_x}{Dt}$ is the "fluid" derivative

$$\frac{DV_x}{Dt} = \frac{\partial V_x}{\partial t} + V_x\frac{\partial V_x}{\partial x} + V_y\frac{\partial V_x}{\partial y} + V_z\frac{\partial V_x}{\partial z} \tag{2}$$

Equation 1 may be simplified to

$$\rho\frac{DV_x}{Dt} = -\frac{\partial P}{\partial x} + \frac{\partial \tau_{yx}}{\partial y} + \frac{\partial \tau_{zx}}{\partial z} \tag{3}$$

which may be integrated to yield, for two dimensional flow,

$$\tau_{yx} = \int_0^y \rho\frac{DV_x}{Dt}\,dy + \int_0^y \frac{\partial P}{\partial x}\,dy \tag{4}$$

where y = 0 at the position where $\tau_{yx} = 0$

The eddy viscosity, ϵ_{mx} , is related to the shear, τ_{yx} , by the expression

$$\tau_{yx} = \rho(\epsilon_{mx} + \nu)\left(\frac{\partial V_x}{\partial y} + \frac{\partial V_y}{\partial x}\right) \tag{5}$$

which permits evaluation of $\epsilon_{mx} + \nu$ as

$$\epsilon_{mx} + \nu = \frac{\int_0^y \rho \frac{DV_x}{Dt} dy + \int_0^y \frac{\partial P}{\partial x} dy}{\rho\left(\frac{\partial V_x}{\partial y}\right)} \tag{6}$$

if $\frac{\partial V_y}{\partial x}$ is assumed negligible with respect to $\frac{\partial V_x}{\partial y}$.

Equation 6 may be simplified for steady state conditions in two-dimensional flow to the form

$$\epsilon_{mx} + \nu = \frac{\int_0^y \rho\left[V_x \frac{\partial V_x}{\partial x} + V_y \frac{\partial V_x}{\partial y}\right] dy + \int_0^y \frac{\partial P}{\partial x} dy}{\rho\left(\frac{\partial V_x}{\partial y}\right)} \tag{7}$$

For the special steady state condition in two-dimensional flow for which $V_y = 0$ and V_x is independent of x, Equation 2 reduces to

$$\frac{\partial \tau_{yx}}{\partial y} = \frac{\partial P}{\partial x} \tag{8}$$

which is integrable to

$$\tau_{yx} = y\left(\frac{\partial P}{\partial x}\right)$$

or, in more familiar form,

$$\tau_{yx} = \tau_{0yx}\left(y/y_0\right) \tag{10}$$

The equation for eddy conductivity as a function of position in the wake is obtained from an energy balance for a volume element. A rectangular coordinate system and a volume element $\delta x\, \delta y\, \delta z$ are established as before. The energy balance for the element is

$$\begin{aligned}
&\left[c_p \sigma \theta v_x - \frac{\partial}{\partial x}\left(c_p \sigma \theta v_x\right) \frac{\delta x}{2} \right] \delta y\, \delta z \\
&- \left[c_p \sigma \theta v_x + \frac{\partial}{\partial x}\left(c_p \sigma \theta v_x\right) \frac{\delta x}{2} \right] \delta y\, \delta z \\
&+ \left[c_p \sigma \theta v_y - \frac{\partial}{\partial y}\left(c_p \sigma \theta v_y\right) \frac{\delta y}{2} \right] \delta x\, \delta z \\
&- \left[c_p \sigma \theta v_y + \frac{\partial}{\partial y}\left(c_p \sigma \theta v_y\right) \frac{\delta y}{2} \right] \delta x\, \delta z \\
&+ \left[c_p \sigma \theta v_z - \frac{\partial}{\partial z}\left(c_p \sigma \theta v_z\right) \frac{\delta z}{2} \right] \delta x\, \delta y \\
&- \left[c_p \sigma \theta v_z + \frac{\partial}{\partial z}\left(c_p \sigma \theta v_z\right) \frac{\delta z}{2} \right] \delta x\, \delta y \\
&- \left[(\epsilon_x + k) \frac{\partial \theta}{\partial x} - \frac{\partial}{\partial x}\left\{ (\epsilon_x + k) \frac{\partial \theta}{\partial x} \right\} \frac{\delta x}{2} \right] \delta y\, \delta z
\end{aligned} \tag{11}$$

$$+\left[(\epsilon_x+\kappa)\frac{\partial\theta}{\partial x}+\frac{\partial}{\partial x}\left\{(\epsilon_x+\kappa)\frac{\partial\theta}{\partial x}\right\}\frac{\delta x}{2}\right]\delta y\,\delta z$$

$$-\left[(\epsilon_y+\kappa)\frac{\partial\theta}{\partial y}-\frac{\partial}{\partial y}\left\{(\epsilon_y+\kappa)\frac{\partial\theta}{\partial y}\right\}\frac{\delta y}{2}\right]\delta x\,\delta z$$

$$+\left[(\epsilon_y+\kappa)\frac{\partial\theta}{\partial y}+\frac{\partial}{\partial y}\left\{(\epsilon_y+\kappa)\frac{\partial\theta}{\partial y}\right\}\frac{\delta y}{2}\right]\delta x\,\delta z$$

$$-\left[(\epsilon_z+\kappa)\frac{\partial\theta}{\partial z}-\frac{\partial}{\partial z}\left\{(\epsilon_z+\kappa)\frac{\partial\theta}{\partial z}\right\}\frac{\delta z}{2}\right]\delta x\,\delta y$$

$$+\left[(\epsilon_z+\kappa)\frac{\partial\theta}{\partial z}+\frac{\partial}{\partial z}\left\{(\epsilon_z+\kappa)\frac{\partial\theta}{\partial z}\right\}\frac{\delta z}{2}\right]\delta x\,\delta y$$

which may be simplified to the form

$$\frac{\partial}{\partial x}(C_p\sigma\theta V_x)+\frac{\partial}{\partial y}(C_p\sigma\theta V_y)+\frac{\partial}{\partial z}(C_p\sigma\theta V_z)$$

$$(12)\qquad =\frac{\partial}{\partial x}\left\{(\epsilon_x+\kappa)\frac{\partial\theta}{\partial x}\right\}+\frac{\partial}{\partial y}\left\{(\epsilon_y+\kappa)\frac{\partial\theta}{\partial y}\right\}+\frac{\partial}{\partial z}\left\{(\epsilon_z+\kappa)\frac{\partial\theta}{\partial z}\right\}$$

The equation of continuity

$$(13)\qquad \frac{\partial(\sigma V_x)}{\partial x}+\frac{\partial(\sigma V_y)}{\partial y}+\frac{\partial(\sigma V_z)}{\partial z}=0$$

may be used to reduce Equation 2 to the form

$$(14)\qquad \sigma\left\{V_x\frac{\partial C_p\theta}{\partial x}+V_y\frac{\partial C_p\theta}{\partial y}+V_z\frac{\partial C_p\theta}{\partial z}\right\}$$

$$=\frac{\partial}{\partial x}\left\{(\epsilon_x+\kappa)\frac{\partial\theta}{\partial x}\right\}+\frac{\partial}{\partial y}\left\{(\epsilon_y+\kappa)\frac{\partial\theta}{\partial y}\right\}$$

$$+\frac{\partial}{\partial z}\left\{(\epsilon+\kappa)\right\}\frac{\partial\theta}{}$$

Equation 14 involves ϵ_x, ϵ_y and ϵ_z because of the non-vectorial nature of the energy balance (as contrasted with the force balance) and is therefore not susceptible to solution of the form indicated by Equation 6 without introduction of various simplifying assumptions. For example, in two-dimensional flow for which θ is also independent of x

$$\epsilon_y + K = \frac{\sigma \int_0^y v_y \frac{\partial c_p \theta}{\partial y} dy}{\frac{d\theta}{dy}} \tag{15}$$

With the further restriction that $v_y = 0$, Equation 14 reduces to the familiar form

$$(\epsilon_y + K) \frac{d\theta}{dy} = \text{Constant} = -\frac{\dot{q}}{c_p \sigma} \tag{16}$$

Propositions Submitted by Glenn Wagner Billman

Ph. D. Oral Examination, May 26, 1948, 09:00 A.M., Crellin Conference Room

Committee: Professor Sage (Chairman), Professors Clark, Kirkwood, Lacey and Lindvall.

Chemical Engineering

1. It is desirable for submarine application to develop a carbon dioxide removal system which, with make-up oxygen, will permit a Diesel engine to operate on the recycled exhaust gas.. A system employing polyethylene amines in aqueous solution is proposed.

2. It is proposed that silicones or halogen derivatives of silicones be employed as heat transfer media in the "fluid heat" systems of large bakeries or restaurants. The stability, low viscosity index and moderate heat capacity of this family of compounds make it particularly satisfactory for this application.

3. The definition of eddy viscosity employed by various authors (References* 7 and 8) is unsatisfactory because of difficulty encountered in evaluation of this quantity near maxima or minima in the velocity distribution. A theoretical analysis indicates the source of this difficulty and suggests a possible modification of the definition to avoid the computational difficulty.

4. The logarithmic velocity distributions proposed by various authors (References 7 and 8)give gradients which are discontinuous near maxima and minima in the distributions. A velocity distribution is proposed which is based upon an empirically determined parabolic distribution of mixing length in the conduit and which possesses continuous velocity gradients throughout the conduit.

5. It is proposed that a composition correlating line rather than tie lines be employed to indicate compositions of coexisting phases in ternary diagrams. These composition correlating lines would permit quick extimation of the composition of the coexisting phases throughout the entire two-phase region rather than at the isolated experimental points. Several types of correlating line may be employed. One, whose construction involves only simple graphical operations, is obtained in the manner described below and indicated by example in the sketch.

- -

* The reference numbers for the propositions correspond to those employed in the text of the thesis.

5. (continued)

(i) Lines of constant per cent B are drawn through the experimentally determined compositions rich in A.

(ii) Lines of constant per cent C are drawn through the experimentally determined compositions rich in C.

(iii) The correlating line is drawn through the intersections of corresponding lines from steps (i) and (ii). It is apparent that in systems with a critical composition at the temperature and pressure of the diagram the termini of the line are the critical composition (c) and the binary composition (b) rich in C.

The employment of this correlating line to obtain compositions of coexisting phases throughout the entire two-phase region is apparent from the manner of construction.

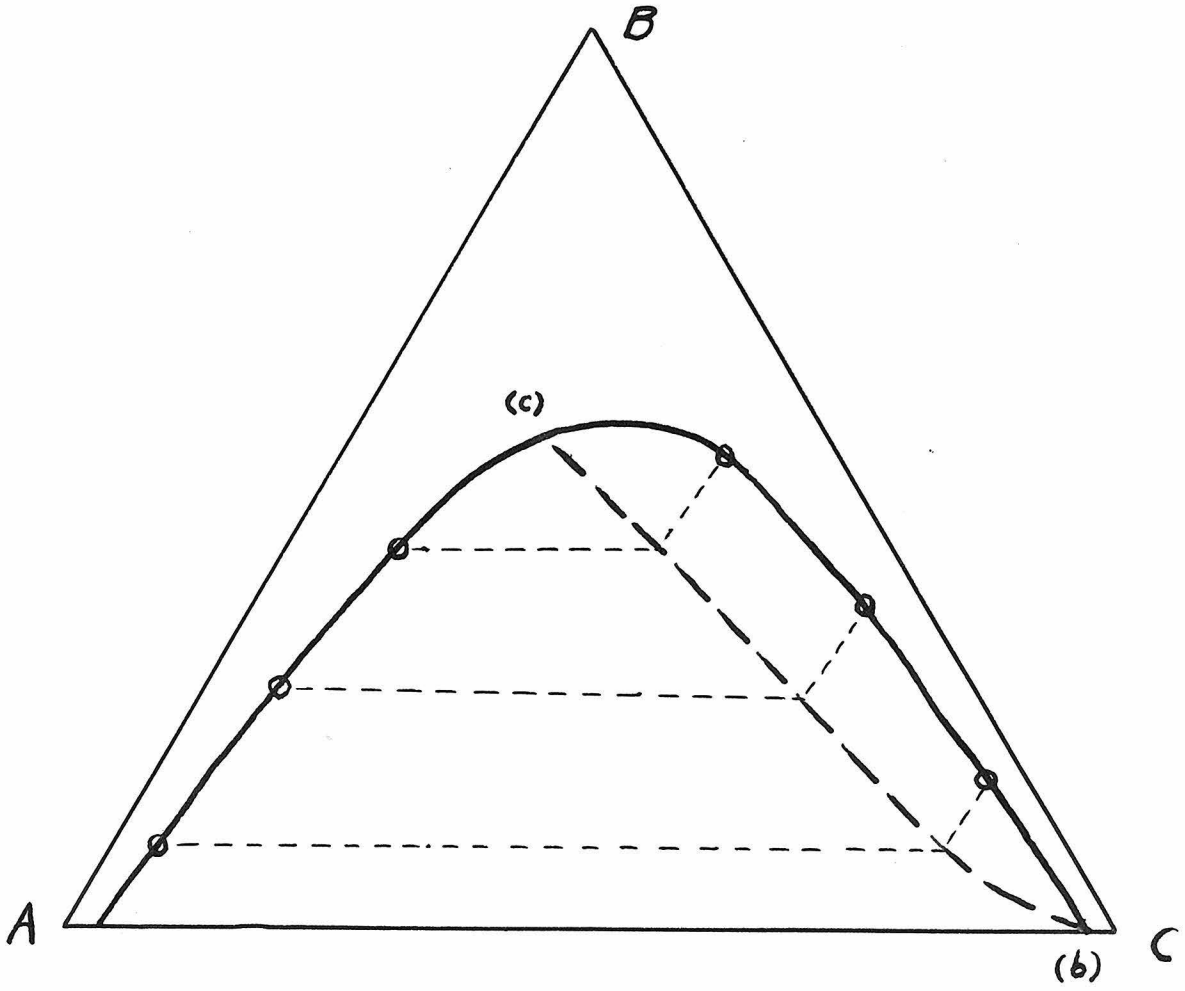

Mechanical Engineering

1. McAdams (Reference 13, Page 186) describes velocity distributions in laminar flow which are associated with thermal transfer of energy. The flex point shown in Figure 87, curve B of the reference is demonstrably impossible under the conditions described. A mathematical demonstration is provided to cover the case of flow both with and without appreciable pressure gradient along the conduit.

2. It is proposed that strain gages be employed to prevent excessive overloads during operation of power driven equipment. The strain gages would operate through appropriate electronic circuits and associated mechanisms to reduce power input to the equipment when such overloads develop.

3. A simple extension is proposed to the method of spur gear selection originated by Professor Clapp of the California Institute of Technology. This extension is for the case of wear controlling and relates the diametral pitch to various pertinent gear parameters.

Chemistry

1. Chromite ores in the Western United States commonly possess an iron-chromium ratio too large for commercial exploitation as sources of chromium metal. It is suggested that beneficiation of these ores could be accomplished by selective reduction of iron in the ores with natural gas followed by acid-leach removal of metallic iron. This process would supplement the domestic supplies of chromium ore during periods of national emergency when the additional cost is not a deciding factor.

2. For tactical purposes in submarine warfare, it is occasionally desirable to produce a large dispersion of stable bubbles in sea water. Carbon dioxide produced from carbonate-acid mixtures has been commonly employed for this purpose in the past. It is proposed that acetylene or hydrogen (from carbides or hydrides of the alkali or alkaline earth metals) would be more satisfactory for this purpose because of the lower solubility of the gas and the relatively large ratio of gas to gas producer volume.